EXPANDING THE UTILITY OF SILK FIBROIN MICRONEEDLES:

AN INVESTIGATION OF DEVICE AND FABRICATION PROCESS IMPROVEMENTS FOR TRANSDERMAL VACCINATION AND BROADER APPLICATIONS

A Thesis

Submitted By

Jordan A. Stinson

In Partial Fulfillment of the Requirements for the Degree of

Master of Science

in

Biomedical Engineering

TUFTS UNIVERSITY

August 2015

Advisor: David L. Kaplan

Committee Members: Fiorenzo G. Omenetto and Ayşe Asatekin

Abstract

Thin-film microneedle patches have emerged as an exciting alternative to hypodermic needles as they offer a simple, minimally-invasive approach to drug and vaccine delivery. Despite extensive research, many materials chosen for use in microneedle patches limit the total device scope through poor processing, stability, or mechanical properties. Silk fibroin protein from *Bombyx mori* offers the potential to bridge the gaps in microneedle fabrication associated with other materials as it offers a suite of properties including mechanical strength, biocompatibility, tunable release, and simple processing conditions compared to metals, glasses, and polymers. While silk microneedle patches are an excellent platform for transdermal delivery of drugs and vaccines, there exist limitations with their use due to existing fabrication methods. In the present work, the investigation of device and fabrication process improvements to recapture some of the advantages of silk over other materials is reported. Through demonstration of conformable microneedle patches, successful influenza vaccination, and novel device formats, the broad utility of silk microneedles is demonstrated. This work provides evidence of the capability of the silk microneedle platform to be designed for drug or vaccine delivery, biosensing, and tissue engineering applications.

Acknowledgments

During the course of my undergraduate and graduate career at Tufts, I've learned a lot about myself and what makes me tick. To those that have been there along the way, to help me reflect and guide me when I've strayed from the path, I thank you. I appreciate the feedback I have received from everyone throughout this project, especially from my advisor, David Kaplan; professors, Fiorenzo Omenetto and Bruce Panilaitis; and my research mentor, Waseem Raja. I would also like to thank Professor Ayşe Asatekin for graciously joining my committee and providing another perspective on this work. I'd like to thank Stephen Tutunjian for his guidance early on in this process. I also appreciated the graduate community in the department, especially those members of my mini-groups with whom I was able to interact and provide feedback.

To my parents, Brian and Keiko, as well as Jim, Kendall, and Will, I appreciate the support throughout all of my time at Tufts. Through all of the highs and lows, the good times and the bad—I couldn't have done it without all of you. To my friends and housemates, who've helped encourage me to step out of my comfort zone and kept me excited about my research by providing context, I thank you. Finally, to all of the undergraduate students who I've had time to mentor and teach—Alex, Nat, Dan, Adam, and Scott—you guys have taught me a lot about how to not only manage my time, but to manage others' and I appreciate your patience throughout that learning process. A final thanks to everyone else in the department who contributed to my education and research experience, you've helped me become who I am today and I hope to make you all proud.

Table of Contents

Table of Contents (Continued)

Table of Contents (Continued)

Table of Contents (Continued)

List of Tables

List of Figures

List of Figures (Continued)

List of Figures (Continued)

EXPANDING THE UTILITY OF SILK FIBROIN MICRONEEDLES:

AN INVESTIGATION OF DEVICE AND FABRICATION PROCESS IMPROVEMENTS FOR TRANSDERMAL VACCINATION AND BROADER APPLICATIONS

1. Introduction

Developing nations face a significant public health challenge in the form of improving vaccination coverage. It was recently estimated that of 129 million children born in 72 different developing countries, only 66 percent received a hepatitis B vaccine, 29% received a type B influenza vaccine, 8% received a rotavirus vaccine, and 7% received a meningococcal vaccine [1]. Unfortunately, the access to vaccines in these nations is limited by financial costs and distribution logistics. The activity of vaccines and many antibiotics is extremely sensitive to temperature and demands refrigeration throughout the distribution and transportation processes [2]. These limitations have driven the development of vaccine and antibiotic delivery devices that are simple, cheap to manufacture, and thermostable. Transdermal devices, intended for delivery across the skin, meet some of these important criteria and are considered promising for vaccination. The skin has unique immunological properties, including the presence of dendritic cells, which process particles entering the skin and present these antigens directly to T cells [3]. Many new transdermal delivery devices strategically target and deliver therapeutic payloads to these dendritic cells in the skin to induce T-cell mediated responses [4]. One such transdermal vaccination approach is through the use of microneedle devices, which are patches with arrays of needles less than a millimeter tall. These devices offer the ability to stabilize vaccines in the solid phase and be self-administered, removing the barriers of cold storage distribution and access to a physician which can limit vaccine coverage in remote locations of the world. These devices also offer advantages over existing parenteral administration methods in developed nations by reducing the pain and

anxiety associated with hypodermic injections. With over 10% of the American population suffering from belonephobia—the fear of needles and sharp objects—any technique to deliver drug in a more convenient fashion without sacrificing efficacy is an improvement [5]. This could also lead to the benefit of improving patient compliance by improving patient comfort through a less-invasive delivery format.

While microneedle devices have been investigated extensively over the last two decades, no existing product has fully demonstrated all of the potential advantages of transdermal delivery. The devices that have gained FDA-approval are essentially hypodermic needles that have been miniaturized and do not offer delivery or *in situ* stability of solid phase therapeutics. The reason many of these devices have failed to progress to the envisioned use-case is due to the fabrication methods and materials used to create these microneedle patches. Many fabrication processes can reliably generate microneedle devices, but are limited in the materials amenable to the process. Other fabrication processes allow biocompatible polymeric materials to be used as microneedle substrates, but these materials fail to meet all of the criteria necessary to produce a platform device capable of delivering different types of therapeutics. Silk fibroin is an attractive material for these devices as it can stabilize bioactive species at elevated temperatures and has been demonstrated to have good mechanics in a microneedle format previously [6, 7, 8] (Figure 1).

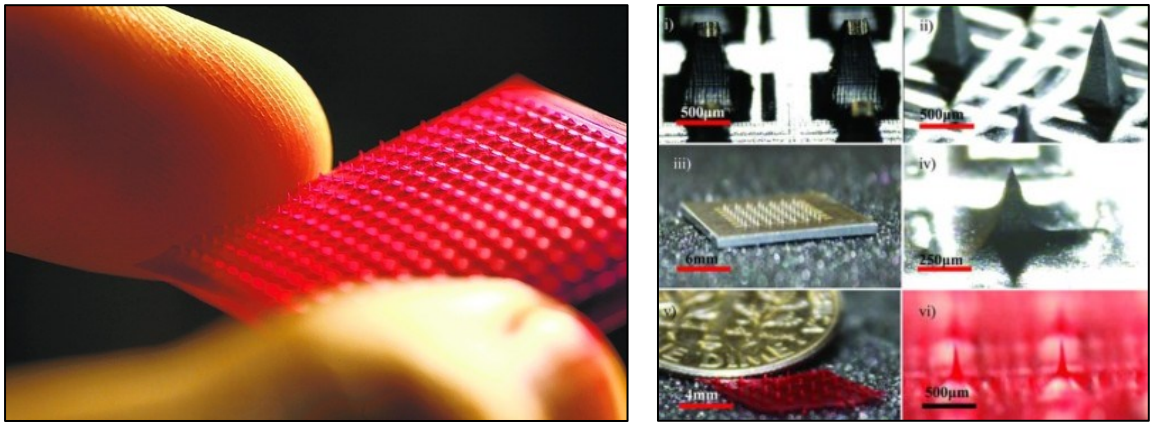

Figure 1. Silk fibroin microneedle devices, loaded with a red 120 dye for visualization. Microneedle devices have been previously investigated using silk fibroin, a biomaterial with excellent mechanical properties and biocompatibility. Challenges have been previously encountered with these devices, which this research aims to solve. This work will demonstrate the potential of these devices in the traditional application of transdermal drug or vaccine delivery as well as other applications. Borrowed from [7].

While these devices have been tested extensively *in vitro* and briefly *in vivo* with positive results, there remain challenges with silk microneedles that have prevented their acceptance as a leading microneedle platform candidate. In the present work, we report our efforts to improve the silk microneedle devices, demonstrating their potential as a platform for drug and vaccine delivery as well as other biomedical applications.

2. Background

2.1 Transdermal Drug Delivery

2.1.1 Introduction

The skin is the largest and most easily accessible organ in the human body, and has been used as a route of administration for thousands of years. Throughout history, humans have created substances for topical application to the skin to produce local therapeutic effects. In the 1960s, researchers began to study the barrier properties of the skin and how the stratum corneum—the outer layer of the epidermis—limits the permeability of drug compounds [9, 10]. However, it was soon demonstrated that some compounds had significant percutaneous diffusion and could produce systemic pharmacologic responses [11, 12, 13]. This finding led to the subsequent study of topical ointments and eventually to the development of adhesive transdermal delivery devices.

These transdermal patch devices offered improved control over dose, application area, and pharmacokinetics relative to previously developed topical ointments, creams, and gels [14]. These inherent advantages led the US Food and Drug Administration (FDA) to approve the first adhesive patch device in 1979 for the transdermal administration of scolopamine hydrobromide to prevent and treat motion sickness [15]. Since that time, many different drug products have been approved by the FDA and are currently available in transdermal patch delivery system formats (Table 1). As interest in the transdermal administration route has grown, the associated delivery devices have evolved and progressed from passive delivery vehicles (creams, ointments, patches) to more active methods that enable a broader range of compounds to be used.

Table 1. List of current FDA-approved drug products available in transdermal patch or transdermal delivery system formats. The first transdermal patch was approved by the FDA for scopolamine delivery in 1979; the list has since grown to 21 active compounds. [16]

Active Compound(s)	Product Name(s)	Indication	First Date of Approval
Buprenorphine	Butrans®	Analgesia	2010
Clonidine	Catapress TTS®	Hypertension	1984
Diclofenac Epolamine	Flector®	Acute pain due to minor sprain/strain	2007
17β-Estradiol	Alora®, Climara Esclim®, Estraderm FemPatch®, Menostar®, Minivelle®, Vivelle®, Vivelle-DOT®	Hormone replacement	1986
Estradiol/ Levonorgestrel	Climara Pro®	Menopausal symptoms	2003
Estradiol, Norethindrone Acetate	Combipatch®	Hormone replacement	1998
Ethinyl Estradiol/ Norelgestromin	Ortho Evra®, Xulane®	Contraception	2001
Fentanyl	Duragesic®	Analgesia	1990
Granisetron	Sancuso®	Prevention of chemotherapy-related nausea and vomiting	2008
Lidocaine	Lidoderm®	Post-herpatic neuralgia	1999
Lidocaine/ Tetracaine	Synera®	Local analgesia	2005
Menthol/ Methyl Salicylate	Salonpas®	Pain relief	2008
Methylphenidate	Daytrana®	Attention Deficit Hyperactivity Disorder (ADHD)	2006
Nicotine	Nicoderm®, Habitrol®, Prostep®	Smoking cessation	1991
Nitroglycerin	Transderm-Nitro®, Nitro-Dur®, Minitran®	Angina	1981
Oxybutynin	Oxytrol®	Overactive bladder	2003
Rivastigmine	Exelon®	Dementia associated with Alzheimer's Disease and Parkinson's Disease	2007
Rotigotine	Neupro®	Parkinson's Disease, Restless Legs Syndrome	2007
Scopolamine	Transderm Scop®	Motion sickness	1979
Selegiline	Emsam®	Major depressive disorder	2006
Testosterone	Androderm®, Testoderm®	Hypogonadism	1993

Within the last two decades the transdermal route has gained momentum in the research community, vying with oral administration as the most innovative area in drug delivery research and challenging the paradigm of hypodermic injections as well [17]. Relative to these routes of administration, transdermal delivery offers a less-invasive and painless approach while also avoiding the first-pass clearance mechanism of the gastrointestinal tract, which can limit the bioavailability of certain therapeutics [18]. Transdermal delivery also has the potential to reduce the amount of sharps waste that is generated from hypodermic injections. While this reduction of waste is important from a disposal standpoint, it has the added health benefit of lowering the risk of disease transmission through the re-use of needles, which is a serious problem in underdeveloped regions of the world [19]. Finally, most transdermal delivery devices can be self-administered and are relatively low-cost to produce, which should improve patient compliance and therapeutic outcomes [17].

2.1.2 Human skin function and anatomy

Before the progression of transdermal delivery devices can be addressed, the function and anatomy of human skin tissue must be discussed to provide context for drug diffusion, percutaneous vaccination, and device design. The skin is the primary organ in the human integumentary system and serves as the interface between the internal and external environments of the body. In such a position, the skin has the responsibility to maintain homeostasis, which refers to the stabilization of internal body conditions despite changing external conditions. This state is achieved through the many functions of the skin, including assisting with thermoregulation, helping retain water, functioning as a

sensory organ, and synthesizing vitamin D [20, 21, 22]. Most importantly though, human skin must function as a barrier, providing protection against physical, chemical, immune, pathogen, ultraviolet radiation, and free radical damage [23]. Unfortunately, this property hinders transdermal drug delivery as the skin inherently resists the passive diffusion of most therapeutic molecules.

The barrier function of the skin is largely due to its unique structure and composition, compared with other tissues. This organ is considered to be one of the most complex in the body as its structure manifests from five different cell types and also contains components from the immune and circulatory systems [23]. Human skin is composed of three major layers which are, progressing from superficial to deep: the epidermis, which is a thin layer of epithelium consisting of keratinocytes and melanocytes; the dermis, which is composed of collagen and fibroblasts; and the hypodermis, which is well-vascularized and consists of adipose and other connective tissue. (Figure 2). The epidermis originates from the ectoderm germ layer of the embryo during development, while the dermis and hypodermis originate from the mesoderm, leading to different cell types and functional roles in mature human skin [24].

The epidermis is generally 150–200 micrometers thick, depending on the location of measurement on the body. Keratinocytes are the main cell type (90-95%) in the epidermis; they are continuously dividing to serve as the protective layer of the skin. These cells start with cuboidal or columnar appearance in the basal layer of the epidermis (stratum basale) and undergo biochemical and morphological changes as they advance through the epidermal layers until they are shed from the skin after approximately 30 days [25]. In the stratum spinosum, keratin filament content in the cells increases as they

migrate towards the surface of the skin [23]. These keratinocytes begin to flatten in the stratum granulosum, where the synthesis of filaggrin matrix protein aggregates the keratin filaments into bundles which allow the cell to collapse [26, 27]. The presence of the stratum lucidum is observed in thick regions of the skin, such as the palms of the hands or the soles of the feet. The outermost layer of the epidermis, the stratum corneum, is only 10–20 micrometers thick but provides a majority of the skin barrier function due

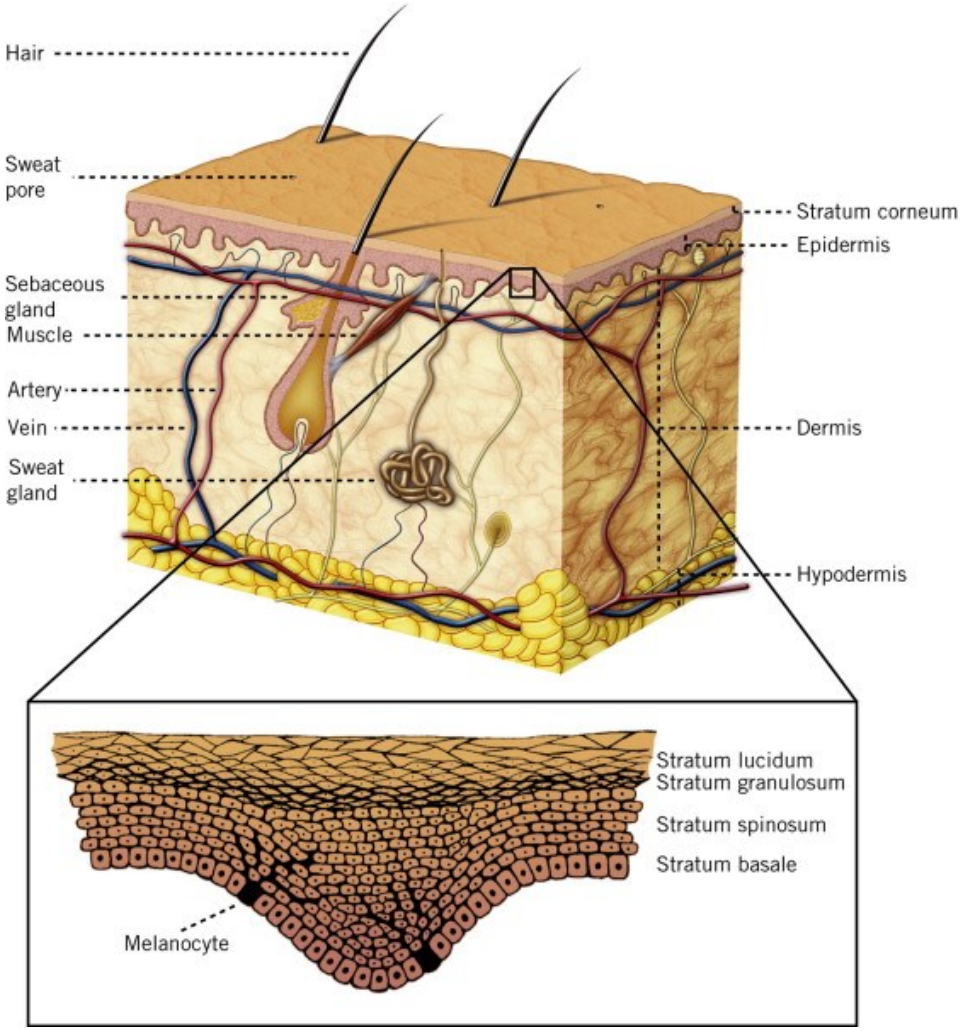

Figure 2. Illustration of the major layers of the human skin, including the epidermis, dermis, and hypodermis. Each layer has different functions that contribute to the overall role of the organ. The presence of immune, nervous, and circulatory components make the skin one of the most complex organs in the body. Diagram borrowed from [28].

to its “brick and mortar” structure. This structure includes corneocytes (terminally differentiated keratinocytes) that have a lipid envelope of omega-hydroxyceramides, allowing the cells to tightly pack and interdigitate the lipid secretions from lamellar bodies [29]. The lipid “mortar” forms regions of semi-crystalline, gel, and liquid crystal domains that prevent intracellular diffusion of molecules through the stratum corneum [30]. The other 5-10% of cells in the epidermis includes melanocytes, which are cells that produce the skin pigment melanin, and Langerhans cells, which are antigen presenting cells involved in the adaptive immune response of the human body [25].

The dermal and hypodermal layers impart strength and flexibility to the skin while supporting the exterior epidermis. This dermis is thick and contains many nerve endings to collect sensory information about pain, temperature, and pressure. Sweat glands, hair follicles, and blood vessels are all present in the dermis as well. Fibroblasts are the main cell type in this tissue layer, which produce collagen fibers (primarily type I and type III in the dermis) that are responsible for the mechanical strength of the skin and account for 98% of the mass of dried dermis [25]. A small amount of elastin is also present in the dermal layer of the skin. There is also a greater immune presence in the dermis than in the epidermis, with two types of dermal dendrocytes present as well as mast cells [31]. These cells provide an excellent target for transdermal vaccine delivery devices. Below the dermis is a layer of fatty tissue, which provides nutritional storage for the rest of the skin, aids thermoregulation through insulation, and also protects the body from injury. Adipocytes, or fat cells, are the major cell type in the hypodermis. The vasculature present in the hypodermis innervates and provides nutrients to the more superficial layers of the skin.

2.1.3 Transdermal delivery approaches and devices

There are many benefits to the transdermal delivery route compared with other traditional routes of administration, including reduced pain, avoidance of first-pass hepatic clearance (increased bioavailability), minimal biohazard/sharps waste generation, and simplicity through self-administration [17, 18, 19]. To exploit these advantages, researchers have developed a variety of drug formulations and devices amenable to the transdermal route of administration. As mentioned, the first modern approach to transdermal drug delivery leveraged passive diffusion across human skin to generate a therapeutic response. Gels, creams, and ointments were developed for topical application to the skin, while adhesive patches were the first transdermal delivery devices. Although these transdermal delivery patches were successful in the non-invasive delivery of therapeutics and still exist today, the passive diffusion approach is severely limited in scope due to the nature of the skin barrier. Research of the specific structure and composition of human skin led to a better understanding of its protective function and how inherently limiting this barrier is to most drug compounds. The skin is very hydrophobic due to the high lipid content in the stratum corneum that binds the dead keratinocytes together. Only drug molecules that have low molecular masses (below a few hundred Daltons), are highly lipophilic, and are efficacious at very low doses are amenable to diffusion-based transdermal delivery [17]. The delivery of hydrophilic compounds, peptides, and DNA/small-interfering RNA has been challenging to date using this passive approach [32]. Therefore, the next generation of transdermal delivery devices sought to increase the permeability of the skin in order to expand the range of therapeutics that could be delivered across the skin.

While enhancing the transport of drug molecules across the skin is an important objective, it was recognized that this improvement could not come at the expense of harm to underlying tissues or extended disruption of the integrity of the skin barrier. There are a variety of different transport enhancement methods that balance improved permeability with temporary disruption or damage to the skin barrier. These techniques include chemical/biochemical enhancers, iontophoresis, electroporation, noncavitational/ cavitational ultrasound, thermal ablation, and microneedles [17]. Many chemical penetration enhancers work by fluidizing the lipid bilayers in the "mortar" of the stratum corneum, partitioning the membrane and allowing hydrophilic drugs to diffuse intracellularly [33]. Liposomes and dendrimers are interesting chemical enhancers as they not only improve partitioning of drug molecule into the skin, but also improve drug solubility in the formulation [34]. Iontophoresis uses an electrical current to help drive charged drug molecules into the skin, while electroporation uses short voltage pulses to create pores for drug diffusion [35, 36]. Noncavitational ultrasound uses pressure waves to disturb the packing of corneocytes and lipids in the skin barrier, improving delivery of drugs transdermally [37]. Alternatively, cavitational ultrasound can produce small bubbles in the hydrogel placed over the surface of the skin. When these bubbles collapse larger drug molecules loaded in the hydrogel are jet into the skin by the shock wave [38]. Thermal ablation causes perforations in the stratum corneum by rapidly heating the skin surface for millisecond durations [39]. Microneedles offer the most straightforward way to deliver therapeutic molecules across the stratum corneum and into the dermis [17]. There are advantages and disadvantages to each of these methods, but the simplicity of microneedles make them very promising transdermal delivery devices.

2.2 Microneedle Devices

2.2.1 Motivation for development

When researchers are developing a new drug product and its associated dosing regimen, pharmacokinetics and pharmacodynamics are two of the most important parameters that must be considered. Safety and stability aside, a drug product must be designed and well-characterized in terms of what the body does to the drug (pharmacokinetics) and what the drug does to the body (pharmacodynamics) in order to be successful. The traditional drug delivery paradigm requires a drug product to enter the body through a particular route of administration (e.g. parenteral injection [intramuscular, subcutaneous, or intravenous] or oral pill), move into the bloodstream, and then be distributed throughout the body. Once the drug has been distributed, it must reach a concentration necessary to elicit the therapeutic response. Research over the last few decades has focused on improving both the upstream drug delivery and downstream drug action processes of this paradigm [14, 40, 41, 42]. However as drug products have become more potent, specific, and complex, some protein- and nucleic-acid-based therapeutics are no longer compatible with standard delivery formats [42, 43]. Degradation of the drug product in the gastrointestinal tract (strongly acidic pH environment) and clearance through the hepatic first-pass mechanism may prevent formulation of these high molecular weight therapeutics into an oral pill [14, 44, 45]. The therapeutic may not be amenable to a liquid formulation either, eliminating injection as a route of administration—which is also inconvenient and can be painful for the patient [44, 46].

As mentioned, the transdermal route of administration overcomes many of the limitations associated with gastrointestinal delivery or parenteral injection and has become one of the most innovative areas of drug delivery research [17]. The primary advantage of this delivery route is its simplicity: the skin is the most accessible organ and delivery can be as easy as placing a drug product on the epidermis. In most cases however, this concept is more nuanced and requires engineering to help deliver therapeutics that cannot easily diffuse across the skin barrier. Of the proposed methods to improve transdermal delivery of a broader range of therapeutics, microneedles represent the most straightforward approach. The concept of shrinking down the hypodermic needle into an array of sub-millimeter-scale solid needles was first presented in 1998 and has blossomed into a significant subset of current transdermal delivery research [43]. Microneedle devices were originally produced from silicon as the fabrication methods were adapted from microfabrication techniques used in the microelectronics industry (Figure 3) [43]. Since that time, new fabrication methods have been developed which permit the use of other types of materials, including metals, glass, polymers, and natural biomaterials, expanding the scope and applicability of these devices.

(A) (B)

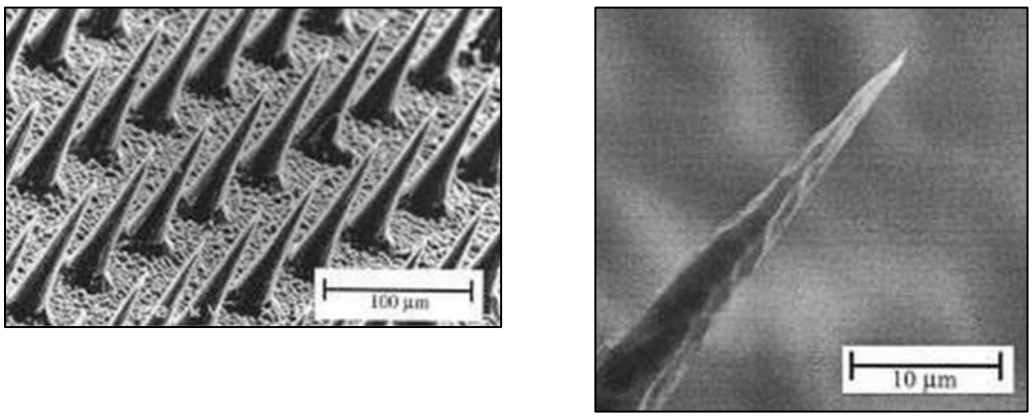

Figure 3. SEM images of the first microneedle array device. Microfabrication processes used in the microelectronics industry were adapted to produce the first microneedle devices, limiting the material selection to silicon but allowing the creation of very fine tips. Since 1998, new fabrication methods have been developed that enable the use of alternative materials that expand the scope of the devices and their commercial viability. Image borrowed from [43].

Microneedle devices offer many significant advantages over other routes of administration that have made them extremely attractive transdermal delivery devices. The devices are designed to be pain-free compared to hypodermic needles, as they are small enough to reduce stimulation of intradermal nerves and therefore the pain sensation [47, 48, 49]. The devices do not necessarily require a trained medical professional to administer a dose of drug or vaccine and there is reduced risk of needle-stick injury or the transmission of pathogens due to needle re-use [48, 50, 51]. Most importantly, the device designs can be modified to permit formulation with macromolecules, nucleic-acid-based therapeutics, and biologics which can be diffusion-limited with other transdermal devices [48, 52]. Microneedle devices are appealing to both patients and clinicians as they are a relatable and straightforward transdermal delivery approach.

2.2.2 Device categories and design considerations

While microneedle devices are simple in concept and application, their designs have evolved to become much more complex and feature various mechanisms for drug delivery. These devices can be broadly categorized into four groups based on their design and degree of delivery functionality. These categories are: (1) solid microneedles to permeabilize the skin for subsequent topical drug application, (2) solid microneedles prepared with dry drug or vaccine coating for dissolution inside the dermis, (3) degradable polymer/biomaterial microneedles with bulk-loaded drug or vaccine for controlled or rapid bolus release, and (4) hollow microneedles for liquid intradermal injections (Figure 4) [47, 52, 53, 54].

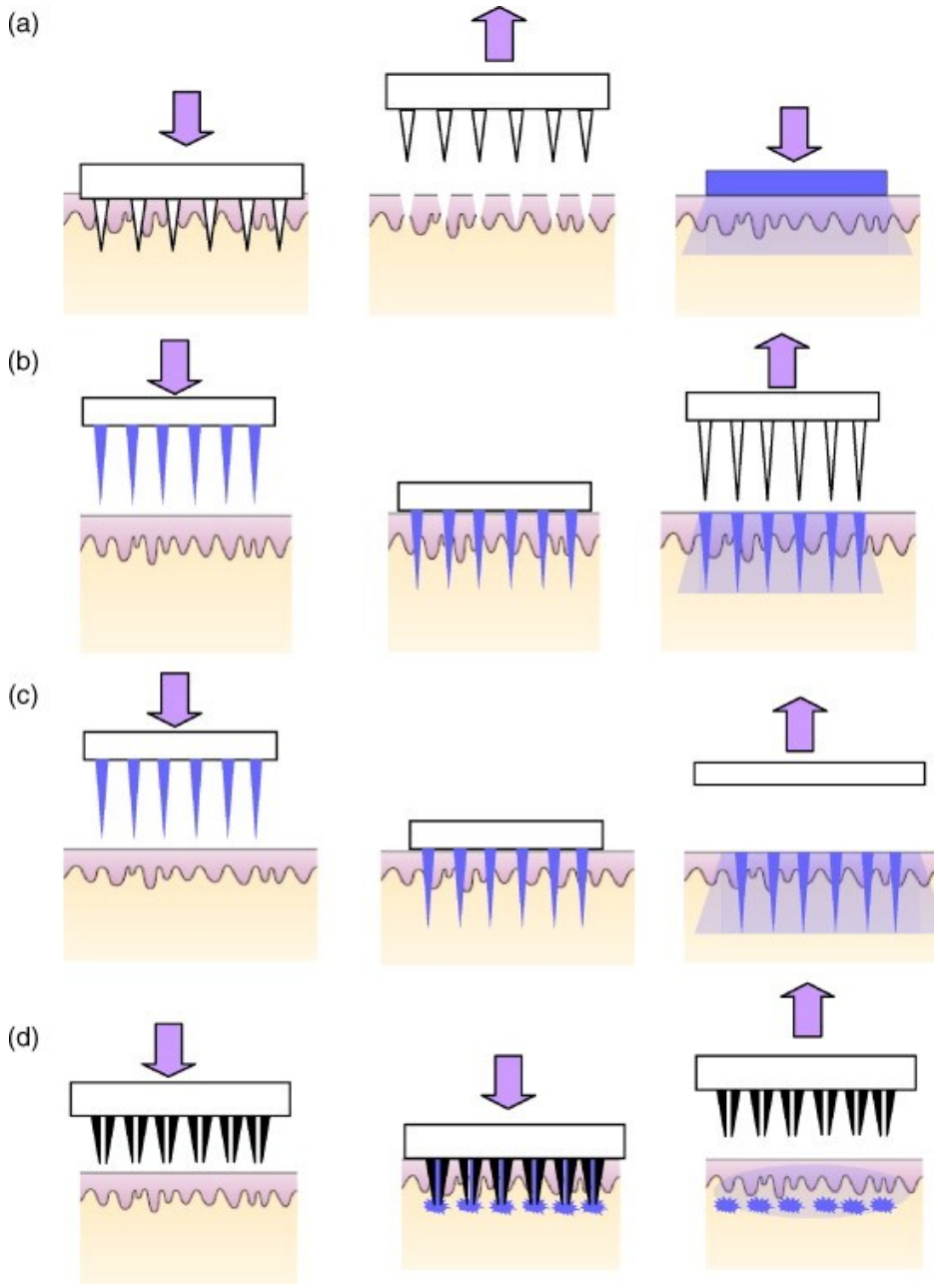

Figure 4. Microneedle device delivery method categories. There are four major categories by which microneedles deliver therapeutics transdermally, including: (a) solid for permeabilization of the skin and subsequent topical administration—"poke and patch"; (b) solid coated microneedles—"coat and poke"; (c) degradable polymer/biomaterial microneedles loaded with therapeutic—"poke and release"; and (d) hollow microneedles for liquid formulation—"poke and flow". Figure borrowed from [52].

The first microneedle patch devices investigated were used to create micropores in the stratum corneum to aid passive diffusion of topical drug products. The pores are produced by either pressing the patch onto the skin or scraping it along the stratum corneum. With this initial microneedle design, researchers demonstrated increases of model drug permeability by a single order of magnitude for insulin and bovine serum albumin (BSA) [55], three orders of magnitude for plasmid DNA [56], and four orders of magnitude for calcein [54]. Through this microneedle approach, the integrity of the skin barrier is only compromised for a two hour period while the micropores remain open in the stratum corneum [52].

Coated microneedles are designed to carry a water-soluble drug formulation into the skin, which rapidly dissolves once the needles have penetrated the tissue [57]. By placing the drug onto the surface of the needle, the subsequent topical drug application step is eliminated thereby simplifying the transdermal delivery process. These devices also offer more rapid delivery of macromolecular drugs relative to topical formulations and the potential for longer-term stability due to solid-phase storage of the therapeutic on the microneedles [50]. As an example of this solid-phase stability, over 98% of desmopressin coated onto microneedles was retained after storage for 6 months at room temperature [57]. Influenza vaccine is another target that has been investigated for storage stability on microneedle devices [58, 59]. While this category of microneedle devices can be used to rapidly deliver drugs or vaccines into the skin, the total delivered dose is limited to the amount that can cover the surface area of the needles themselves, which typically amounts to a dose of less than one milligram [50].

To increase the maximum transdermal delivery dose, researchers developed the third class of microneedles: degradable polymer or biomaterial needles. These devices are fabricated from water-soluble or biodegradable materials which are formulated to contain the drug or vaccine in their bulk. When inserted into the skin, these needles can rapidly dissolve and release a larger bolus dose or be engineered to degrade slowly and release the therapeutic in a much more controlled manner [60, 61]. Many of these biodegradable polymers, such as polylactic acid (PLA), polyglycolic acid (PGA), and polylactic-co-glycolic acid (PLGA), are known to be biocompatible, strong and elastic, and amenable to low-cost soft lithography fabrication techniques enabling the production of cheap and safe devices [62, 63]. The primary drawback to this category of devices is the duration of administration: some patches must be left on for at least five minutes to allow degradation of the polymer or detachment of the needles from the patch [54]. Other microneedle designs, such as arrowhead polymer needles, have recently emerged to overcome this limitation [60, 64].

Hollow microneedles are the final class of these devices and enable liquid formulations of drug or vaccine to be delivered into the skin. This approach is amenable to any drug or vaccine already existing in liquid format with no limitation to delivered dose. In addition, hollow microneedles have broader functionality; they can be used for interstitial fluid/capillary blood extraction for biosensing or diagnostic applications [65]. This minimally-invasive approach for blood extraction and biochemical analysis has been investigated and adapted into commercial products such as Seventh Sense Biosystems' Touch-Activated-Phlebotomy™ platform. For drug delivery applications however, this microneedle device category sacrifices the benefit of patient convenience as patients must

visit a clinic to have the dose measured and administered by a physician [54]. Overall, when designing a microneedle system there are many options available that have been developed to be compatible with different types and doses of therapeutics.

2.2.3 Fabrication methods, associated materials, limitations

In 1998 research on microneedle arrays began exploring the use of fabrication processes borrowed from the microelectronics industry to produce these transdermal delivery patches. These initial attempts were quite successful in producing sub-millimeter-scale needles from a silicon wafer and demonstrated the medical potential for these transdermal delivery devices [43]. Since this time, microneedle research has grown significantly with efforts from both academia and industry. Patches have developed from solid needles to permeabilize the stratum corneum ("poke and patch" approach) to coated microneedles ("coat and poke") to degradable needles ("poke and release"), becoming more advanced in their geometries and mechanisms of action [48, 51]. As these devices have expanded in the scope and complexity of their designs, the associated fabrication methods have been adapted to permit a broader range of materials and to enable additional needle geometries (Figure 5). There are three primary categories of fabrication techniques used to create microneedles: (1) photolithography, (2) replica molding, and (3) micromachining [48]. These general fabrication categories will be outlined to provide an overview of the capabilities and limitations of each technique, which must be considered when designing a microneedle delivery system.

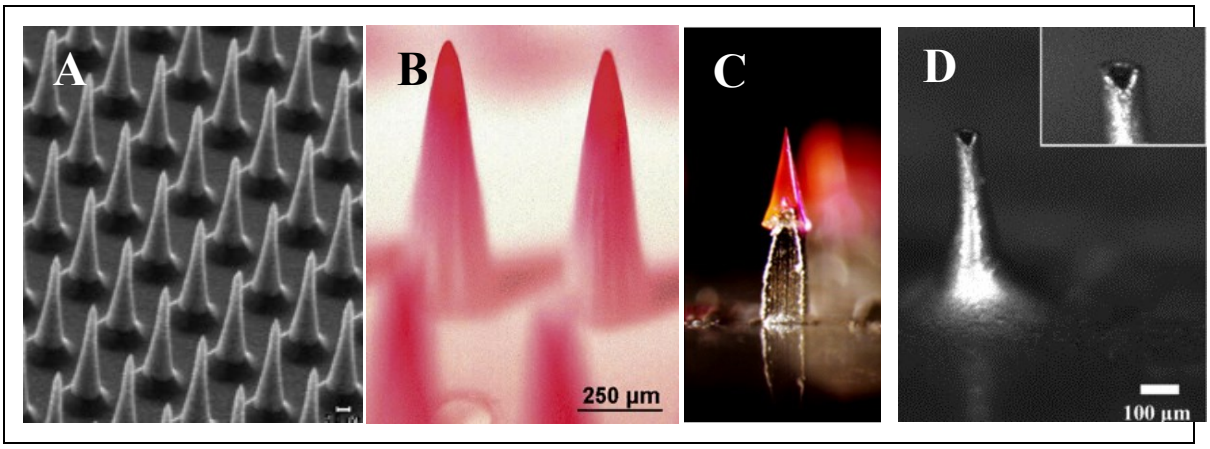

Figure 5. Evolution of microneedle design and material selection. Over the past 17 years, microneedle array devices have grown more complex in design and mechanism of action, with new fabrication techniques enabling the use of a variety of materials. Examples of the hundreds of devices in literature, include: (A) an array of 25-um silicon microneedles fabricated through lithographic and etching techniques [46]; (B) an array of rapidly dissolving polyvinylpyrrolidone (PVP) microneedles fabricated through ultraviolet polymerization [66]; (C) an arrowhead microneedle designed for detachment of the tip in the skin and subsequent dissolution of the polymer [64]; and (D) a hollow microneedle formed through electrodeposition of nickel metal onto a polymer mold, followed by sacrifice of the polymer mold [67].

Fabrication techniques from the microelectronics industry provided the first conduit for solid microneedle production. These processes, including photolithography and deep reactive ion etching, had been developed for the mass production of microscale integrated circuits and were quickly found to be suitable for the fabrication of microneedle devices [43]. Silicon wafers are used as the device substrate in this approach to create microneedles. The wafer is patterned through photolithography, which uses electromagnetic radiation in the visible, UV, or X-ray regions to transfer 2-D shapes from a photomask onto a separate photoresist layer. This photoresist layer is then developed through a subsequent chemical exposure step. Wet etching using additional chemical solutions or dry etching (such as deep reactive ion etching) using gas plasmas can remove remaining photoresist as well as exposed silicon in the wafer. These fabrication

techniques offer the benefit of very sharp microneedles with smaller tip radii than polymeric or metal devices [68]. This approach is highly-reproducible and also scalable as the technology is used in microelectronics fabrication [43,69].

The microelectronics fabrication approach also offers the ability to include biosensing and interfacing capabilities as well as micropumping action not achievable through alternative microneedle production techniques [43, 68, 70, 71]. For this reason, this category of fabrication has led to the development of in-plane microneedles to complement standard out-of-plane microneedles. These in-plane microneedles can be more easily created with microfluidic geometries to handle biospecimens such as blood or interstitial fluid extracted from the dermis [72]. These hollow devices have the flexibility to handle both drug delivery and lab-on-a-chip responsibilities, making them an important class of microneedle devices [73]. There are limitations with silicon microneedle devices: the material is fragile and the needles can easily break and remain in the skin during the administration of the device [52, 62, 68]. The material is not biocompatible and can elicit an immune response from the body, especially at the needle tips [74, 75]. The final device must also be treated as biohazard sharps waste, creating a logistical disposal challenge after administration of the microneedle patch.

From a practical standpoint, the microfabrication methods are cost and time intensive, requiring sophisticated equipment, materials, and a cleanroom environment [68]. These devices are limited in the maximum dose they can deliver, as they can only be coated with the therapeutic or vaccine. The material selection for the devices is also limited to those compatible with the suite of cleanroom microfabrication processes: silicon in the wafer and non-degradable photocurable polymers (photoresists) such as

SU-8 epoxy or polymethyl-methacrylate (PMMA) [54, 55, 68, 76, 77, 78]. While there are limitations to the microneedle devices produced through this approach, the suite of cleanroom-based microfabrication techniques provide excellent control over the geometries of the needle projections. For this reason, this approach is often used to create a master positive mold that is subsequently used in other fabrication techniques to create microneedle devices. These alternative fabrication methods allow the devices to be fabricated from a range of other materials, including ceramics and polymers [54].

Replica molding is a fabrication technique that falls under the category of soft lithography, which refers to the methods that use elastomeric molds and stamps to transfer patterns and structures to castable materials [79]. This molding technique allows the features from a master positive mold to be replicated in a different material, such as biodegradable polymers or ceramics, by using an intermediate negative mold. The negative molds are typically created from polydimethylsiloxane, an elastomer that can be cast around the master features and retain the relief pattern following curing and lift-off. Similar negative molds have also been produced from poly vinyl alcohol (PVA) to create PMMA microneedle devices [80]. This fabrication approach is a low-cost and time-efficient (i.e. single step) alternative to cleanroom processing that can also be easily expanded in production scale [53, 62]. Another significant benefit of replica molding is that it enables the use of polymers with well-established safety profiles that also have the viscoelasticity to avoid shear-induced breaking when inserted into the skin [49, 81]. A list of materials, as well as some of the advantages and disadvantages associated with these materials, is provided below to demonstrate the amenability of the replica molding fabrication approach to a broad range of substrates (Table 2).

Table 2. Comparison of materials used in replica molding fabrication of microneedles. These materials have good biocompatibility and most are designed to degrade inside the skin. The limitations to using many of these materials include high processing temperatures, UV light for crosslinking, or susceptibility to ambient humidity levels.

Cast Material	Fabrication	Advantages	Disadvantages	Sources
Polylactic acid (PLA); Polyglycolic acid (PGA); Polylactic-co-glycolic acid (PLGA)	Melt polymer casting	- Controlled degradation into biocompatible products - Demonstrated mechanical strength to pierce skin	- High curing temperature (150°C) is required	[60, 62, 77, 82, 83, 84]
Polycarbonate (PC)	Hot embossing	- Biocompatible - Excellent mechanics for skin penetration	- Embossing technique exposes therapeutics to high temperature, pressure - Coating with therapeutic only, limitation to dose	[85, 86, 87]
Polymethylmethacrylate (PMMA)	Hot embossing	- Biocompatible - Good mechanics and material strength	- Embossing technique exposes therapeutics to high temperature, pressure	[80, 88, 89]
Polyvinylpyrrolidone (PVP)	Melt polymer casting and photo-polymerization	- Biocompatible - Highly water soluble - Mechanically strong	- UV exposure for 30 minutes necessary to induce cross-linking of PVP - High encapsulated dose needed to elicit same immune response as IM injection	[61, 66]
Maleic anhydride/ methylvinyl ether co-polymer (Gantrez AN®)	Solvent casting and evaporation	- Good mechanics and skin penetration demonstrated - Non-toxic material - Room temperature processing	- Incorporation of drug caused softening of needle structures - Limited drug loading concentration (1% w/w)	[90]
Polyvinylalcohol (PVA)	Solvent casting and evaporation	- Create separable device (needle from backing) with this material - Biocompatible - Water soluble material	- High temperature (60°C for 2 hours) for material preparation and drug encapsulation	[64, 91]
Polyoxymethylene (POM)	Injection molding	- Scalable process - Good mechanics and insertion into pig skin demonstrated	- Exposure to high temperature - Coated devices only or hollow devices for liquid formulation injection	[92]
Carboxymethylcellulose (CMC) with Amylopectin	Solvent casting and evaporation	- Biocompatible, rapid degradation - Thermal stabilization of lysosome reported - Bolus or sustained release possible	- Increased temperature needed during processing to concentration CMC for adequate mechanics (70°C) - Incomplete insertion of needle shafts due to weaker mechanics	[93, 94]
Chondroitin sulfate	Solvent casting and evaporation	- Water soluble and biocompatible - Bulk loading and bolus release	- Poor demonstrated bioavailability (potentially due to poor mechanics)	[95, 96]
Chitosan	Solvent casting and evaporation	- Biodegradable material with non-cytotoxic products - Immune stimulating material	- Oven drying needed (37°)	[97, 98]
Hyaluronic acid	Solvent casting and evaporation	- Natural biological material, water soluble disaccharide polymer (FDA approved) - Demonstrated mechanics for penetration	- Susceptible to degradation in high relative humidity environments	[99, 100]
Maltose	Melt polymer casting	- Sufficient strength to penetrate stratum corneum - Safe material for drug delivery systems	- Humidity can cause degradation of needle structures - High temperature needed to melt material and formulate with drug (140°C)	[100, 101, 102]
Galactose	Melt polymer casting	- Sufficient mechanical strength - Biocompatible, safe material	- Spontaneous dissolution at high relative humidity - High processing temperature (160°C)	[100]

The replica molding fabrication approach enables the use of a broad range of materials with better biocompatibility and controlled release properties than those encountered with microfabrication. This molding process requires a master positive mold to create devices out of the desired material but this master mold does not necessarily need to be fabricated through cleanroom processes. Micromachining of either the bulk substrate or the surface of a material, laser ablation, or two-photon polymerization can be used to generate a master mold from which replica devices can be produced [81]. These fabrication approaches also enable the direct use of other materials, removing the molding steps from the process. Metals, such as titanium, palladium, or nickel, can be directly machined to make solid microneedle structures instead of the typical electroplating techniques used to make hollow devices from these materials [103, 104]. Laser ablation can also be used to fabricate solid metallic microneedles [105]. Ceramic materials possess excellent mechanical properties for transdermal drug delivery and are low-cost, offering advantages over more expensive biocompatible metals and cleanroom materials. Ceramic-polymer hybrid microneedles have been fabricated through two-photon polymerization in a scalable process and have been demonstrated to have no significant cytotoxic effects [106].

Thermal drawing is one specialized fabrication technique that does not fall under the categories of microfabrication, replica molding, or micromachining. This technique enables the fabrication of microneedles from glass as well as dextrin [95, 107, 108]. Glass microneedles are prepared by using a thermal micropipette puller with borosilicate glass and then melting the needle tip shut with a Bunsen burner to increase strength and smoothness [107]. These needles are only suitable for delivery of liquid formulations or

for interstitial fluid/blood extraction for diagnostic applications as the needles are hollow. As dextrin is another polysaccharide material, it suffers from the same susceptibility to humidity-induced degradation reported for galactose and maltose [100]. However, dextrin can be dissolved in solution without elevated temperature to form a glue-like paste allowing reduced loss of incorporated drug or vaccine activity. Drying of these devices is performed in a desiccator without the addition of increased temperature [95, 108]. Overall, there are a variety of methods that have been developed to permit microneedle fabrication with a broad range of materials enabling control over mechanics, drug release kinetics, and stability. This has allowed these devices to be studied extensively both *in vitro* and *in vivo*, with a multitude of drug and vaccine cargoes.

2.2.4 Transdermal microneedle drug and vaccine delivery

Over the 17 years since the first microneedle patch device was reported, researchers have used microneedle devices to transdermally deliver a broad range of therapeutics both *in vitro* and *in vivo* to demonstrate proof of principle. Each engineering innovation made concerning the design and fabrication side of these devices enabled the use of an expanding list of drug and vaccine products. Initially, these devices were used to deliver fluorescent payloads (calcein and BSA) with little clinical relevance to simply demonstrate their ability to penetrate the skin and release their payload [43]. Since that time, these devices have been studied for the delivery of small molecule therapeutics, including: nicarpidine hydrochloride [109], sumatriptan [110], theophylline [90, 111], naltrexone [112], alendronate [113], pilocarpine [114], and diclofenac [70]; and biopharmaceuticals including: insulin [107, 108, 115, 116], erythropoietin [95], heparin

[117, 118], human growth hormone [119, 120], parathyroid hormone [121], desmopressin [57], lysozyme [93], leuprolide acetate [96], siRNA [122, 123], and DNA/plasmid-DNA [124, 125].

Using microneedles for vaccination is the ultimate objective as this application leverages all of the major benefits of a minimally-invasive transdermal delivery device. The microneedle devices enable vaccine antigens to be delivered in close proximity to the immunogenicity cellular component of the skin, eliciting comparable responses to intramuscular injections in some cases [59, 61, 126]. The devices can reduce biohazardous sharps waste generation in the dissolving needle format and offer the potential to ease global distribution through temperature stabilization in the solid phase [19, 81]. Most importantly, the devices are simple enough to be self-administered which could remove a significant global public health barrier to vaccination. Vaccines are not amenable to the oral administration route and transdermal delivery offers an exciting alternative to the traditional hypodermic injection. Many vaccine targets have been investigated in coordination with microneedle devices--whether through the "poke and patch", "coat and poke", "poke and release", or "poke and flow" delivery approaches. A list of the vaccine antigens that have been examined for immunogenicity *in vivo* has been compiled to demonstrate the broad flexibility of this platform for a number of diseases (Table 3). It can be observed that these devices could be used as seasonal vaccination devices for influenza or as dose-sparing devices for lifetime protection against measles. For these reasons, microneedle devices have great potential in the vaccination space and represent a major shift towards a more patient-friendly and accessible means of drug and vaccine delivery.

Table 3. List of vaccine targets studied *in vivo* with microneedle delivery. A list of animal models has been provided to show the progression with certain antigens from basic rodent models to more advanced animals and non-human primates.

Target Disease/Antigen	Studied *in vivo* Animal Model	Sources
Influenza	Mouse (BALB/c, C57BL/6) Guinea pig (IAF HR/HR Hartley)	[58, 59, 126, 127, 128]
Tetanus	Rat (Hairless)	[126]
Diphtheria	Rat (Hairless)	[126]
Malaria	Mouse (BALB/c)	[126]
Anthrax	Rabbit (New Zealand White)	[129]
Measles	Rat (Female 6-week-old Cotton) Rhesus macaque (Female 2-year old *Macaca mulatta*)	[130, 131]
Hepatitis B Antigen	Pig (3-4 week old Land Race Cross)	[132]
Human Papillomavirus (HPV)	Mouse (C57BL/6)	[133]
West Nile Virus	Mouse (BALB/c)	[134]
Chikungunya Virus	Mouse (BALB/c)	[134]
Bacillus Calmette-Guerin (BCG) for Tuberculosis	Guinea pig (Female Hartley)	[135]
Inactivated Polio Virus (IPV)	Rat (Female Wistar Han) Rhesus macaque (Female 2-year old *Macaca mulatta*)	[136, 137]

2.3 Silk Protein Microneedles

2.3.1 Silk fibroin biomaterial

With ancient roots in the textile industry, silk fibroin protein has become an exciting biomaterial due to its outstanding properties. Silk proteins are produced from the specialized glands of Lepidoptera larvae, such as the silkworm *Bombyx mori* and the spiders *Nephila clavipes* and *Araneus diadematus*, and spun into fibers that are used for various structural functions, including forming a protective cocoon capsule, building a nest or web to capture prey, and supporting the organism as a dragline [138, 139, 140]. There is inherent variability in the composition and properties of the silk proteins produced for these various uses by different species. However, silk fibers from the silkworm *Bombyx mori* have been especially well characterized due to their use for centuries as a medical suture material.

Silk fibers produced from domesticated *Bombyx mori* silkworms consist of two major protein components: a center, structural core of silk fibroin and an outer, glue-like coating of hydrophilic sericin protein [138, 139]. The silk sericin coating (20-310 kDa) helps hold the fibers in the cocoon together, but is removed from the fibroin protein before use as it has been demonstrated to cause an immune hypersensitivity response [141, 142]. The purification of silk fibroin from raw cocoons is accomplished through the boiling of the material in an alkaline solution, removing the sericin which accounts for 25-30 percent of the total mass [143]. The remaining silk fibroin fibers consist of two distinct proteins: a light chain (~25 kDa) and heavy chain (~390 kDa) which exist in an equal 1:1 ratio [144]. These chains are linked by a cysteine-cysteine disulfide bond between the 172nd-residue in the light chain and the 20th-residue from the carboxyl

terminus of the heavy chain [145]. A third component, the P25 glycoprotein, is also found in the silk fibroin fibers and associates with the two fibroin chains through hydrophobic interactions [145].

Many fibrous proteins, such as collagen, are characterized by their highly repetitive amino acid sequences. Silk fibroin is not unique in this repetitive nature and largely consists of G-X blocks (94% of total primary sequence), where G refers to the amino acid glycine (45.9% of total residues) and X is alanine (64% of G-X repeats), serine (22%), tyrosine (10%), valine (3%), or threonine (1.3%) [146]. In the fibroin heavy chain, these G-X blocks form twelve crystalline domains that are linked by amorphous sequences containing charged residues; these domains can each adopt parallel or anti-parallel β-sheet structure [146]. Through van der Waals forces between the stacked β-sheets in the crystalline domains and through hydrogen bonding within and between β-sheets, silk fibroin protein is extremely stable and has excellent mechanical properties [147]. The mechanical features of silk, coupled with all-aqueous processing and biocompatibility have led to the extended study of the material in solution, sponge, film, powder, hydrogel/aerogel, and electrospun-tube formats [148, 149, 150, 151] (Figure 5). The ability of silk protein to be fabricated into different presentations has enabled the engineering of three-dimensional silk scaffolds for a range of target tissues, including: bone, cartilage, fat, intestine, and brain [152, 153, 154, 155, 156]. In addition to tissue engineering, silk fibroin has also shown great promise in the field of drug delivery.

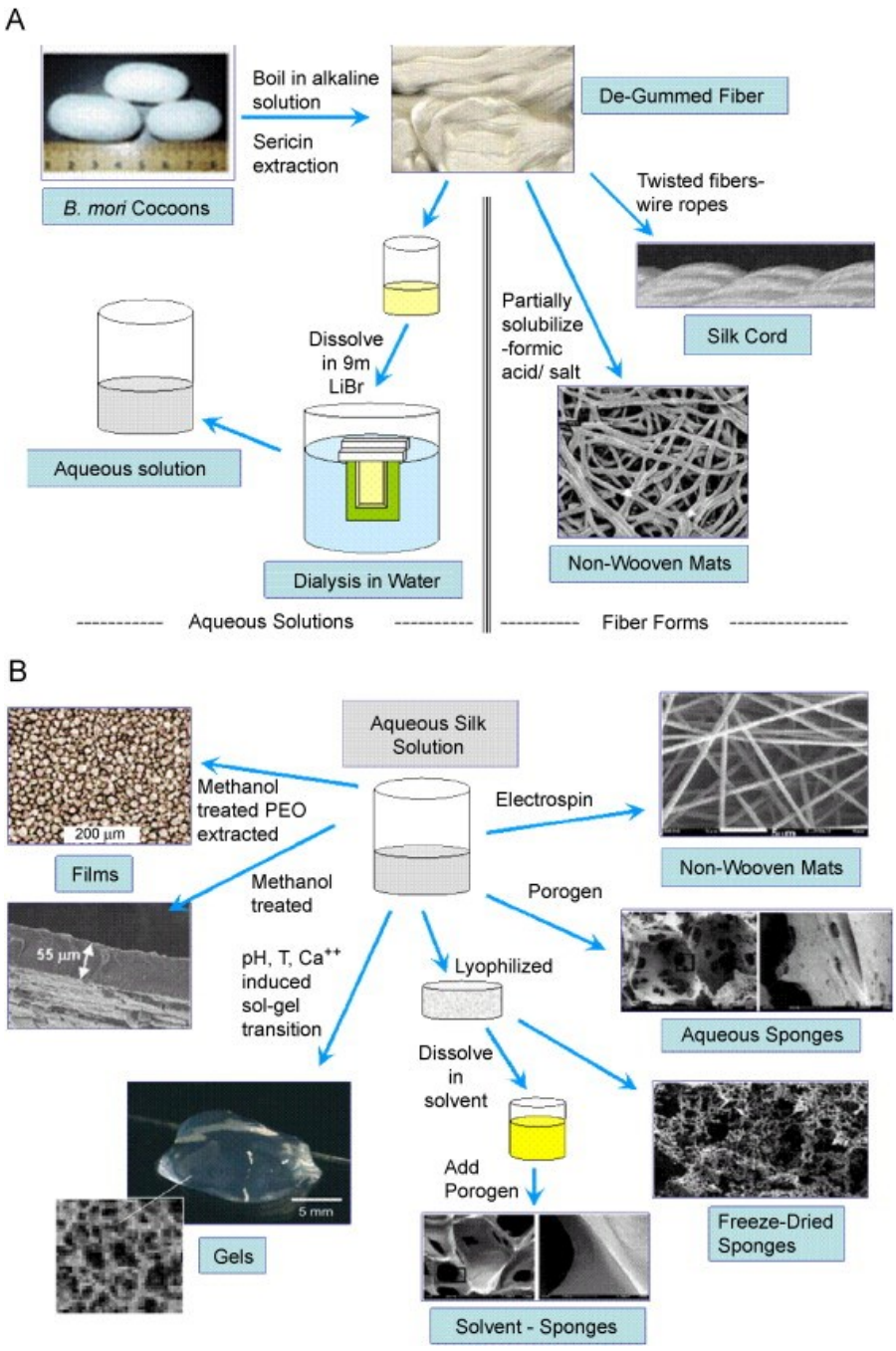

Figure 6. Silk fibroin can be processed under benign conditions into a variety of material formats. (A) All-aqueous processing removes the sericin protein from the silk fibers which can be used in solid form or can be returned to the liquid phase by dissolution in lithium bromide chaotrope and subsequent dialysis. (B) Silk solution can be used to produce solid biomaterials in formats suitable for a range of biomedical applications. Figure borrowed from [143].

2.3.2 Silk for drug delivery

Drug products are some of the most highly scrutinized and regulated commodities in the modern world to ensure their safety, stability, and efficacy when prescribed to the general population. If a therapeutic molecule or delivery device fails to meet certain standards in any of these broad categories, it will never proceed beyond clinical trials. For those drug products that do present well in these categories, development does not simply end--efforts are made to improve the convenience of the drug product to the end user. Patient compliance with drug products and their dosing regimens is critical to the positive outcome from the treatment. However, non-compliance is a significant issue with certain drug products that are required to be taken frequently to maintain a therapeutic level in the body or must be administered in an inconvenient manner (e.g. injection). Thus, research efforts in the drug delivery field focus on more convenient routes of administration, device formats, and controlled release systems to reduce the burden on the patient [157].

Silk fibroin possesses a unique combination of properties that lend itself well as a material to be used in drug delivery systems. The protein can be processed under benign conditions into a variety of formats [148, 158]. Other biomaterials require harsh processing conditions such as UV-crosslinking or high-temperature which prevent formulation of the material with sensitive therapeutics or biologics. Silk fibroin is also biocompatible and can biodegrade *in vivo* at controllable rates into non-inflammatory peptide and amino acid products [139, 142, 159, 160, 161, 162]. The mechanical properties of silk are robust and can also be tuned through post-processing of the material. While this post-processing enables control over mechanics and form-factor, it

also permits control over the release of therapeutics loaded into the bulk silk material. Through water annealing or methanol treatment, the β-sheet content in the silk is increased, rendering the material water insoluble [139, 163]. Finally, the material has been shown to preserve the activity of encapsulated molecules, including enzymes and vaccines, when stored at elevated temperatures [8, 159]. This is a significant property of the material that could eliminate the cold-storage chain, increasing patient access to temperature-sensitive diagnostics, vaccines, or therapeutics through silk-based devices and formulations.

2.3.3 Silk microneedles: performance, and limitations

Compared with alternative biomaterials and polymers, silk offers the same biocompatibility and mechanical strength while obviating the need for ultraviolet crosslinking, elevated curing temperature, or high molding pressure. Silk fibroin can also be water-vapor annealed to increase β-sheet content, eliminating any susceptibility to humidity-induced degradation which is a significant problem for sugar-based microneedles [100, 139, 163]. The material can be processed in a non-cleanroom environment unlike metal or silicon-based microneedles, reducing overall cost and improving scalability of the devices. With outstanding material properties and the processing benefits over alternative natural and synthetic materials, silk fibroin has been used to fabricate microneedle devices for transdermal drug delivery [7, 120, 164, 165, 166] (Figure 7). These devices have been designed to rapidly degrade in the skin [166], remain applied for an extended period of time to provide extended release [6, 7, 165], or combine long-term delivery with an initial bolus release to augment immune response

[164]. Mechanical strength of silk microneedles has been investigated and found to be superior to PLGA and PVP [98], adequate to pierce the stratum corneum of cadaver porcine skin [7, 165], and histologically proven to breach murine skin *in vivo* [6]. These initial published studies demonstrate the broad applicability of silk microneedles for transdermal drug delivery due to their programmable release kinetics.

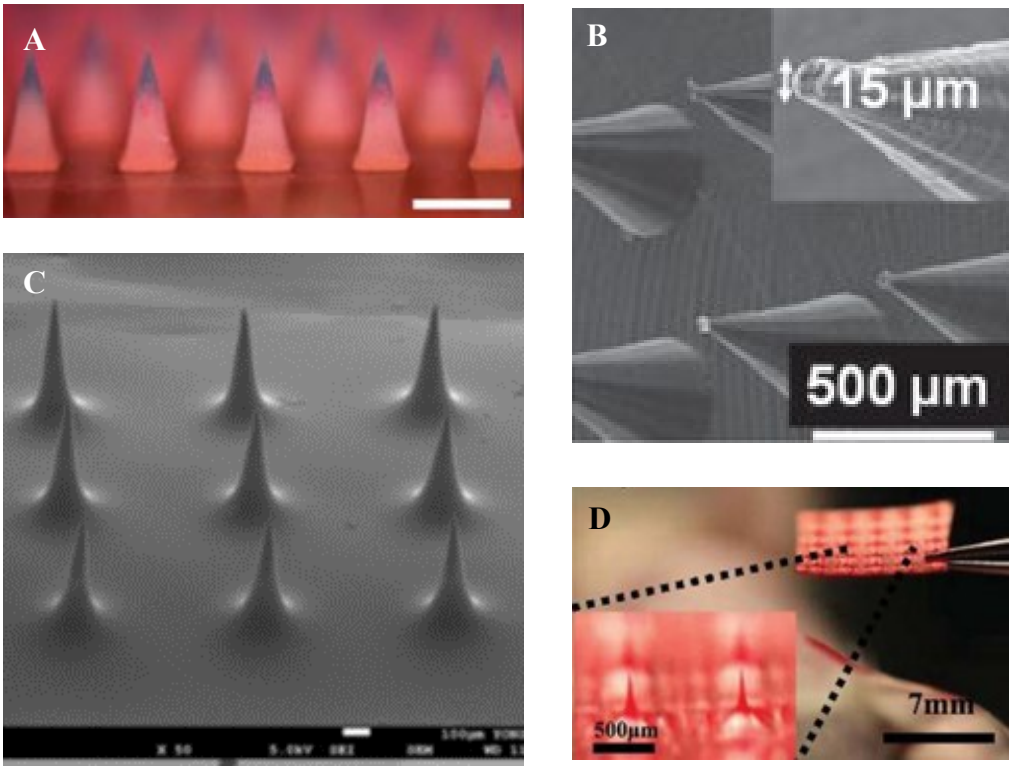

Figure 7. Silk microneedle devices have been studied both *in vitro* and *in vivo* and can be processed into different geometries. (A) Composite silk fibroin microneedle tips with polyacrylic acid bases for programmed vaccine release [164]. (B) HFIP silk microneedles produced from a micromachined master mold [7]. (C) Microneedles can be cast into PDMS molds produced from thermally-drawn PLGA master molds [165]. (D) Silk microneedles can be bulk-loaded with drug for long-term release [6].

Previous work on silk microneedles at Tufts has demonstrated the performance of silk microneedles for delivery of therapeutics *in vivo* as well as *in vitro* [167]. The goal of all microneedle devices is vaccine delivery, as the product offer the ability to remove logistical barriers to access (via solid-phase stability and self-administration) with maintained efficacy through transdermal delivery. Ovalbumin (OVA) has been studied as a model vaccine as it can elicit a quantifiable immune response from rodent models. Silk microneedles successfully delivered ovalbumin transdermally, generating an immune response that resulted in an increased anti-OVA antibody titer [167]. While silk microneedle patches are an excellent platform for the transdermal delivery of therapeutics, challenges have been reported with device performance *in vivo* due to poor patch conformance to the curved rodent skin surface. In addition, silk microneedles loaded with sulphorhodamine B dye or OVA demonstrated slower release over a 24-hour period compared to surface-coated microneedles [7, 167]. As mentioned, surface-coated microneedles are limited in scope by their maximum deliverable dose and do not fully eliminate biohazardous sharps waste. Despite these limitations, silk microneedle devices maintain their advantages over devices produced with other materials and can even be combined with complementary materials to design programmable vaccination microneedles [164]. Thus, the present work has aimed to preserve the broad scope and applicability of the silk microneedle platform by investigating methods to improve mechanical flexibility of the patches to aid conformance, demonstrate the continued performance of coated devices with a commercial vaccine, and develop a more rapid and scalable fabrication technique providing greater control over release kinetics and enabling other microneedle device formats.

3. Research Objective and Project Aims

Microneedle devices represent an exciting change to the existing parenteral drug delivery paradigm, particularly for the administration of vaccines. While these devices have been extensively researched over the last two decades, there remain limitations with the fabrication processes used to produce these devices. Access to a cleanroom facility, harsh chemical cross-linking, ultraviolet-radiation exposure, and high temperature or pressure are all drawbacks associated with current processes used to produce microneedle devices. Additionally, some of these methods are limited in the scope of process-compatible materials providing further limitation to the utility of the final products. Many materials have been investigated for their use in microneedle devices, demonstrating good mechanics for skin insertion and drug or vaccine release. However, every tested material falls short in at least one critical device property that is necessary for the use of microneedles as a platform for the delivery of a wide variety of therapeutics (Table 4).

Table 4. Limitations with microneedle materials and the potential for silk fibroin. Of the most popular materials used in microneedle delivery systems, no single material offers all of the critical properties for device success and broad applicability. Silk fibroin, previously studied in a microneedle format at Tufts, does offer the full array of properties but requires improvement to recapture some of these advantages over other materials.

Microneedle Material	Device Property							
	Demonstrated Biocompatibility	Good Mechanics	Stable Material	Provides Therapeutic Stability	Simple Aqueous Processing	No UV, Chemical, or High Temperature Required	Allows Coated Formulations	Allows Loaded Formulations
Silicon		●	●				●	
SU-8 Polymer	●	●	●				●	
Polylactic/Polyglycolic Acid (and PLGA co-polymer)	●	●	●	●	●			●
Nickel Metal	●	●	●				●	
Hyaluronic Acid	●	●		●	●	●		●
Maltose	●	●		●	●			●
Silk Fibroin	●	●	●	●	●	●	●	●

Silk fibroin biomaterial offers excellent material properties, including biocompatibility/biodegradation into non-inflammatory products, tunable mechanical properties, temperature stability of therapeutics, simple processing under benign conditions, and controlled release [8, 139, 142, 148, 159-162, 168]. This material covers the gaps encountered with other microneedle materials, offering the potential to be used

in a microneedle platform for transdermal drug delivery and additional applications. To this end, our research objective was to expand upon previous studies at Tufts using silk microneedles and demonstrate the broad utility of this device platform. Specifically, we sought to solve some of the challenges and limitations previously encountered with the silk microneedle devices and demonstrate their ability to be used *in vivo*. We also desired to adapt the silk microneedle devices for other traditional and non-traditional research applications including biosensing and tissue engineering, respectively. Our research was organized into four research aims, including:

- **Aim I:** Investigation of materials and methods to produce silk microneedle devices for better conformance to curved skin substrates for improved delivery efficacy and performance consistency.
- **Aim II:** Evaluation of the *in vivo* delivery of an existing commercial vaccine to demonstrate the viability of the silk-based devices for transdermal immunization.
- **Aim III:** Development and evaluation of improved fabrication techniques to recapture some silk material potential sacrificed with previous methods.
- **Aim IV:** Exploration of microneedle devices for additional applications including: liquid delivery or fluid extraction, biosensing, and tissue engineering.

The silk microneedle platform previously developed at Tufts leveraged the material properties and processability of silk fibroin, but did not fully unlock all of its advantages over alternative biomaterials. In the present work, we describe approaches to recapture some of the potential lost with spin-cast microneedle fabrication and improvements to the silk-based platform. This research will impact the potential of microneedle devices by providing an all-in-one material platform that can be adapted for specific therapeutic targets and overcomes limitations with previous materials. While FDA-approved microneedle devices exist, they require the use of an applicator and do not

maintain the most important benefit of transdermal delivery devices: self-administration. With a number of tunable properties, silk fibroin represents a flexible platform that can be engineered for different applications and provides the best route to the creation of a self-administrable microneedle device.

4. Materials and Methods

4.1 Silk Fibroin Preparation

Silk fibroin protein solution was prepared from *Bombyx mori* cocoons according to the standard methods as previously described in the literature [143]. B. mori cocoons were cut open to remove the silkworm and were subsequently diced into pieces roughly 3-4 square centimeters in size. Five grams of prepared cocoons were boiled for 30 minutes in an aqueous alkaline solution of 0.02 M sodium carbonate (Sigma-Aldrich, St. Louis, MO) to remove the gum-like silk sericin protein. Following a deionized (DI) water rinse process, the silk fibroin was allowed to dry overnight in a fume hood before being dissolved in a 9.3 M lithium bromide solution (Sigma-Aldrich, St. Louis, MO) for four hours at 60°C. This dissolved silk solution was then transferred to Spectra/Por dialysis membrane tubing (3,500 Da, SpectrumLabs) for dialysis for two days, with six periodic water changes performed. Resulting solution (~5–6 w/v%) was concentrated overnight on the bench to achieve a final concentration of 7–8 w/v%. This solution was centrifuged two times for twenty minutes at 8600 revolutions per minute (RPM) before storage in the 4°C refrigerator to remove any residual particulate matter. Final concentration was determined by weighing the residual silk mass after drying a known volume of solution.

4.2 Spin-Cast Microneedles

4.2.1 Mold design and fabrication

Negative molds for silk microneedle fabrication used in this body of work were prepared from existing master positive molds. These positive molds had been fabricated according to the methods described in literature [7, 167] (Figure 8). Briefly, computer numerical control (CNC) machining techniques were used to drill a chamber 5mm deep in a wax block. This chamber was then milled with drill bits that had the desired microneedle cone profile to create a template array of microneedles. A profile tool was then pressed into each machined needle well to remove any surface irregularities and create the final microneedle geometry. This machining process provides good reproducibility of the microneedle profiles while also being a much faster prototyping method than cleanroom fabrication.

The master positive mold was prepared from the master wax negative mold by casting epoxy into the machined well and curing for at least 24 hours at high temperature (80°C). This epoxy material (Electron Microscopy Sciences) is mixed in a volume ratio of 1 : 0.9 : 0.03 of dodecenyl succinic anhydride (DDSA), Araldite 502, and 2,4,6-tris(dimethylaminomethyl)phenol (DMP-30), respectively, and produces a very robust mold that preserves the needle tip features through repeated replica molding. The elastomeric polymer polydimethylsiloxane (PDMS; Sylgard 184, Dow Corning) was then cast around the master positive mold to form a negative mold from which silk microneedles could be produced. To scale up the fabrication process, the Araldite epoxy can be cast into the PDMS mold to generate a replica positive master mold. This back-and-forth process between PDMS and epoxy can quickly generate many negative molds

to increase device throughput and enable more efficient research efforts. The final molds were designed to produce 1.5 cm by 1.5 cm arrays of 400 microneedles, each with the geometry of 700 μm height, 15 μm tip diameter, and 360 μm base diameter.

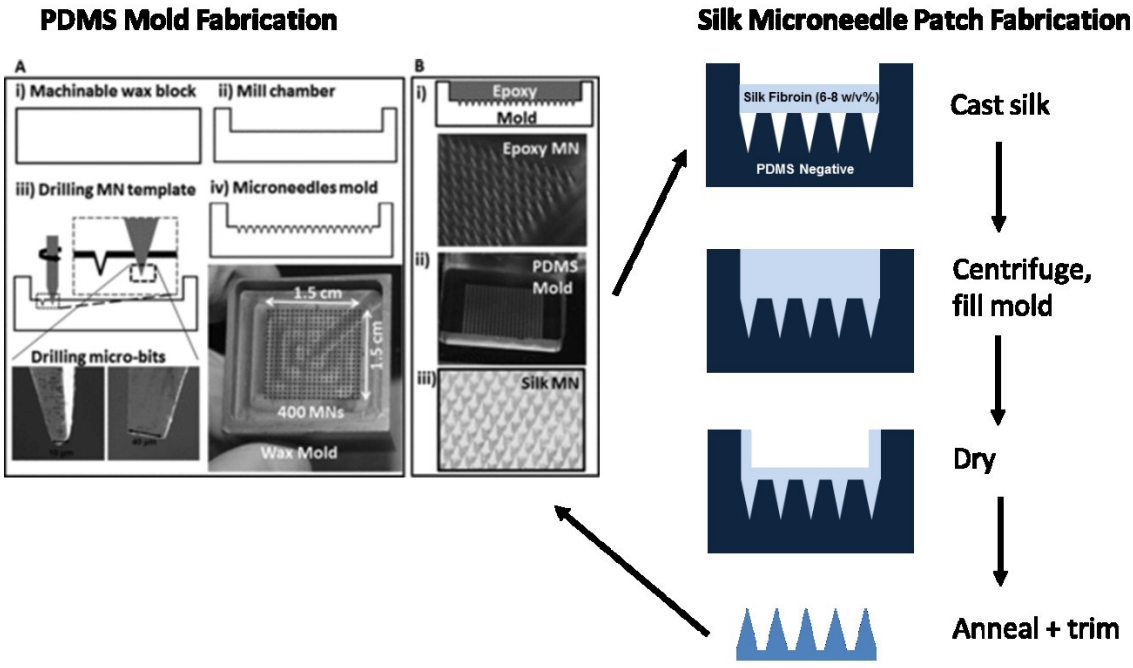

Figure 8. Overview of baseline silk microneedle fabrication process. The master molds are produced through a micromachining approach with good reproducibility, followed by replica molding in Araldite epoxy and PDMS [borrowed from 7]. Silk microneedles are produced by casting solution in the PDMS molds, a centrifugation and filling step, followed by drying and annealing of the patches to increase their strength and water insolubility.

4.2.2 Silk microneedle processing

Baseline silk microneedles were prepared using the techniques developed at Tufts and reported in the literature [7] (Figure 8). A small volume (800 μL) of prepared silk fibroin solution (~6–8 w/v%) was pipetted into the negative PDMS molds and centrifuged at a rate of 5000 rpm for 20 minutes at 4°C. This centrifugation step helps force the solution into the tips of the needle molds, evacuating any air trapped in the needle wells during the initial silk solution casting step. After centrifugation, any remaining bubbles are removed with a pipette, and the mold trenches are completed filled with silk solution (total volume ~3.5mL). The filled molds are left on the bench and typically take 2–3 days to fully dry, depending on ambient humidity. The dried silk microneedle devices are removed from the molds and placed in a vacuum chamber to water-vapor anneal for 24 hours. The water-annealing process increases the amount of beta-sheet content relative to the amorphous silk structure, rendering it water-insoluble while also improving the mechanical strength of the material [169]. After annealing, the edges of the patches are manually trimmed and the patches are pinned down onto a PDMS surface to ensure that they dry flat before subsequent use.

4.2.3 Therapeutic (drug or vaccine) coating

Before silk microneedles can be used in in vitro or in vivo release studies, the devices must be prepared with the therapeutic compound. Although the compound can be formulated into the bulk material of the silk devices, faster release kinetics and better immune responses have been observed from coating formulations [7, 167]. Coating of the microneedle devices is performed in a two-step process to first wet the microneedle

surfaces and then distribute the final therapeutic formulation across the area of the device. To pre-wet the microneedles, 100 uL of deionized water is pipetted into multiple (5-10) droplets on the surface of the device making sure to prevent the pipette from contacting the microneedle tips and potentially damaging them. These droplets are left on the microneedles for 3-5 minutes to hydrate them and are combined on the surface of the device to increase the wetted surface area. Once the surface has been pre-wet, the water is pipetted off and replaced with the therapeutic coating solution. A volume of 100 uL or less is recommended, as a greater volume could take more than 24 hours to dry on the surface of the device and is also susceptible to leaking off during drying. Previously, coating formulations have been examined with 1% (w/v) silk fibroin to impart thermal stability to the therapeutic and provide some control over initial release kinetics. These silk-therapeutic coatings have been demonstrated to change the surface morphology of the microneedle devices without any change to the overall tip size and needle dimensions [167].

4.3 Flexible Silk Microneedle Patches

4.3.1 Multi-material approach: silk needles and blend patch-backing

Microneedle patches were fabricated with separate materials used for the microneedle tips and the film backing in the patch. The same methods were used to create the needles in these devices as are used to create spin-cast microneedle patches, with the total silk mass in baseline and multi-material patches remaining constant (Figure 9B). The volume of silk fibroin solution (~6–8 w/v%) used to fill the PDMS negative molds was halved to create pure silk needles with a thin-film backing. These devices were dried and subsequently water-annealed in the PDMS molds before a second material addition step to create the blend patch-backing. A blend solution of silk fibroin and glycerol (Sigma-Aldrich, St. Louis, MO) was created at a weight ratio of 40% (glycerol to dry silk mass), which is reported to be above the critical threshold for making the blend film insoluble while decreasing the stiffness of the film by two orders of magnitude [170]. A simple polyol, glycerol is safe for human consumption as it is commonly used as a food additive and was therefore deemed appropriate for these studies. The volume of silk-glycerol solution needed to reach the same total silk mass as baseline patches was calculated, and then cast onto the water-annealed silk microneedles to create a blend backing over the pure silk microneedles.

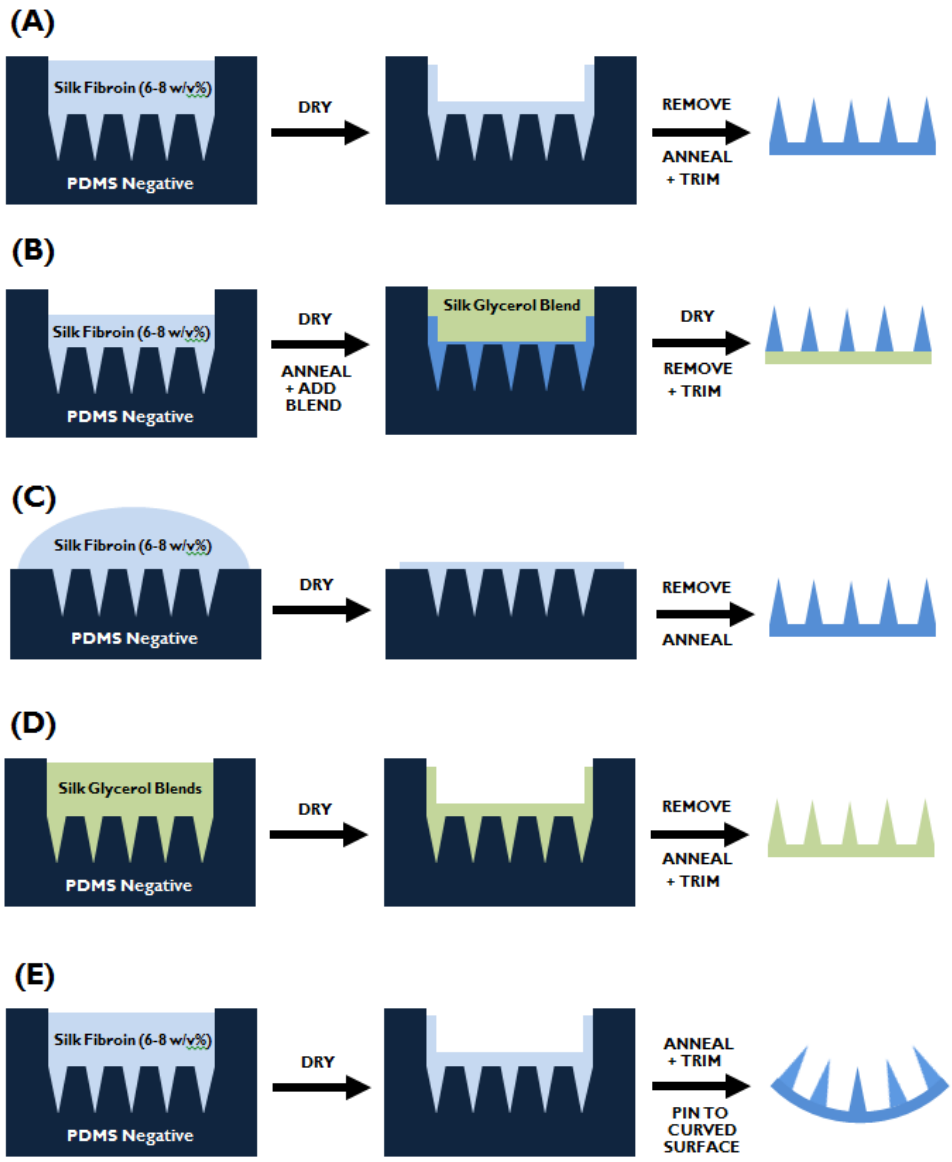

Figure 9. Process flow diagram for the creation of baseline microneedle patches, as well as alternative fabrication and material strategies to generate more flexible patches. (A) The baseline processing steps for creating microneedle patches include spinning down silk in the PDMS negative molds and allowing it to dry before annealing the patch, trimming the edges, and pinning it down to dry flat. (B) The first strategy to produce multi-material microneedle patches utilized a second addition step to incorporate a silk-glycerol blend backing into the patch. (C) Drop-casting fabrication was investigated as a more efficient production process and required manual scraping to remove bubbles from the PDMS mold tips. (D) Whole-patch blend microneedles were created using the same processing steps as (A) with a silk-glycerol blend substituted for pure silk fibroin solution. (E) Curved microneedle patches were formed by pinning baseline (A) patches to a curved PDMS mold to impart the rounded shape to the patch.

4.3.2 Whole-patch material blends

Flexible microneedle patches were investigated using a material blend of silk and glycerol instead of neat silk solution, obviating any additional fabrication steps (Figure 9D). Glycerol and silk were mixed to create solutions with weight ratios of 0, 5, 10, and 20 percent (glycerol to dry silk mass). These weight ratios were selected as a trade-off between improved flexibility and the mechanical strength of the needle features themselves [170]. After 800 uL of the blend solutions were spun down in the microneedle molds, different volumes of solution were added to the mold trenches to create microneedle patches with final silk fibroin masses of 0.125 g ('LO'), 0.165 g ('MID'), 0.200 g ('HI'), and 0.250 g ('XHI'). The final masses include the mass of the patch edges which are normally trimmed off after annealing. These microneedle patches with a range of glycerol blends and total silk masses were then mechanically assessed for flexibility.

4.3.3 Curved patch fabrication

Curved microneedle patches were created from both baseline silk microneedles as well as silk-glycerol blend microneedles. Relative to the standard methods used to produce the flat devices, the only difference was in the drying step after water vapor annealing. The microneedle patches were manually pinned down to a piece of PDMS with a curved surface, allowing them to take on the shape of the material as they dried (Figure 9E). The curved drying molds were prepared by casting PDMS around 50-mL Falcon conical tubes, creating a concave surface with an approximate radius of curvature of 3.0 cm.

4.3.4 Flexible drop-cast microneedle patches

Briefly, this alternative fabrication technique was investigated as a method to create flexible microneedle patches with reduced material waste and improved processing time (Figure 9C). This work led to further analysis as will be detailed later. Drop-casting is a fabrication technique that combines the simple aqueous processing of silk fibroin with the concepts of soft-lithography to produce patterned silk films [171]. To allow a PDMS microneedle mold to be used in the drop-casting technique, the edges of the well were removed to allow a solution droplet to form on the microneedle-negative surface. A 500-uL drop of silk fibroin solution (~6–8 w/v%) was cast onto the surface of the trimmed PDMS mold. The device was placed in a desiccator under vacuum conditions, which was cycled on and off five times in a 20 minute period to promote infiltration of silk solution into the needle wells. A pipette tip was then used to physically scrape the surface of the mold to release any remaining trapped air bubbles in the microneedle tips and to help spread the droplet evenly on the surface of the mold. These bubbles were removed with a pipette and an additional 0.5–1.0 mL of silk solution was added to the mold surface depending on the final desired mass. The silk was allowed to dry overnight and was subsequently annealed before mechanical testing.

4.3.5 Mechanical evaluation: Three-point flexural bend test

Silk microneedle patches were mechanically tested to determine their baseline flexibility and to quantitatively measure any mechanical differences due to the formulation with glycerol plasticizer. Patch flexibility was evaluated through a three-point flexural bending test, which is commonly used to determine the bending strength of

biomaterials [172, 173]. In summary, the testing apparatus was assembled by placing a microneedle patch on two triangular supports spaced 10 mm apart. The rounded testing plunger was centered above the rounded supports and the microneedle patch, and was attached to a ±5 N load cell used on a uniaxial mechanical tester (Figure 10, Instron Model 3366, Norwood, MA). All flexural testing was performed with a cross-head extension rate of 1 mm/min and a data sampling rate of 10 Hz.

The raw extension-load data was pre-processed before the patch flexibility could be quantified. First, the compressive extension of the raw mechanical data was zeroed for each sample to standardize the initial point of compression. This data was then truncated to select the elastic deformation region (characterized by a linear period of deformation). The slope of the elastic deformation region was extracted from the processed data using the trendline function in Microsoft Excel, and was used to determine the modulus of elasticity in bending, also called the flexural modulus, through the following equation:

$$E_{flexural} = \frac{mL^3}{4BH^3}$$

where m is the slope of the linear elastic region of the load-extension curve in N/mm, L is the length of the support span in mm, B is the width of the tested microneedle patch in mm, and H is the height of the tested microneedle patch in mm [174]. The flexural moduli for the microneedle patches at different silk masses and glycerol weight ratios were averaged and plotted with error bars displaying one standard deviation. Statistical significance between silk mass conditions and glycerol weight ratios was examined using one-way analysis of variance (ANOVA) calculations.

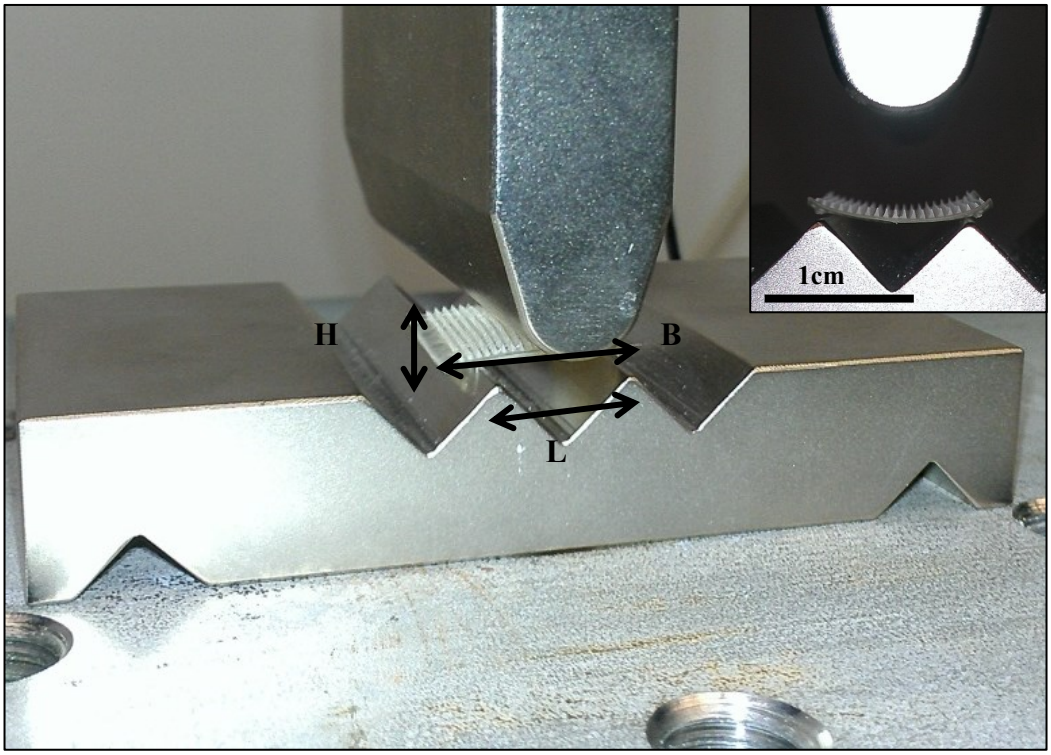

Figure 10. Three-point flexural bending test setup on Instron 3366. The testing apparatus consisted of two triangular supports spaced at a distance L, with a microneedle patch of height H and width B. The rounded plunger was moved at a cross-head rate of 1 mm/min by the Instron 3366 instrument. The ±5N load cell was used to sample load and compressive extension at a rate of 10 Hz.

4.3.6 Mechanical evaluation: Single needle axial compression test

The strengths of single silk fibroin and blend silk-glycerol needles were evaluated to determine whether flexible-patch material compositions would preserve microneedle ability to penetrate the stratum corneum. PDMS negative molds were fabricated for a single microneedle, following the methods previously described in section 4.2.2. Single microneedle patches were created at the same silk mass and glycerol weight ratio conditions as used for flexibility testing, after adjusting for a smaller mold trench volume.

These needles were subjected to an axial compression test on the Instron with the ±5 N load cell, using flat plates to both support the microneedle patch and to compress the needle tip. Needles were compressed at a crosshead rate of 100 μm per minute, and data collection was performed at a rate of 10 Hz. The needle strength was determined from the raw data as the point of needle tip fracture, as previously described [7].

4.3.7 Controlled release of enzymatic model drug

The release of horseradish peroxidase (HRP, Sigma-Aldrich, St. Louis, MO) from coated baseline silk fibroin and flexible blend microneedles was examined into three-dimensional collagen gels as reported with similar devices [6]. Briefly, baseline (XHI, 0%) and flexible (HI, 20% glycerol [glycerol mass to silk dry mass]) microneedles were prepared, with an additional dicing step performed after the annealing process to generate 4 quarter-patches from one standard-sized patch. The microneedle surfaces were wetted with DI water to improve the evenness of the final coating. Horseradish peroxidase (HRP) solution was prepared at a concentration of 0.45 mg/mL, and patches were coated with 20 μL of HRP and allowed to dry overnight. The collagen gels were prepared by boiling 40 mL of water with 4.5 g of gelatin powder (Knox Unflavored Gelatine), and pouring the solution into a Petri dish. The solution was allowed to cool overnight, and was diced into 1-cm X 1-cm squares. For testing, the collagen gel pieces were placed on 3–4 paper towels that had been wet with DI water to prevent dehydration. A piece of plastic wrap was placed over the gels to mimic the stratum corneum, and patches were applied to the gels. A glass slide was placed over the samples and a weight was added to provide 0.5 N of force.

Five release times were examined: 10 minutes, 1 hour, 4 hours, 12 hours, and 24 hours. After removing the patches, we placed the gels in 1 mL of 1 mg/mL collagenase solution and left them in a 37°C oven for two hours to digest. Negative controls of blank collagen gels were also prepared to remove any background absorbance during the colorimetric assay. Additional HRP-coated patches were washed with DI water to remove the coating, and this solution was assayed as a positive control for full release. Triplicate wells of a 96-well plate (Falcon 353077, Corning) were coated with 100 uL of the digested collagen gels containing HRP, as well as the patch rinsate controls. To perform the HRP assay, 100 µL of 3,3',5,5'-tetramethylbenzidine (TMB supersensitive for ELISA, Sigma-Aldrich, St. Louis, MO) substrate was added to 100 uL of each sample solution. The reaction was stopped after 5-10 minutes of incubation through the addition of 2M sulfuric acid solution. A microplate reader was then used to examine the absorbance of samples at 450 nm. Percent release was calculated from comparisons between samples and their paired positive controls.

4.3.8 Evaluation of release on curvilinear surfaces

The release performance of baseline and flexible microneedle patches was examined in a curved porcine cadaver skin model. Skin from a porcine donor is the most commonly used xenograft for the treatment of burn wounds and is also accepted as a good model of human skin [175, 176]. Patches were prepared with both standard and 20% (w/w) glycerol material formulations, with two patch shapes—flat and pre-formed, as described in section 4.3.3. Microneedle patches in each of these four conditions were coated with 50 µL of 25 mg/mL ovalbumin-Texas Red conjugate solution (Life

Technologies, Carlsbad, CA) and allowed to dry overnight on the bench in a light-protected environment. Porcine skin was thawed and placed on wet paper towels before being shaped around a metal rod (radius of curvature 4.25 cm, McMaster-Carr, Robbinsville, NJ; Figure 11). Rubber bands were used to hold the skin in place during testing. We dried the skin surface and then applied the coated patches for 15 minutes, using the rubber bands to provide some force to the patches. Patches were then removed and the skin surface was imaged both under standard and ultraviolet illumination. No additional image modifications or corrections were performed.

Figure 11. Curved porcine skin release model. The setup for evaluating release of a model drug into cadaver porcine skin consisted of the porcine skin sample placed over wet paper towels to maintain hydration. This sample was formed around a cylindrical stainless steel rod with 4.5cm radius of curvature, closely resembling a human forearm.

4.4 In Vivo Vaccine Delivery

4.4.1 Animal selection, care, and vaccine target

Silk microneedle devices have been studied *in vivo* previously with the model vaccine ovalbumin, which was demonstrated to elicit an immune response when delivered transdermally [164, 167]. These studies examined both a rat (Sprague Dawley) and mouse (C57BL/6) model, respectively, each chosen for the extensive background literature on immunizations performed on these animals. For this study, BALB/c mice were chosen as a model organism due to easier housing requirements than rats which allowed increased sample sizes. While the C57BL/6 strain is the most commonly used laboratory mouse, the BALB/c strain is used more often for immunological studies as their immune response tends towards a T-helper (Th) lymphocyte type 2 response [177]. This type 2 response generates a strong antibody response from extracellular pathogens while the type 1 response in C57BL/6 produces a stronger cellular response [178]. This results in specific antibody production in rodent models, with type 1 responses tending towards immunoglobulin (IgG) 2a and type 2 responses tending towards IgG1, IgE, IgG2b, and IgG3 [179]. In humans, most T-helper-mediated responses result in the production of IgG1 antibodies [180]. For this reason, the BALB/c mouse model was chosen for study with our vaccine target. All animal studies were approved by the Tufts Institutional Animal Care and Use Committee (IACUC) and were performed following NIH (National Institutes of Health) guidelines for animal care.

We have chosen to study the transdermal delivery of influenza vaccine using silk microneedle devices. This vaccine target is one of the most widely studied in literature as its annual use warrants the need for a simpler administration technique that has the same

efficacy of subcutaneous injection. This target has been successfully delivered into murine skin using other microneedle materials and device formats, with ongoing clinical trials and an FDA-approved product in Sanofi Pasteur's Fluzone® Intradermal device and vaccine formulation [58, 59, 127, 128, 129, 181]. We aimed to demonstrate the ability of silk-based microneedle devices to deliver a commercially-available seasonal influenza vaccine (Fluzone Quadrivalent Vaccine, Sanofi Pasteur, Swiftwater, PA) and provide stability at elevated temperatures over a two-week period.

4.4.2 Microneedle administration to mice

Female BALB/c mice (8-10 weeks old, Charles River Labs, Wilmington, MA) were obtained for the *in vivo* release experiments. Pre-experiment blood samples were obtained through the facial vein technique and were collected in serum separator tubes (Amber Microtainer 365978, Becton Dickinson, Franklin Lakes, NJ). Serum was collected from the tubes following centrifugation at 13400 RPM for 5 minutes and stored at -20°C when not being used. To administer microneedle patches, the animals were first anesthetized with vaporized isofluorane in an isolation chamber. The animals were then transferred to the benchtop where they remained under anesthesia with a face mask. The upper region of the back was then prepared by shaving with hair clippers and subsequent application of hair removal cream (Nair™ Sensitive Formula, Church and Dwight). The cream was removed thoroughly using a damp cloth after five minutes of application and the skin was allowed to dry. The silk microneedle device is then placed onto the prepared skin region and administered by pinching the patch and skin with the index finger and thumb. The patch is immobilized in the skin with a 3 cm by 3 cm piece of adhesive

dressing (Tegaderm™, 3M, St. Paul, MN). Animals receiving microneedle patches for transdermal delivery are caged separately during the administration process to prevent chewing of the patches or bandages. After 24 hours of release, the silk microneedle devices are removed. All injection controls and experimental conditions were administered subcutaneously in the dorsal region between the shoulders.

4.4.3 Dose response study

The first phase of this *in vivo* vaccine delivery experiment was to determine the immune response of the animals to varying doses of influenza vaccine antigen. Based on previous studies in the literature, it has been demonstrated that 6 ug of influenza antigen produced a strong immune response in BALB/c mice and 9 ug elicited a comparable response to intramuscular injection in human subjects [61, 182]. With the silk microneedle system, we sought to determine the strength of immune response to doses spanning this antigen range, including 12 ug per patch (3 ug per individual antigen), 6 ug per patch (1.5 ug per antigen), and 1 ug per patch (0.25 ug per antigen). Reducing the amount of total antigen needed to provide protection offers the benefit of reducing production costs and/or increasing efficacy safety margins. Intradermal vaccination may also spare additional doses by eliciting stronger immune responses during the first administration event [61]. Controls for this immunization dose response study included a negative control (water-coated microneedle patch) and a positive control (12 ug subcutaneous injection). All experimental groups consisted of five animal subjects to minimize variability. The immunization schedule consisted of a primary immunization with a single boost after two-weeks to induce a stronger IgG secondary immune response.

Antigen coatings were formulated with 1% (w/v) silk fibroin to provide consistency with the thermal stability study. Blood samples were collected via the facial vein prior to each immunization as well as at 4 weeks after the first administration event.

4.4.4 Thermal stability study

The second aspect of the *in vivo* vaccine delivery experiment was to examine the thermal stabilization properties of silk fibroin protein. It has been previously reported that silk fibroin films are able to temperature stabilize enzymes, antibiotics, and vaccines at elevated storage temperatures for periods up to six months [8, 168]. We sought to validate this finding *in vivo* with commercial influenza vaccine instead of measles, mumps, and rubella (MMR) vaccine for the reasons described in section 4.4.1. For this study, unaltered liquid influenza vaccine was compared head-to-head for immunogenicity with vaccine stored in the solid phase with 1% (w/v) silk protein on the surface of microneedles. Coated silk microneedle patches and vaccine vials were stored at three elevated temperatures for two weeks prior to administration: 25°C, 37°C, and 60°C. The same immunization schedule (primary immunization and 2-week boost) was followed for this study as for the dose response study; blood sample collections were also identical (prior to immunizations and 4-week time point). A 12 microgram dose was used for both the liquid and solid doses of influenza vaccine, allowing efficacy comparison with the patch conditions from the dose response experiment. Microneedle patches were placed in sealed empty tip boxes that had been cleaned with 70% ethanol and filled with 1 gram of clay desiccant. The tip boxes were covered with aluminum foil to prevent any light-induced degradation from occurring.

4.4.5 Anti-influenza immune response quantification

To evaluate the success of silk microneedle vaccine delivery, the immune response to influenza antigen was quantified through the indirect enzyme-linked immunosorbent assay (ELISA) technique (Figure 12). In this process, the level of serum antibodies against a specific antigen (in this case, 4 influenza strains) is determined. To perform this ELISA, 96-well microtiter plates (Nunc Maxisorp, Thermo Fisher Scientific, Waltham, MA) were coated with 100 uL of influenza vaccine antigen at a concentration of 1 ug/mL in carbonate buffer (0.05 M, pH 9.5) and stored overnight at 4°C. Wash buffer (1X phosphate-buffer saline [PBS] with 0.01% Tween-20) was prepared and used to wash the wells of the microtiter plate three times before the addition of 200 uL of blocking solution (1% bovine serum albumin [BSA] in wash buffer). The blocking solution helps coat any residual open surface in the microtiter well with protein to prevent any later non-specific binding of primary or secondary antibody. The 96-well plates are incubated at room temperature for 2 hours before washing 3 times again. Aliquots of primary serum samples, defined as the serum obtained from the animals in the dose response and stability experiments, are pooled and subsequently prepared in serial dilutions of 1/100, 1/500, 1/2500, 1/12500, 1/62500, and 1/312500 in PBS-Tween 20 (0.01%). A volume of 100 uL of each serum dilution is added to triplicate wells in the 96 well plate and incubated for 2 hours at room temperature. For the preliminary bleed data, only the first three dilutions were used as it was not expected to observe anti-influenza titers without previous exposure to the antigen. Another wash step (3X) was performed before the addition of 100 uL biotinylated secondary antibody in PBS-Tween 20 (0.05%). The secondary antibody is incubated in the wells for 1 hour before another wash step and

the addition of 100 uL of streptavidin-peroxidase substrate in PBS-Tween 20 (0.05%). This is incubated for 30 minutes at room temperature before a final wash step and development. The colorless substrate 3,3',5,5'-tetramethylbenzidine (TMB, Sigma-Aldrich, St. Louis, MO) is added to each well and is converted to a blue product by the HRP enzyme. After 5-10 minutes of development (enzyme conversion), a 100 uL volume of 2M sulfuric acid is added to stop the reaction and convert the product to a yellow color. The absorbance of the wells can be read at a wavelength of 450 nanometers.

The endpoint titer is determined as the maximum dilution that produces an absorbance value at least two times greater than the average background signal (no primary antibodies present). Two secondary antibodies were used to quantify the endpoint titers for all anti-influenza immunoglobulins (biotinylated goat anti-mouse IgG [H+L], Sigma-Aldrich, St. Louis, MO) and IgG-specific antibodies (biotinylated goat anti-mouse whole IgG, Sigma-Aldrich, St. Louis, MO). By using these two detection antibodies, the total immune response can be measured as well as the IgG-specific secondary response. When an animal is first exposed to a vaccine, there is a short lag phase while the antigen is processed. Eventually, the primary immune response occurs with the production of predominantly IgM-subtype antibodies. It is not until the second exposure to the antigen that the immune system produces IgG antibodies, which are associated with immunological memory and long-term protection [183]. The results regarding total immune response and secondary immune response should provide insight to the protection against influenza virus through silk-microneedle based immunization as well as the optimal dose regimen.

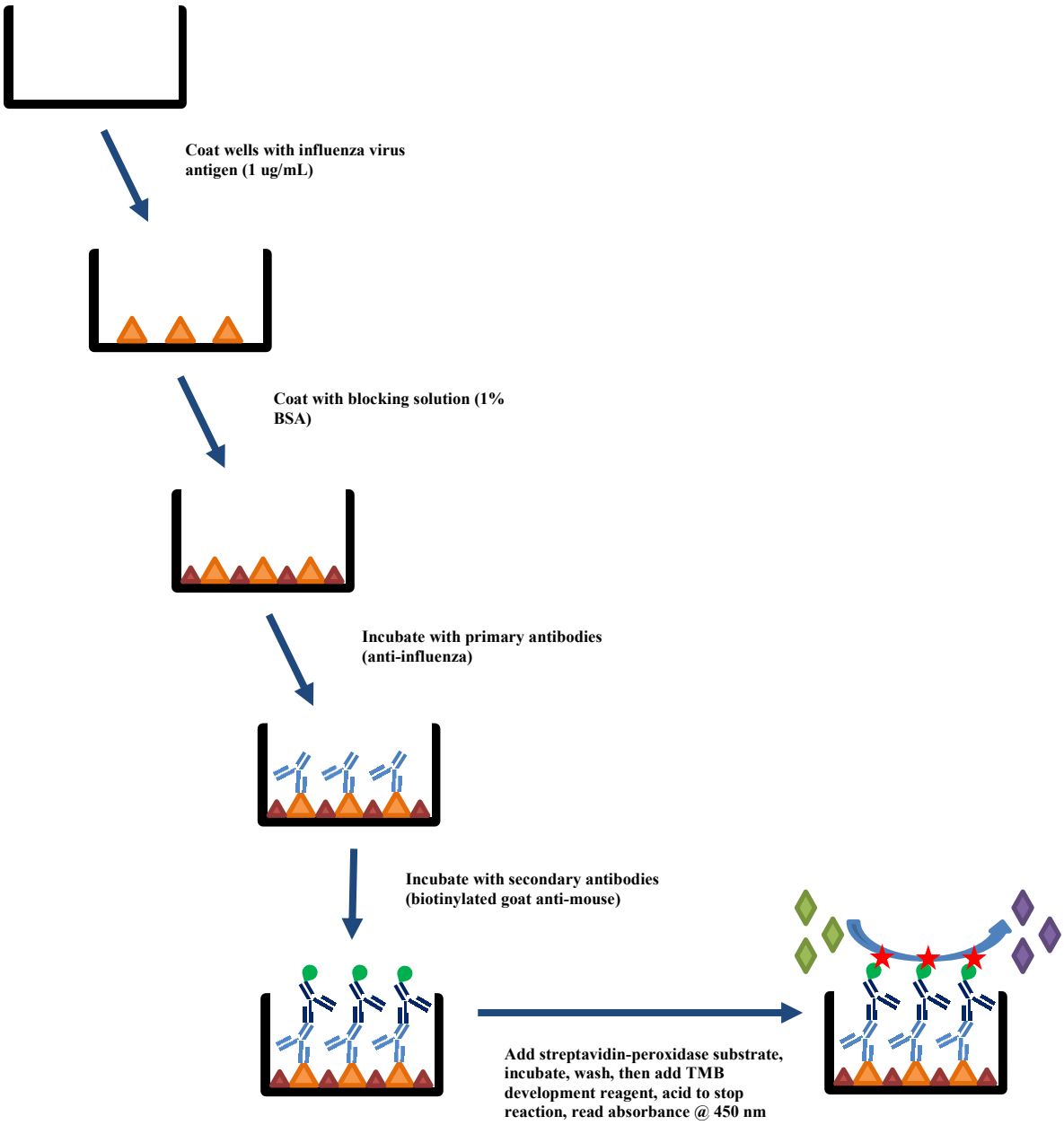

Figure 12. Overview of indirect enzyme-linked immunosorbent assay method using to quantify anti-influenza immunoglobulin titers following immunization. The indirect method uses a target antigen to capture any antibodies in serum samples with paratopes specific to the epitopes of the antigen. A secondary antibody from a different animal species against the Fc domain of the primary antibody from the mouse results in a second binding event. The HRP molecule can be directly conjugated to the secondary antibody, or can be bound to a streptavidin molecule which binds to a biotinylated secondary antibody to provide increased assay sensitivity. The assay is developed with the addition of 3,3',5,5'-tetramethylbenzidine (TMB) substrate, which is catalyzed to a colored product by HRP which can be spectrophotometrically quantified through an absorbance reading after the reaction is stopped with the addition of sulfuric acid solution.

4.4.6 Anti-silk immune response quantification

In addition to anti-influenza indirect ELISAs, anti-silk ELISAs were performed to quantify the immune response to the biomaterial itself. Silk fibroin is FDA-approved for use as a suture material and has been demonstrated to be biodegradable into non-inflammatory amino acid and peptide products [139, 142, 159, 160, 161, 162]. However, in the microneedle delivery format, the silk material as well as the vaccine are being presented to the dendritic cells in the skin to elicit an immune response. For the devices to remain efficacious in the clinical setting, the coating formulation of silk with vaccine must not generate any adverse reaction upon primary or secondary antigen presentation. In the same indirect protocol outlined for anti-influenza ELISAs, anti-silk ELISAs were run with 4 ug/mL silk fibroin (30 minute boil). Total immune response was examined with the same secondary antibodies as before, since it can detect the conserved regions of IgA, IgM, and IgG antibodies. To improve throughput with the ELISAs, pooled serum samples from the five animals were used instead of individual samples to determine if any immunological memory against the biomaterial is raised in the murine models for each experimental group.

4.5 Rapid and Scalable Microneedle Fabrication

4.5.1 Drop-cast fabrication development

One of the major limitations of the standard microneedle fabrication process is the drying step. After centrifugation, the molds are completely filled with silk solution (~3 mL) and require two or three full days to dry depending on the ambient humidity. For this process to be potentially scaled-up, efficiency and throughput must be considered—and having a mold in-use for greater than 24-hours is not efficient. Thus, we sought to improve this fabrication process by investigating the drop-cast fabrication method as it had been previously noted that the devices dried much more quickly with this technique. To begin, we used the same PDMS molds that are utilized in the spin-cast fabrication of microneedles. The vertical edges of these molds were removed, leaving a 1.5 x 1.5 cm PDMS surface with the 20 x 20 array of microneedle wells. On these molds, we cast different volumes to characterize the maximum droplet size that could be contained on the surface of the device. Additionally, we investigated methods to remove air from the needle wells and promote the infiltration of silk solution into these structures.

With spin-cast microneedles, a significant amount of material dries into a film along the vertical walls of the PDMS mold trenches. These silk edges must be trimmed off of the device after the material has been dried and annealed. We sought to characterize how much material is lost and whether we could achieve silk microneedle patch masses through a reasonable drop-cast volume and silk concentration. Silk microneedles were spun according to the baseline technique (section 4.2.2) and weighed at two points (after drying and after annealing, trimming, and secondary drying) to

determine the material lost as part of the existing fabrication techniques. From a scale-up perspective, material loss should be minimized to reduce overall waste.

Finally microneedle patches produced through spin-casting and drop-casting were characterized to determine if there were any significant differences in the output patches. We performed attenuated total reflection Fourier-transform infrared spectroscopy (ATR-FTIR) to characterize the crystalline structure of the silk fibroin protein in devices produced through the two techniques. In addition, the flexibility of patches produced through the drop-cast technique were compared to the glycerol-blended patches from section 4.3.2 to confirm there were no significant differences in mechanics of the output devices.

4.5.2 Dissolving microneedle investigation

Another limitation with the current spin-cast silk microneedle patches is that even without water-vapor annealing, the devices often dry to an insoluble form. It has been reported that when the drying rate of silk solution is decreased it forces the material into an insoluble silk I conformation with high β-turn content rather than the soluble amorphous form observed after more rapid drying [184]. It was hypothesized the slow release from bulk-loaded therapeutics in the spin-cast devices was observed as a result of drying to an insoluble form. In the insoluble silk matrix it would be challenging for the loaded therapeutic to diffuse, especially when the silk needles are not porous. While this is a beneficial phenomenon for slow, controlled release, it hinders the ability of these devices to be used for rapid delivery of a drug or vaccine dose. With previous studies, the devices were coated with drug or vaccine to shift the release kinetics to a 24-hour

timescale [167]. As the drop-cast fabrication was being developed, we began to examine the ability to fabricate dissolvable silk microneedles simply through the improvements to drying time. This would allow a single fabrication process to be used to create devices with tunable release kinetics, recapturing a major advantage of the silk fibroin biomaterial.

To begin, we fabricated a three-needle device for studying the effect of various fabrication and material variables. Three 30° conical profile tools (Bits & Bits, Silverton, OR) were inserted into a pre-cured 1.0 mm layer of PDMS in a Petri dish. Liquid urethane plastic (Smooth-Cast 321, Smooth-On, Macungie, PA) was cast and cured around the bits to create a master positive mold. PDMS negative molds were then prepared by casting onto the plastic master mold. Using these molds, we investigated the ability to produce a device with soluble needle tips and an insoluble backing. This would allow the needles to be loaded with the therapeutic molecule, minimizing the waste that would occur with loading into the backing matrix in a single casting step (Figure 13). The three-needle molds were originally studied with a plasma-treatment step to improve solution infiltration to the needle wells. Vacuum pulling and manual removal of the bubbles were also investigated. From the observations made with these three-needle devices, we began to study the original drop-cast molds (20 x 20 arrays) to determine if we could produce fully dissolvable microneedle arrays for administration to alternative tissue targets, such as the buccal or sublingual mucosa.

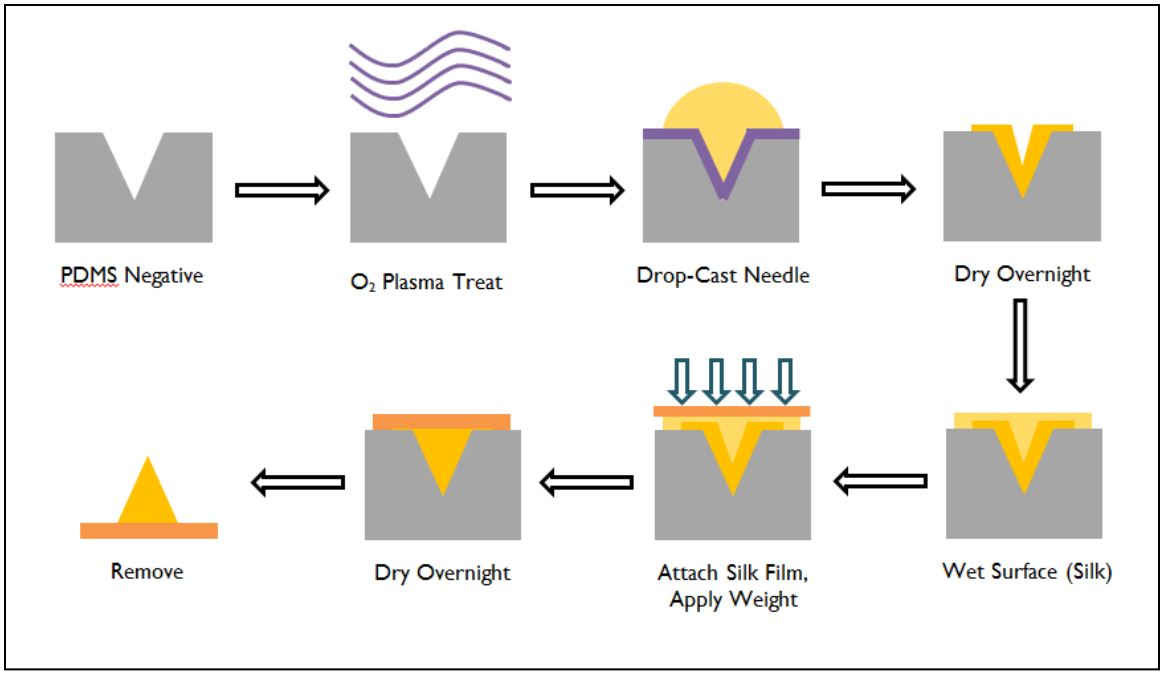

Figure 13. The initial drop-cast fabrication approach for dissolving silk microneedles. A PDMS mold was briefly plasma-treatment to make the surface hydrophilic, promoting solution infiltration to the needle wells during the drop-casting step. Silk solution was added to the mold and allowed to dry overnight, although the drying could be completed in less than 8 hours depending on the initial volume. The surface of the dried needles was then wet with a small (5-10uL) volume of silk solution and a pre-annealed silk film was added to the needles. Force was applied during drying to mimic an embossing process, and the devices were removed from the molds after 24 hours of drying.

4.5.3 Dissolution and release studies

The designed dissolving silk microneedles were examined for their ability to rapidly degrade and release a model payload in vitro. The two-component devices (needles and backing layer) were first examined for their percent degradation through mass balance studies with a variety of silk concentrations, two boiling times, and the inclusion of glycerol in the bonding solution. These silk microneedles were demolded after drying, weighed for their initial mass, placed in deionized water for 5 minutes before being removed and allowed to dry. Final weights were recorded and the percent

dissolution was calculated as the change in mass divided by the original recorded mass. To measure release, the devices were loaded with HRP enzyme and evaluated for release into a gel model to mimic release into a mucosal membrane. Gelatin solution was prepared (0.25 g/mL, Knox) and formulated with 5% (v/v) TMB substrate to allow visualization of HRP release from the devices in situ. The dissolving devices were placed directly onto the gel and allowed to dissolve and release their enzyme payload for 5 minutes before removal. The gel was then placed in sulfuric acid (2M) stop solution and was sandwiched between two glass slides for imaging.

Moving to full size microneedle patches, we examined the dissolution of silk microneedle patches from the same dissolution perspective as the three needle devices. We aimed to determine if there was a relationship between silk concentration and drop-cast mass that could be used to control or predict the percent degradation and therefore release of bulk-loaded therapeutic. To this end, silk microneedle patches were drop-cast from two different concentrations of silk and multiple volumes to produce distinct series of devices with different masses. The patches were removed after drying, weighed, and placed in water for 5 minutes to promote dissolution before being transferred to a new Petri dish to dry. After drying overnight, the devices were reweighed to calculate the percent degradation.

The release of HRP from full-size drop-cast microneedle patches was examined in two ways. First, we desired to confirm that the drop-cast patches maintained their mechanical strength and would be able to penetrate the skin if used in vivo. A patch applicator was designed and created by a senior undergraduate student and was used to apply the drop-cast microneedle patches to gelatin gels covered with Parafilm to simulate

the stratum corneum of the skin as previously described [7]. The gels were loaded with TMB to allow visual confirmation of HRP release and were also created unmodified for more quantitative assessment. These unmodified gels were digested in collagenase solution at 37°C for two hours, coated onto triplicate wells of a 96-well plate and developed with TMB as described previously (section 4.3.7). The next aspect of these release studies was to examine whether the degradation and HRP release could be controlled simply through the amount of glycerol used in the material blend. Previous work has demonstrated that glycerol can be used to create insoluble silk films in addition to improving their flexibility [170]. We created HRP-doped microneedle patches with 10, 20, and 30% weight ratios of glycerol to silk protein and examined the release into gelatin gels with no Parafilm barrier. The gels were processed in the same fashion as for the applicator-applied patches.

4.5.4 Prototyping of alternative format devices

With traditional solvent-casting techniques with biocompatible polymers, microneedle designs are limited to out-of-plane structures. This is the result of the fabrication process, which may require embossing into a mold or a long drying process to produce a final material form. These materials do not offer the potential to be formed into additional structures after the initial casting. We aimed to demonstrate the form-functionality of silk protein, and how it can be used to create new formats of microneedle devices. First, we examined the ability to create in-plane structures that could be folded out-of-plane into microneedles (Figure 14). A PDMS mold was created for these devices by patterning Teflon tape (0.0115" super-slippery tape made with Teflon PTFE,

McMaster-Carr, Robbinsville, NJ) into the microneedle triangular shapes. These tape pieces were adhered to a layer of PDMS and urethane plastic was then cast over this surface to create a master negative mold. PDMS was then cast over the plastic mold to make positive molds. Silk solution was cast and dried on these molds and the needle features were folded out-of-plane after cutting them out with a laboratory knife. We then developed a more advanced mold that allowed these needle features to be folded out-of-plane by manually pressing-down on the feature and then bending the device (Figure 15).

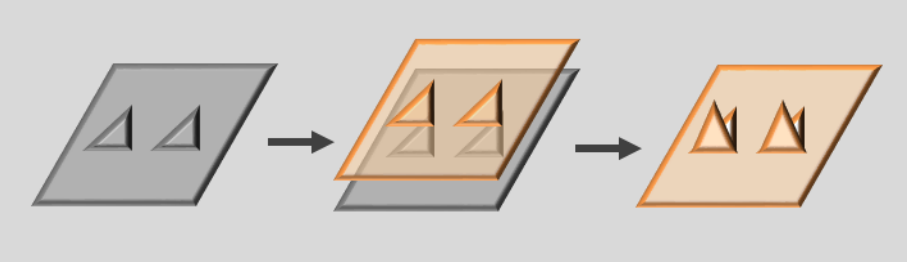

Figure 14. Fabrication of out-of-plane needles from in-plane features. Silk fibroin can be used to create silk films patterned with microneedle features that can be cut out after drying and folded out to create a sharp needle structure.

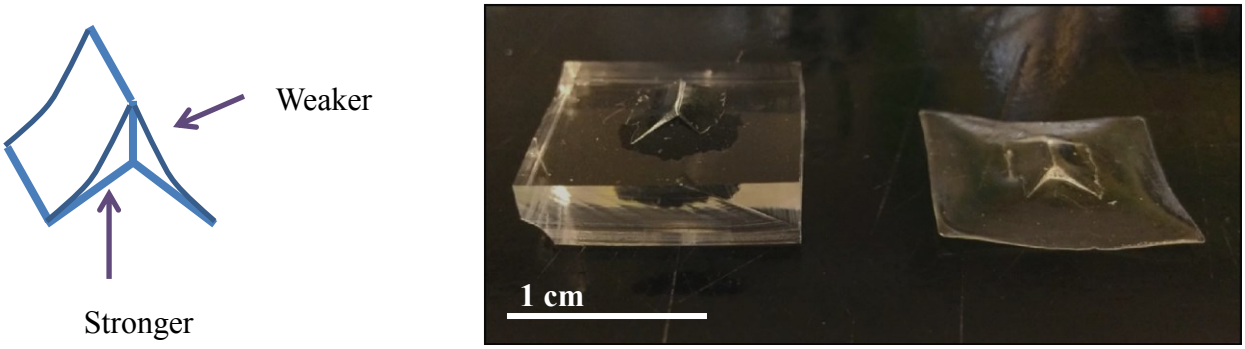

Figure 15. Mold design for self-breakable folding microneedles. Weak joints are designed to break during applied vertically applied pressure, allowing the device to be folded out-of-plane when the device is bent.

Microneedle devices are traditionally flat, again due to the fabrication processes and use of pre-formed materials such as silicon wafers. Silk fibroin films are quite flexible and offer the potential to create non-flat microneedle formats. To this end, we investigated microneedle rings with both axial and radial microneedles (Figure 16). Silk solution with 20% (w/w) glycerol was prepared and cast on sawtooth-patterned PDMS molds. The resultant film was then formed around a 15-mL conical tube and laminated together using a 5 uL droplet of silk solution to produce the axial needle devices. Radial microneedle molds were produced in a sequential process to expand from a single needle to 8 needles. As with the 3 needle device described in section 4.5.2, a layer of PDMS was cast to control the height of the needle features (1 mm). A 30° conical profile tool (Bit & Bits, Silverton, OR) was inserted at a 45° angle to the PDMS surface and urethane plastic was cast around the bit. Two PDMS negative molds were cast from this master positive mold (bit and plastic). The PDMS molds were diced and arranged next to each other with the silk-casting surface face down on a glass slide. Additional PDMS was cast around these negative molds to create a single 2-needle mold. Using the urethane plastic and PDMS this process was repeated to increase the number of needle features until an 8-needle linear mold was produced. Silk-glycerol solution was drop-cast on this mold, dried, and a ring device was created by using a paperclip to hold the laminated layers together.

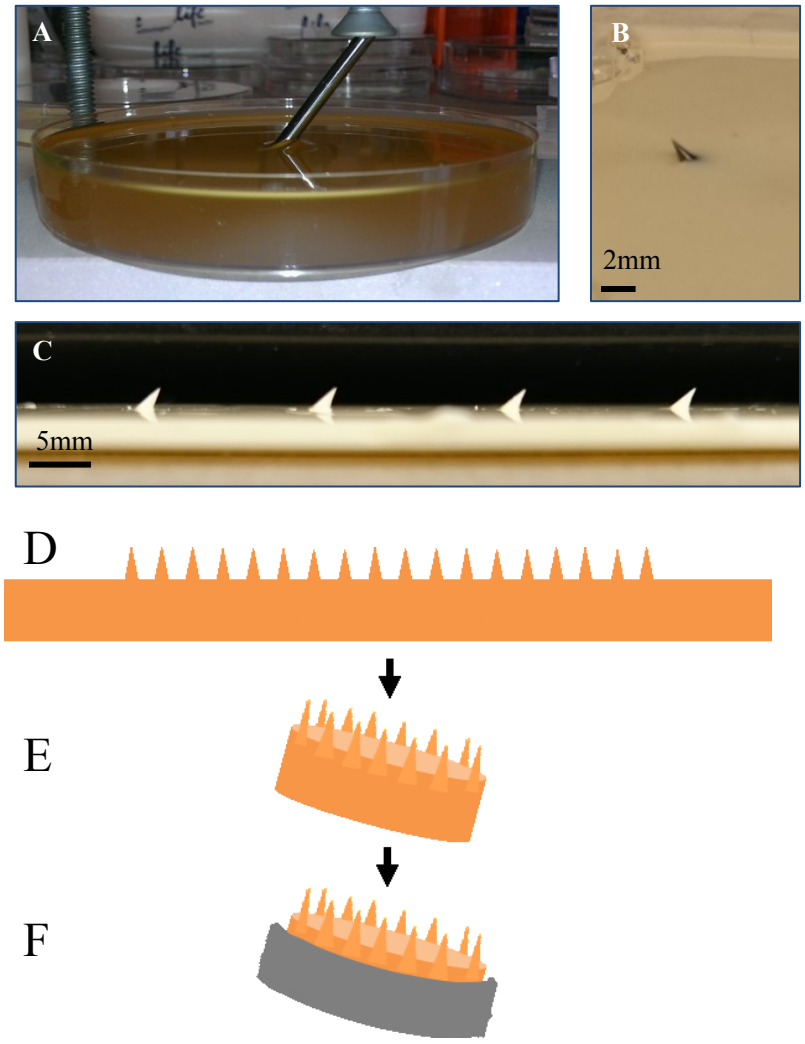

Figure 16. Fabrication scheme for radial and axial silk microneedles. (A-C) Radial needles are produced in a conventional master mold fabrication technique, with the needles angled to permit rotation of the ring to insert the needles into tissue. (D-F) Axial needles are produced on a sawtooth PDMS mold and are then formed into a ring that could interface with a solid device for assistance with insertion or for biosensing readout.

4.6 Adapting Silk Microneedles for Additional Research Uses

4.6.1 Hollow silk microneedles

As described previously, hollow microneedles offer two specific uses during administration to the skin: (1) liquid formulation drug delivery and (2) biosampling of dermal interstitial fluid or capillary blood. To demonstrate the potential to use silk fibroin protein as a biomaterial for such hollow devices, we investigated multiple fabrication approaches to create these devices. Building off the work performed with Dr. Waseem Raja during his time at Tufts, we examined benchtop fabrication techniques to generate master molds compatible with soft lithography mold expansions processes to produce the hollow microneedle devices.

The first fabrication approach was to create a single silk microneedle with the existing molds used for mechanical testing (section 4.3.6 and 4.2.2) and then process the device to make it hollow. Specifically, a laser cutter (Speedy300, Trotec, Canton, MI) was used to bore a central channel through the needle device (Figure 17). A PDMS support containing a microfluidic chamber and female Luer fitting with 1/16" barb (Cole-Parmer, Vernon Hills, IL) was bonded to the hollow silk microneedle with silicone adhesive (3145 RTV, Dow Corning). The ability to use these devices in vivo with a rat model (Female Sprague Dawley, Charles River Labs, Wilmington, MA) was examined.

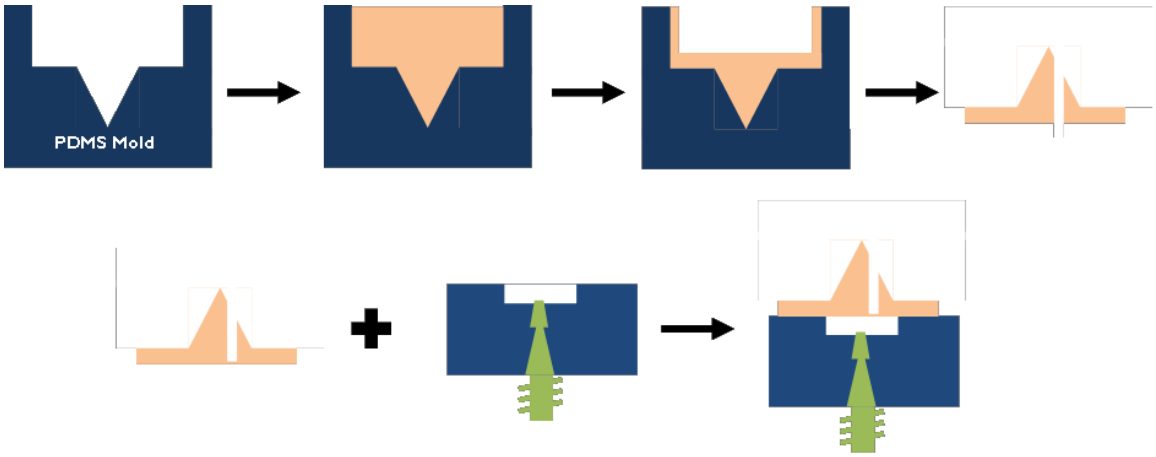

Figure 17. Fabrication process flow diagram for hollow silk microneedles created through standard processing technique. Using the same single needles molds for previous axial compression studies, silk solution (30 minute boil, 6-8%) was cast and centrifuged to evacuate air from the needle wells. After drying, the microneedle was water-vapor annealed to increase crystallinity and then trimmed. The needle was made hollow with a laser cutter aligned slightly off-center from the needle tip to maintain needle strength. The device was then adhered to a PDMS-Luer connected with a silicone adhesive to allow a standard syringe to be used for fluid delivery or sampling.

Another fabrication approach that was investigated was to use a solid material as a removable channel mold. The initial concept was to insert a small diameter Teflon-coated rod (0.006”/154um, McMaster-Carr, Robbinsville, NJ) or stainless-steel acupuncture needle (0.18mm Pipe Ten, DongBang Corporation, Seongnam, South Korea) into the needle well to form a hollow structure after casting silk around this removable shape. The height of the feature was controlled through a pre-measured, patterned layer of PDMS that was then bonded to a separate PDMS block (Figure 18). Upon the initial studies of this fabrication approach, we began investigating vertical fabrication using capillary force up the channel guides rather than into needle depressions in the PDMS mold. These hollow cylinders were cut and sharpened using a handheld rotary tool (Dremel 4000, Mount Prospect, IL).

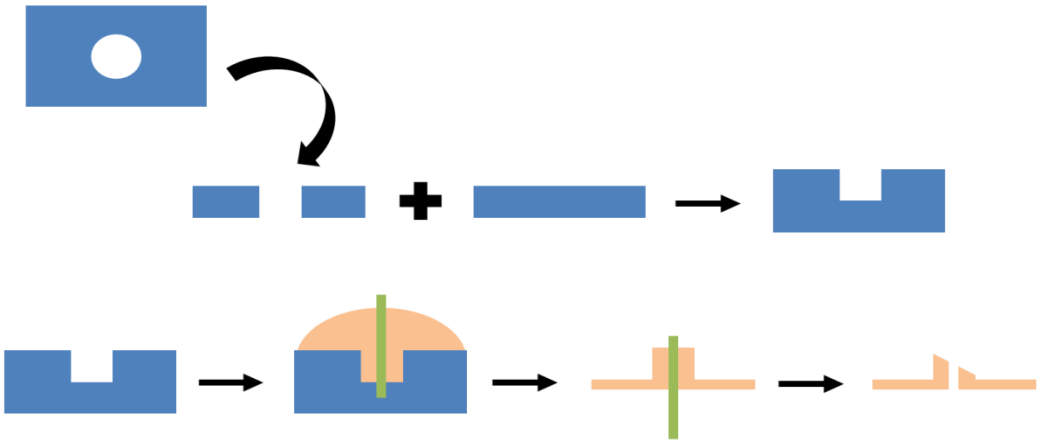

Figure 18. Hollow silk microneedle fabrication around needle bore mold. Needle height is controlled through the thickness of a pre-cast and patterned PDMS layer bonded to a separate PDMS block. Once combined, a needle bore guide (PTFE-coated rod or acupuncture needle) is placed into the center of the needle relief pattern and silk is dropcast around the device. After drying and water annealing, the device is removed from the mold and the channel guide is removed. A handheld rotary tool is then used to sharpen the microneedle structure.

Further prototyping and process development efforts were made to improve these drop-cast hollow microneedles and combine them with microfluidics to demonstrate functionality. First, the profile of the needle bore mold was modified to improve the sharpness of the output silk microneedle. We created positive microneedle molds in PDMS from the negative single needle molds (also PDMS) that were pre-treated with a release agent to improve demolding after the curing step (Ease-Release 200, Smooth-On, Macungie, PA). Silk was cast onto these positive PDMS molds to create needle-shaped hollow silk devices. For the microfluidic portion, we aimed to use a similar drop-casting technique to create an all-silk device. First, we investigated the use of a separate channel-patterned silk film bonded to the initial silk needle. Ultrathin polyimide tape (0.0025”, McMaster-Carr, Robbinsville, NJ) was patterned into a 1 mm wide channel and placed

onto a Petri dish. Sylgard 184 PDMS (Dow Corning) was prepared and cast onto the channel pattern and cured overnight in a 60°C oven. This negative feature (recessed) in PDMS was made into a positive feature through another PDMS casting step onto the negative mold after treatment with release-agent. Silk fibroin could then be drop-cast onto the cured positive mold to create a silk film with a recessed microfluidic channel. This channel film was also water-vapor annealed to increase water insolubility. The two silk components (hollow needle and microfluidic channel) were combined through the wetting of the microfluidic film surface with 10 uL of silk solution and then application of the hollow device. A PDMS ring was then placed around the hollow silk microneedle and weight was applied during drying to improve the bonding process.

A separate all-silk device was investigated through a single drop-casting step. Instead of forming a silk channel film backing and performing bonding, acupuncture needles were inserted perpendicular to the needle axis of the positive PDMS mold. After drop-casting silk onto this mold, the acupuncture needles were removed, leaving behind microfluidic channels with connections directly to the needle bore. The devices were adhered to a PDMS block using double-sided tape to seal the needle bore, and were investigated for microfluidic flow through the channel and out the silk microneedle. Additionally, the ability to create metal contact surfaces within the microfluidic channel was investigated as an option to add biosensing functionality to these devices. A thin layer (300 nm) of gold was deposited onto the surface of the acupuncture needles (NSC 300 magnetron sputter tool, Nanomaster, Austin, TX) prior to incorporating them into the PDMS positive molds. No changes were made to the silk drop-casting technique with these gold-coated acupuncture needles.

4.6.2 Silk microneedle electrodes

Microelectrode arrays are typically used for the recording of electrical activity for neuroscience and cardiology applications [185]. Most of these devices are fabricated through cleanroom micro/nanofabrication approaches and cannot be used for extended periods of time due to poor biocompatibility. Recently, silk fibroin was used in an ultrathin, conformal electrode array for *in vivo* recording of electrical stimulation of a feline brain, offering advantages over other non-conformable materials [186]. We sought to prototype silk microneedle electrode devices to prove efficacy of the material for neural recording or stimulation applications. The first effort to create silk microneedle devices for electrical recording of rat cardiac activity was begun as part of an undergraduate senior capstone project at Tufts. A standard 20 x 20 microneedle array was physically modified to form 7 distinct multi-needle regions which were subsequently deposited with a layer of gold and a connective pathway to allow external connection to a data acquisition device [187] (Figure 19). The devices successfully recorded a signal both *in vitro* and *in vivo* demonstrating the initial potential for silk microneedle electrodes. We aimed to improve these devices with the fabrication of a controlled array and with the developed drop-casting approach to more rapidly generate these devices.

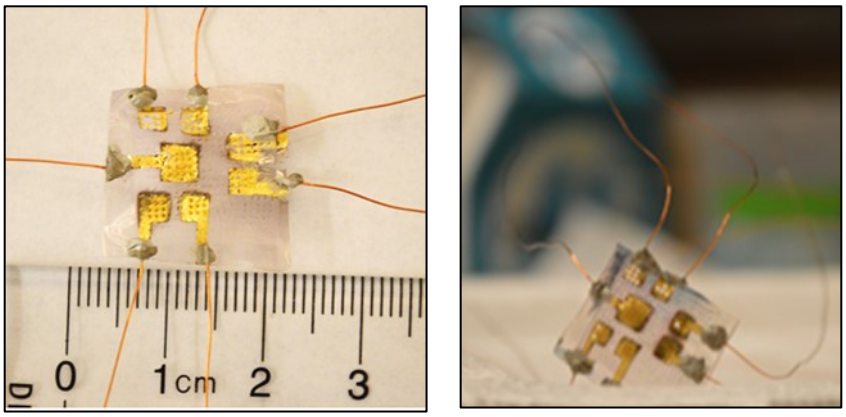

Figure 19. Silk microneedle devices functionalized with gold electrodes. Produced using the standard microneedle molds, these devices provided the foundation for the electrode development work. The devices were used to record electrical signals *in vitro* and *in vivo*. Borrowed from [187].

With the help of two undergraduate students and Scott from the machine shop at the Science and Technology Center at Tufts, we began by fabricating a new master mold using the original micromachining approach. A 4 by 4 array of 1 mm needles was produced with additional area to allow the connection of these needles to connective ribbon tape, providing an easier means to interface with external recording/stimulating devices. Both PDMS and a rapidly-curing castable plastic (Smooth-Cast 321, Smooth-On, Macungie, PA) were used to create positive molds from the wax negative mold. This allowed the fabrication of separate PDMS negative molds (from the plastic postive) or direct silk casting onto the PDMS positive mold. From these two mold types, we attempted to produce solid and hollow silk microneedle electrode devices. For solid devices, we cast silk solution into the negative PDMS molds, using a pipette tip to carefully remove the bubbles from the needle wells after centrifugation. These devices were dried and water-annealed before electrode functionalization. Deposition masks were

prepared by manually patterning laboratory tape and adhering it to the silk film. A 300 nm layer of gold was deposited in a cleanroom environment and the deposition mask was removed to leave the final device. Hollow silk microneedle devices were designed to limit the recorded signal to that of tissue in contact with the embedded microneedle tip, minimizing signal noise from tissue in contact with the conductive pathways of the device. To fabricate these devices, we first created a deposition mask on the PDMS positive mold, used the same sputter deposition technique, and then cast silk on the gold-patterned mold. Both silk devices were examined for basic electrical conductivity by using a multimeter to measure their resistance. As an alternative fabrication approach, the folding microneedle design was examined for compatibility as a silk electrode device. Because the devices are fabricated in-plane, we believed it would be easier to sputter-deposit the conductive pathways than on an out-of-plane feature. We created three-needle devices using the methods outlined in section 4.5.6 and examined the ability to deposit different patterns using a basic deposition masking technique.

4.6.3 Silk microneedles for tissue engineering

Silk fibroin protein has been extensively studied in the field of tissue engineering, specifically as a scaffold material to create more complex three-dimensional tissue models [152, 153, 154, 160]. One such engineered tissue that is currently under investigation at Tufts is the small intestine. Current *in vitro* models in the literature are limited to two-dimensions, with only a few models recapitulating microvilli structures that are a key physiological component in native human small intestine. Researchers at Tufts have developed a novel scaffold fabrication technique that allows three-

dimensional scaffolds with a hollow lumen to be produced. While these devices contain some surface topology, they remain without microvilli and therefore do not fully match the *in vivo* tissue architecture and function. Microvilli are finger-like projections ranging from 0.5–1.6mm in length inside the small intestine, and bear a strong physical resemblance to microneedles. Thus we aimed to include microneedle/microvilli-like projections in the novel three-dimensional scaffold to produce the most advanced small intestine model to date.

We sought to develop a molding technique to produce the microvilli surface topology that would minimally disrupt the overall process flow used to create the previous generation of intestine model. The existing scaffold mold consists of a PDMS chamber device with two ports for a Teflon-coated rod to be inserted through, forming the lumen in the scaffold (Figure 20). Silk solution is cast into this device, frozen overnight at -20°C, and then lyophilized for two days to create a porous silk scaffold. This device is then autoclaved to increase the β-sheet content and make it insoluble. Thus, we decided to replace the Teflon-coated rod with a sacrificial mold material that would transfer the features to the silk scaffold and degrade at some later point in the fabrication process. We selected gelatin as such a material as it is biocompatible and has been previously used as a low-cost, sacrificial molding material [188].

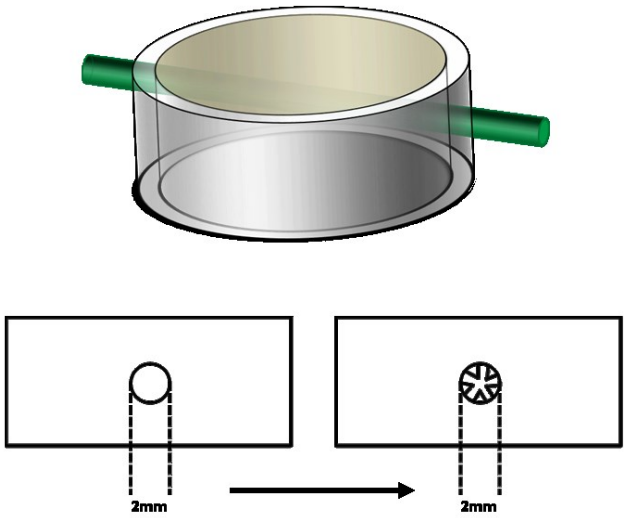

Figure 20. Schematic of 3D intestinal silk scaffold mold and design objective. A PDMS chamber contains an inlet and outlet to hold a Teflon-coated wire (green) in place. Silk solution is cast around this wire in the chamber, frozen, lyophilized, and autoclaved to create the hollow lumen silk scaffolds for small intestine tissue modeling.

We evaluated gelatin first through a two-dimensional fabrication process to confirm its compatibility with our designed process before proceeding to three-dimensional trials (Figure 21). An epoxy mold used for standard microneedle patch fabrication (20 by 20 array, 700 um tall needles) was cast in melted gelatin (0.5 g/mL in PBS, type A from pig skin, Sigma-Aldrich, St. Louis, MO). The gelatin was allowed to cool and set before the epoxy master was carefully demolded. The negative gelatin mold was then filled with silk solution (30 minute boil, 5-6%) and placed under vacuum for 3 minutes to promote bubble release from the needle wells. The devices were then placed into the -20°C freezer overnight and then in the lyophilizer to be freeze-dried over a 48 hour period. Post-autoclaving, the devices were placed in water in a 60°C oven overnight to dissolve any residual gelatin material. The devices were sterilized with ethanol prior to imaging under a macroscope and scanning electron microscope (Field Emission SEM Ultra55, Zeiss, Oberkochen, Germany).

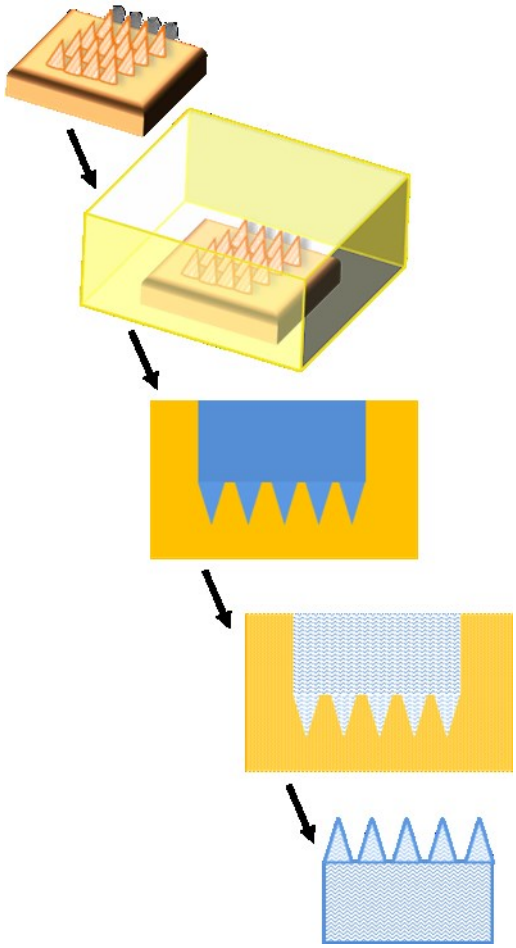

Figure 21. Fabrication process to create flat silk scaffolds with microvilli topology using proposed gelatin-molding process. A standard silk microneedle epoxy mold (positive) is used for this process. The epoxy mold is cast in a molten gelatin solution which is allowed to cool and solidify before being carefully demolded from the epoxy component. Silk solution is then cast in the gelatin mold and placed briefly under vacuum conditions to promote the infiltration of solution into the needle wells. The devices are frozen at -20°C overnight before lyophilization for 48 hours and autoclaving to increase water insolubility. Residual gelatin is dissolved by placing the devices in water in a 60°C oven overnight. The devices are then sterilized in 70% ethanol prior to imaging.

Moving into 3-D, we developed a two-part mold to create a patterned gelatin rod to replace the Teflon-coated wire in the existing scaffold fabrication process (Figure 22). To begin, we created a master negative mold through a micromachining technique. Micromachining was previously used to create the master silk microneedle molds and allowed excellent control over feature profile, density, and size while also enabling rapid prototyping and design optimization to occur. These features make micromachining a more attractive option for master mold fabrication than alternative techniques including photolithography and laser ablation. Liquid urethane plastic (SmoothOn Smooth-Cast 320) was cast inside 2mm internal diameter plastic tubes to form the rod to be machined into the master mold. The larger plastic tubes allow easier operator manipulation of the material during machining. Following machining with a tapered ball end mill, the rod was removed from the tube support and cast in PDMS. The PDMS positive mold was diced into two pieces along the length of the rod, allowing easier de-molding of the gelatin from PDMS. The two pieces will be press-fit back together and gelatin will be cast in the hollow center of this mold. The gelatin will be allowed to set before it is de-molded from the PDMS. The gelatin rod will be inserted into the PDMS chamber to cast silk solution and generate a scaffold.

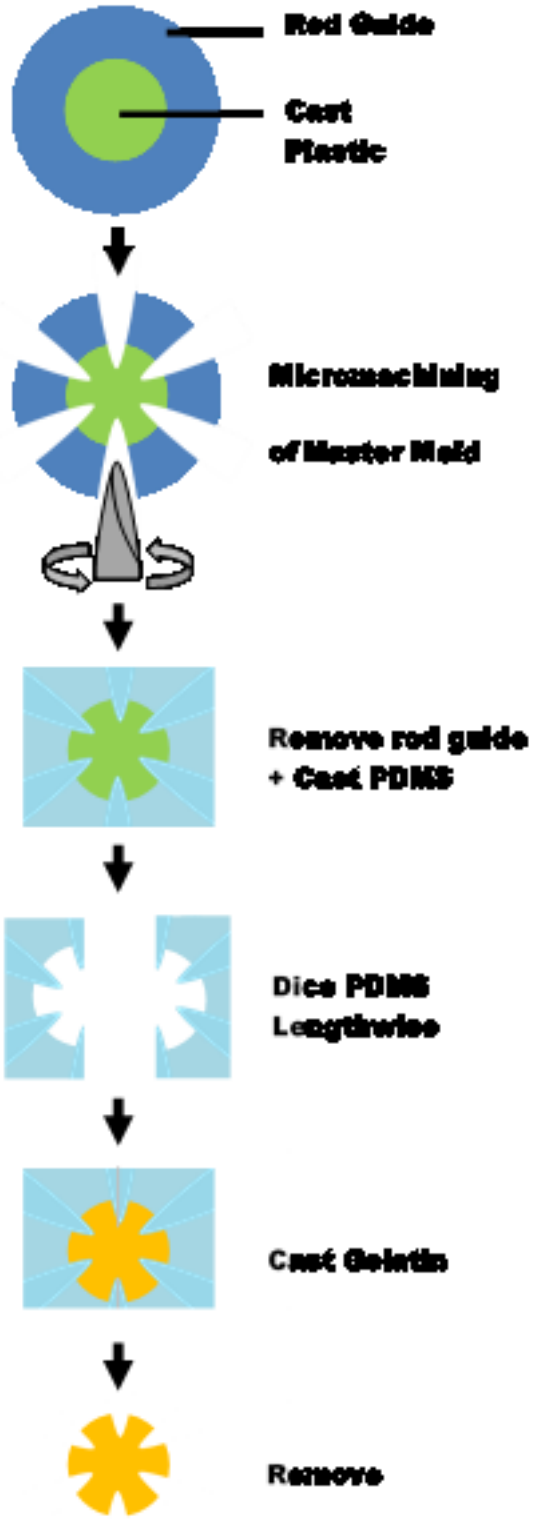

Figure 22. Process flow diagram developed to create patterned gelatin rods for existing scaffold fabrication technique to generate luminal microvilli topology. Plastic was cast inside a tube with the same internal diameter as the existing Teflon-coated rods. An end mill drill bit was used to create radial microvilli structures around the circumference of the rod and along the length of the device. The inner plastic rod was removed and cast in PDMS to create the mold which was carefully diced in half to allow press-fit molding of the gelatin rod. The gelatin is cast in molten form and is allowed to cool and set before being demolded from the PDMS halves.

5. Results

5.1 Silk-Glycerol Blend Microneedle Fabrication Outcomes

5.1.1. Multi-material approach: silk needles and blend patch-backing

The initial approach to create a more flexible, skin-conformal microneedle patch was to modify only the thin-film backing in the device. The rationale was that this would prevent any performance reduction due to changing the material composition of the microneedles themselves. Initial attempts at creating these devices were unsuccessful, as issues were consistently encountered with the silk microneedles (initial layer) delaminating from the PDMS mold during water-vapor annealing. This allowed the silk-glycerol blend to seep underneath the original pure silk fibroin layer during the second addition step to the molds. This caused the formation of dual-layers of microneedles (Figure 23). We attempted to troubleshoot this problem through the formation of silk-glycerol films that were inserted into the molds before the spun silk had dried. The interface between the silk and the silk-glycerol film was better than that of the two-step addition microneedles, but the resultant patches were very brittle. An additional troubleshooting attempt to create these multi-material patches used the drop-casting fabrication technique. Unfortunately, the investigated volume to create the drop-cast needles in the patches was not great enough to create robust microneedle patches after a secondary backing material addition step. In most of these devices, even with a layering process of silk and then silk-glycerol, many of the needles broke off during observation and manual flexing of the patches.

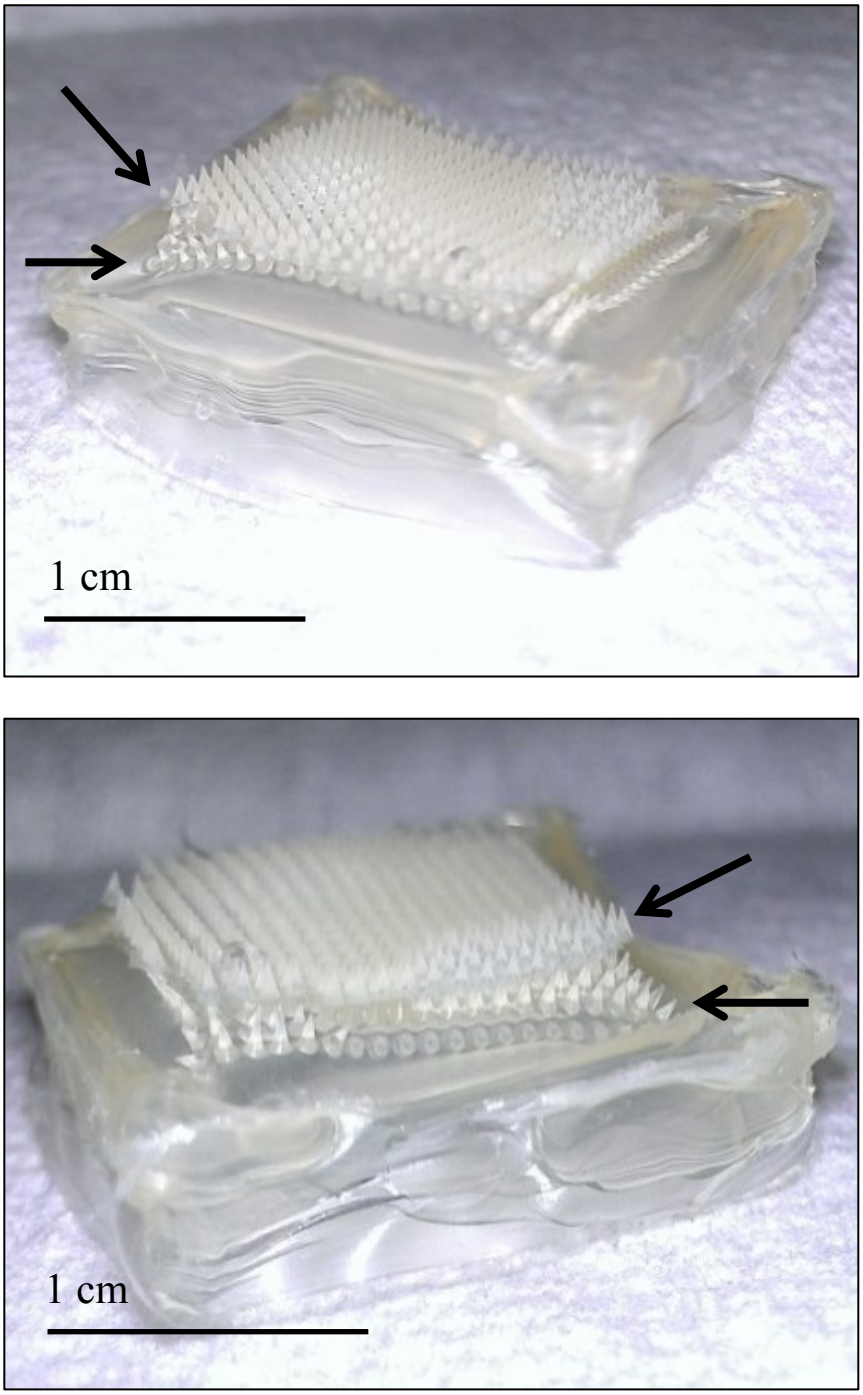

Figure 23. Example of microneedle patch outcomes with multi-material formulations. The arrows demonstrate the areas where the microneedle patches delaminated and the dual-layer of needles resulted.

5.1.2. Whole-patch material blends

After encountering challenges with multi-material microneedle patches, we began to investigate the use of a single blend of silk fibroin and glycerol to generate more flexible devices. The primary benefit of this approach is that the same methods can be used to create the flexible patches as the baseline patches, simplifying the fabrication process relative to the multi-material devices. Initially, we chose to study two material composition factors: silk mass and glycerol weight ratio. For the first round of whole-patch blends, three levels of silk mass were examined, equivalent to creating patches from 3% (w/v) silk ('LO'), 4.5% silk ('MID'), and 6% silk ('HI'). Four levels of glycerol weight ratio were selected (0%, 5%, 10%, 20% weight glycerol to weight silk fibroin) for investigation, based on work previously done with the flexible microneedle patches and that reported in the literature for thin films [170]. These patches were manually flexed during observation, and appeared to have different degrees of bendability at the various material compositions (Figure 24). These blend patches were then moved forward into mechanical testing to quantitatively characterize their flexibility.

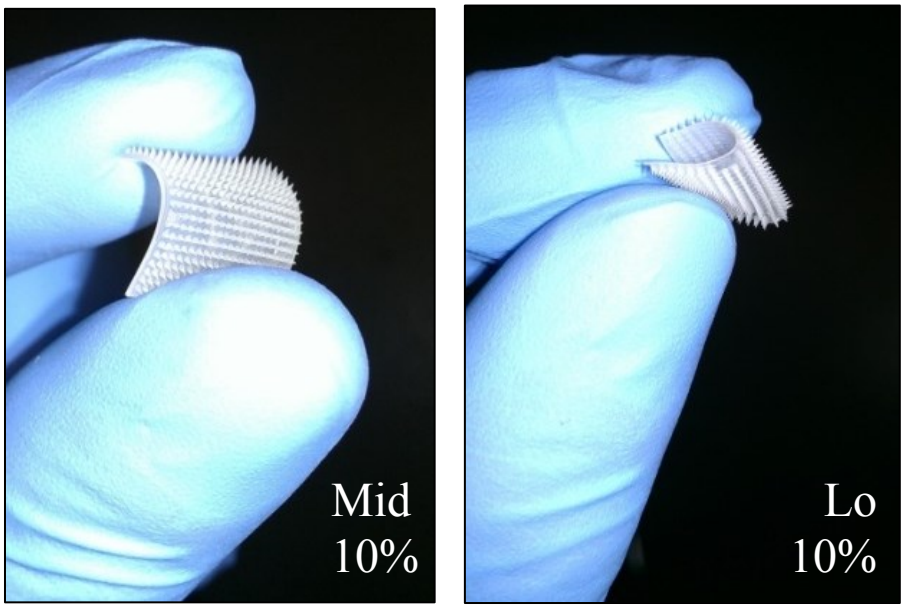

Figure 24. Examples of whole-patch blend flexibility at two different silk masses with the same glycerol weight ratio. Initial observations suggested that whole-patch material blends were a viable method of improving the flexibility of silk microneedle patches. The patches seemed more bendable than baseline devices while maintaining needle structure through the fabrication process.

5.2 Mechanical Comparison of Baseline and Flexible Microneedle Patches

5.2.1. Flexibility testing

Upon observation of the whole-patch blend microneedles, three-point flexural bend testing was performed to quantify the degree of patch flexibility. The first round of tested patches included the three levels of silk mass and the four levels of glycerol weight ratio. After collecting these results and processing the raw data, the experiment was repeated to increase the sample size from two to six patches per material condition. An additional silk mass level was added ('XHI') to provide further insight into the mechanical properties of baseline patches created from more concentrated silk fibroin solution (~8% w/v). The additional patches were tested and the raw data was used with the patch geometries to calculate the flexural moduli for each mass/weight ratio condition. Based on the amount of material used in the patches, the backing thickness was adjusted in direct proportion to the total silk mass plus the mass of glycerol (no volume change during drying). The averages and standard deviations were determined for each material condition (n = 6 for 'LO', 'MID', 'HI'; n = 4 for 'XHI') and plotted (Figure 25). The influence of the glycerol mass ratio variable on the flexibility outcome was statistically significant (one-way ANOVA, $p < 0.01$ for all glycerol ratios); however, the influence of silk mass on flexibility was only significant at lower glycerol concentrations (one-way ANOVA; p = <0.01, <0.01, 0.127, and 0.949 for 0, 5, 10, and 20% glycerol weight ratios, respectively).

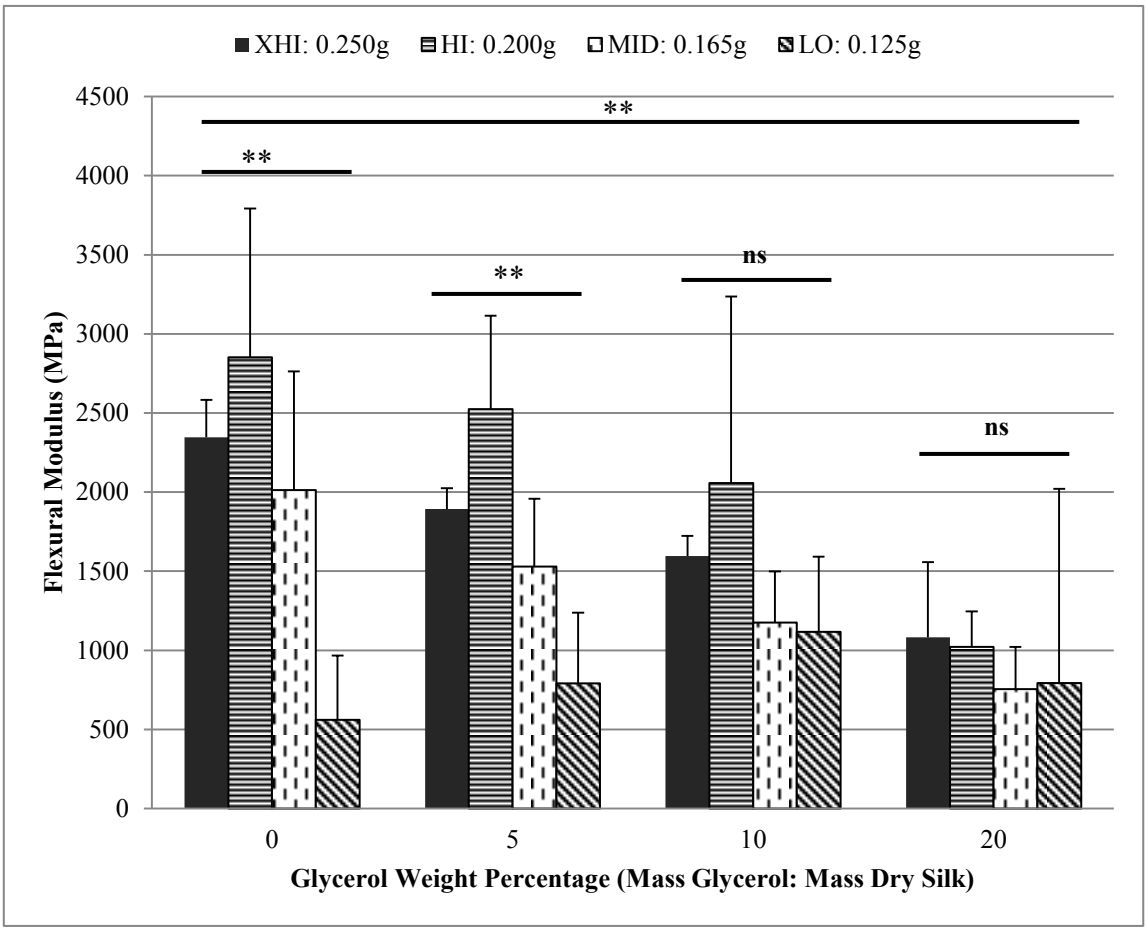

Figure 25. Increasing the glycerol content (mass ratio to dry silk protein) had a significant effect ($p < 0.01$) in decreasing the flexibility of microneedle patches (one-way ANOVA, n = 6 for LO, MID, HI; n = 4 for XHI levels). Increasing the silk mass had a significant effect on patch flexibility at the two lower glycerol mass ratios (one-way ANOVA, $p < 0.01$). Displayed are average flexural moduli for each condition plus one standard deviation. Flexural moduli were calculated from the three-point bend testing raw data by finding the slop of the elastic portion of the load-extension curves and using the patch geometries adjusted for total mass and glycerol content. The mass conditions are for the target total silk protein cast in the microneedle molds and not the final mass of the dried, annealed, and trimmed devices. **: Significance of $p<0.01$; ns: not significant.

5.2.2. Single needle strength testing

One of the most important criteria of this research design project was the ability to maintain the drug release performance characteristic of the baseline microneedle patches in the more flexible ones. This performance depends on the ability of the microneedles to actually penetrate the skin barrier, the stratum corneum, without breaking first. One concern with using a whole-patch blend of silk fibroin and glycerol was that the increase in patch flexibility would come at the expense of weaker microneedles—and that this sacrifice of needle strength would prevent the flexible patches from performing as well. Therefore single needles were fabricated using the same material blends as those tested for flexibility. The needles were subjected to compressive testing, and the force at which the needles yielded was extracted from the raw data and plotted for average plus one standard deviation. Unfortunately, the 'LO' silk mass condition was unable to be tested, as the patch backing was not thick enough to support the needles, resulting in the needles breaking off from the backing during removal from the PDMS molds. Similar issues were encountered with some of the conditions resulting in a sample size of two (standard was n = 3). The majority of the material conditions produced microneedles with fracture forces adequate for skin penetration, based on the threshold of 100 mN as reported in the literature [62] (Figure 26).

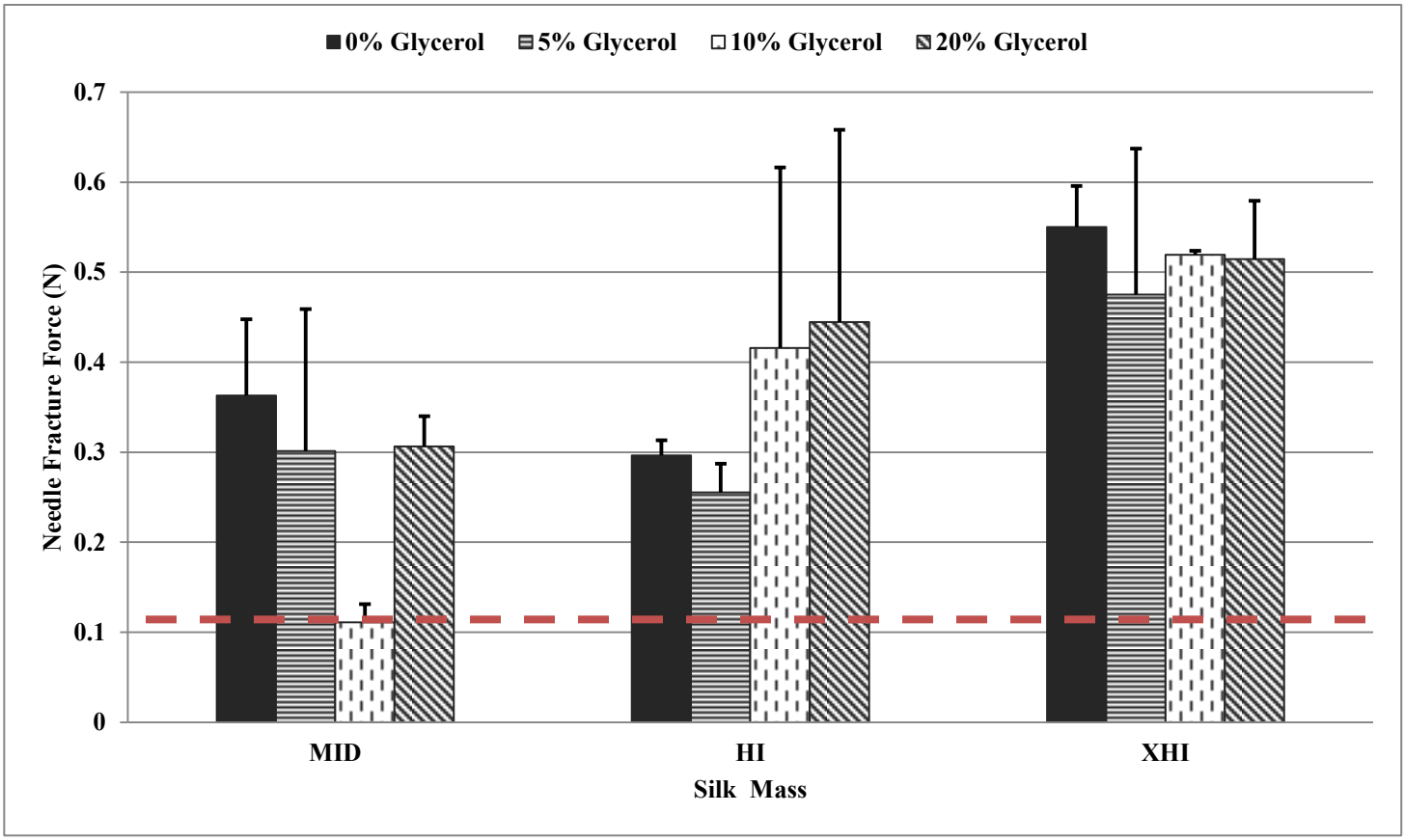

Figure 26. The majority of material conditions used to create more flexible silk microneedle patches possessed adequate needle strength to penetrate the stratum corneum barrier. The threshold for skin penetration (red dashed line) is approximately 100 mN per needle as reported in the literature [62]. This value can vary for different microneedle geometries, but 100 mN provides a good benchmark for microneedle penetration. Plotted are the average fracture forces plus one standard deviation. Sample sizes: n = 2 (MID-0%, HI-0%, HI-5%), n = 3 for the remaining material conditions. Formulation with glycerol had no major effect on the needle fracture force within or between silk mass sample groups. With fracture forces for most of the material conditions recorded well beyond the insertion force requirements, these microneedle devices could be designed with high performance safety ratios (fracture force/insertion force).

5.3 Drug Release Performance of Baseline and Flexible Patches

5.3.1. Controlled release of enzymatic model drug

One of the main objectives of this work was to demonstrate that the drug release performance of silk microneedle patches was conserved through the incorporation of a glycerol plasticizer. After performing single needle studies, a "flexible" patch condition was chosen ('HI', 20% glycerol w/w) due to similar single needle strength to baseline microneedles ('XHI', 0% w/w; 444 ± 214 mN/needle for flexible, 550 ± 46 mN/needle for baseline; Figure 26) with a much lower flexural modulus (7.23 ± 1.59 MPa for flexible, 18.77 ± 1.89 MPa for baseline; Figure 25). The flexible and baseline silk microneedle patches were fabricated and patches were diced into quarters for drug release performance evaluation. The surfaces of the patches were pre-wetted by pipetting droplets of DI water on and off of the devices, and then coating each quarter-patch with 20 μL of horseradish peroxidase solution (0.45 μg/μL). The pre-wetting step improves the evenness of the final drug coating as described in section 4.2.3. These patches were dried overnight on the bench, and then applied to collagen gels that had been prepared with a plastic-wrap coating to mimic the stratum corneum barrier. The application of the patches was staggered such that the removal of the devices from the gels would be coincident, improving the timing of gel digestion and assay completion. The patches were applied to the gels for durations of 24 hours, 12 hours, 4 hours, 1 hour, and 10 minutes, and kept under 0.5 N of weight. Using control patches to determine the percent release from the patches at the time points, it appears that the HRP-coating was released quickly, with no significant difference observed after 4 hours (unpaired t-test, n=4, $p = 0.3571$; Figure 27).

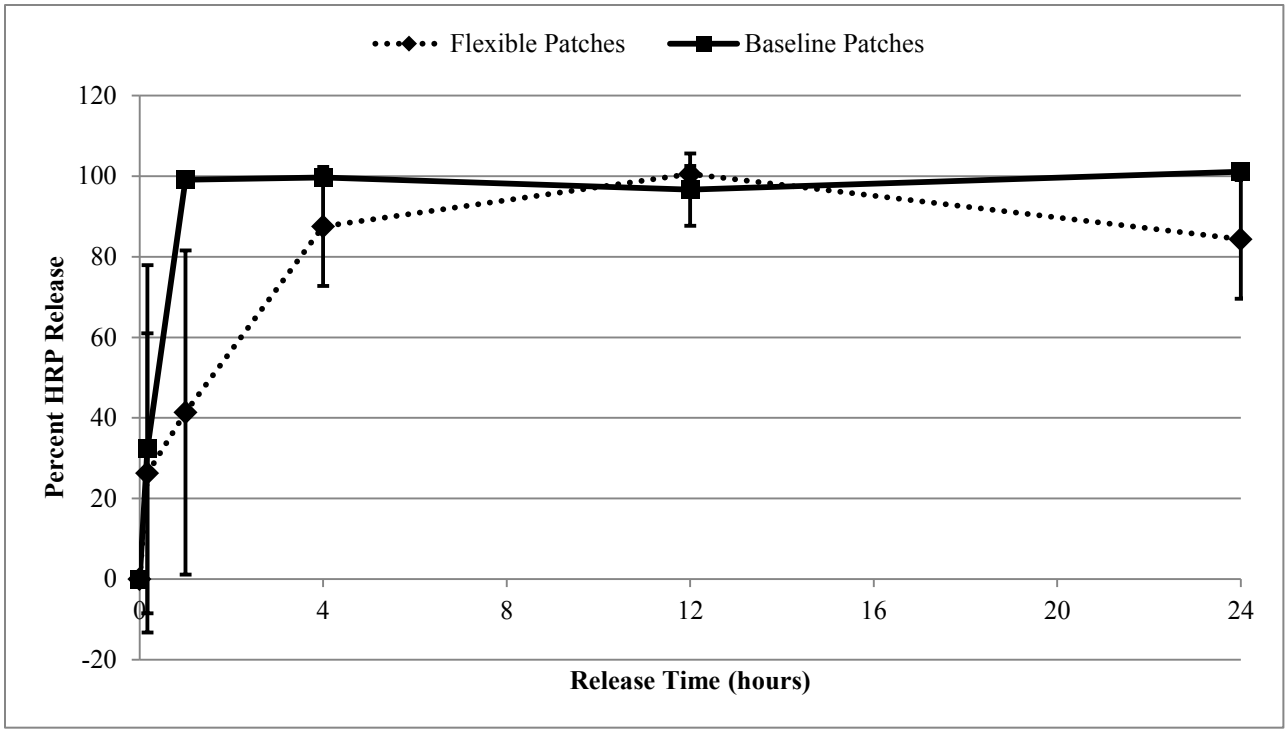

Figure 27. The full coating dose of model drug (HRP) was released quickly from both the flexible and baseline silk microneedle patches into the collagen gel model. Percent HRP release was calculated using patch controls for each drug release time point. No significant difference was observed in the percent release from the baseline and flexible patches after four hours of application (unpaired t-test, $n = 4$, $p = 0.3571$). Plot displays average and ±1 standard deviation for each release time point ($n = 4$).

5.3.2. Evaluation of release on curvilinear surfaces

As previously mentioned, the motivation for conducting this research was the failure of the silk microneedle patches to conform to the curvature of the skin, in some cases limiting the performance of the devices. By improving the overall flexibility of the devices, it was believed that they would better conform to curved surfaces, improving the reliability and efficacy of the devices. We examined the release of baseline and flexible patches into porcine skin that was curved around a metal cylinder with a radius of curvature of 4.25 cm, similar to the curvature of the average forearm (Figure 28A). Baseline and flexible patches were also created using an alternative fabrication method to impart curvature to the patches themselves (described in section 4.3.3). Patches were coated with ovalbumin conjugated with a Texas Red fluorescent dye, applied to the skin manually and kept under the pressure of a rubber elastic band for 15 minutes (Figure 28B). We then removed the microneedle patches and imaged the skin under standard and ultraviolet illumination. Unfortunately, the ultraviolet fluorescence images did not turn out well as the dye could not be seen in the photos. The standard images display a more even needle penetration pattern from flexible, flat microneedle patches than the flat baseline patches (Figure 29A, B). Pre-formed patches also had a greater distribution of needle penetration across the surface area of application (Figure 29C, D).

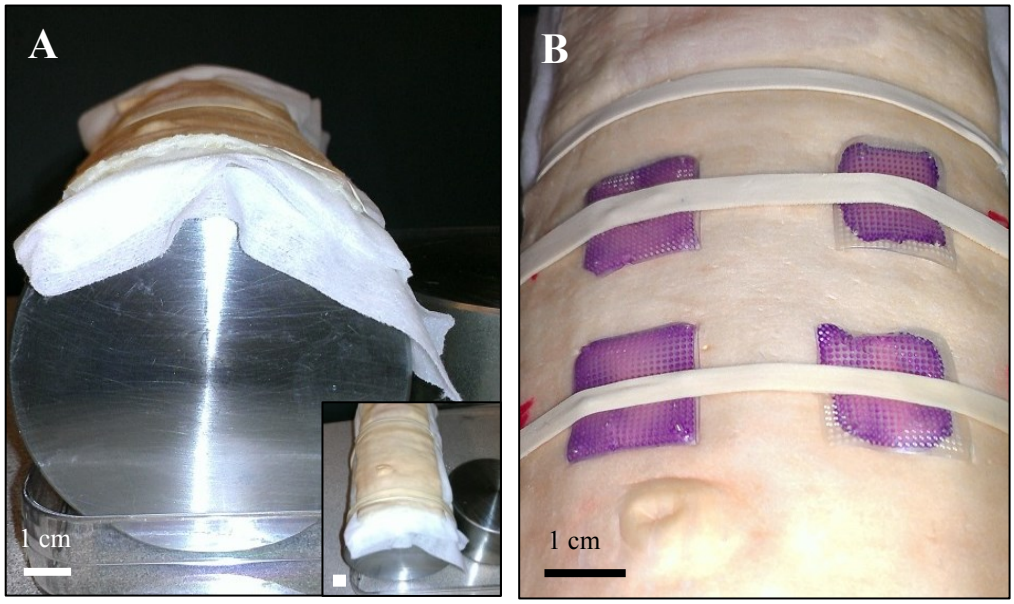

Figure 28. Images of curved skin release study setup. (A) A stainless steel rod of 8.5cm diameter was used as a model for curved the thawed porcine skin into a human "forearm-like" surface. (B) The flexible (left) and baseline (right) microneedle patches were applied for 15 minutes with force applied by a rubber elastic band. Images of release and needle penetration were taken after the patches were removed carefully.

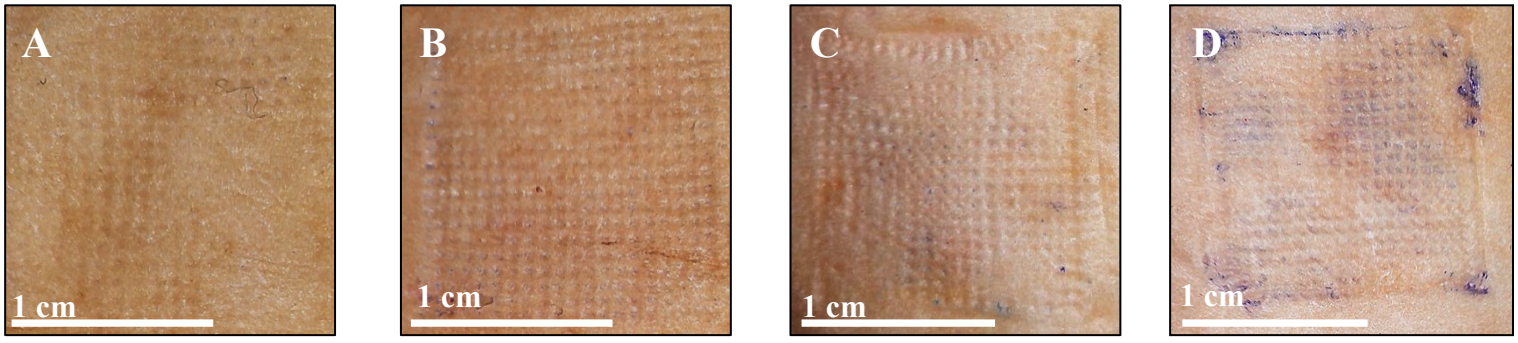

Figure 29. The penetration results of the four silk microneedle patch conditions on a curved porcine skin substrate. (A) Flat baseline microneedle patch displays a vertical needle penetration pattern in the center of the device, but with poor penetration near the edges of the patch. (B) Flat flexible microneedle patches are able to conform to the skin and penetrate throughout the patch area. (C) Pre-curved baseline microneedle patches conform to skin better than the flat baseline patches, but not as well as the flexible and curved microneedles observed in image (D). Purple in the images is the released Texas Red-labeled ovalbumin model drug for release.

5.4 In Vivo Vaccine Delivery Performance

5.4.1 Microneedle administration

For this research aim, we sought to demonstrate the ability to use silk microneedle devices for transdermal vaccination of animal subjects (BALB/c mice) with a commercial influenza vaccine (Fluzone Quadrivalent, Sanofi Pasteur, Swiftwater, PA). Two research studies were performed to evaluate the animal immune response to varying doses and to assess the thermal stability imparted to the vaccine by silk fibroin. Silk microneedles were fabricated as described, and were coated with the vaccine and 1% silk formulation immediately prior to use (dose response) or two-weeks prior to use (stability). Under anesthesia, animals were prepared for immunization by removing the fur on their backs with hair clippers and then 5 minute application of hair removal cream. After using wet paper towels to remove the hair cream, the animal skin was ready for application of a microneedle patch (Figure 30A). The patch was applied to the skin by pinching it between the thumb and index finger, and then was held in place with an adhesive bandage (Figure 30B). The animals that received silk microneedle patches were separated into individual cages overnight to prevent the patches from being chewed off. After 24 hours of administration, the patches were removed from the animals. No issues were observed with patch adherence to the backs of the animals; there were zero cases where the patches were chewed off or had fallen off during the administration window.

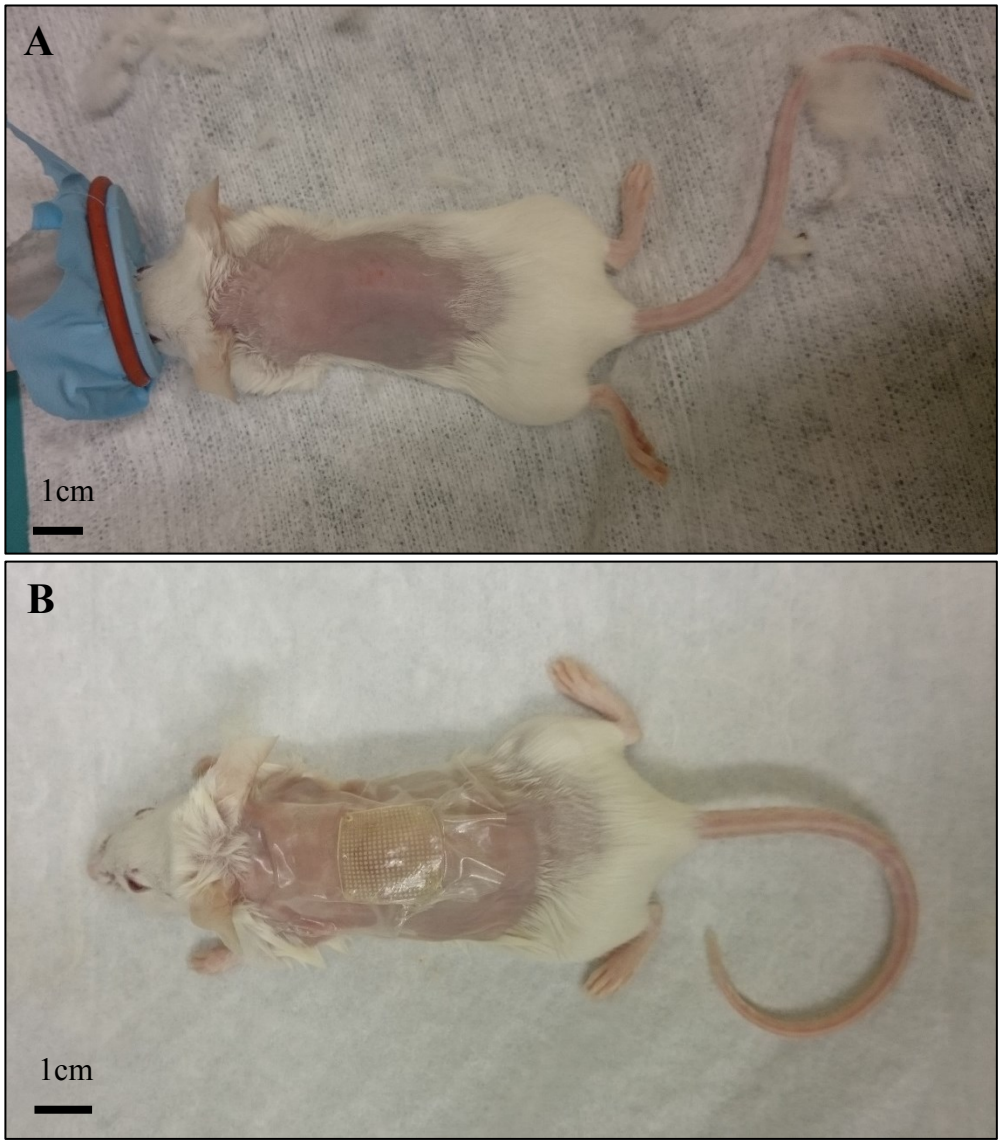

Figure 30. Microneedle administration to BALB/c mice. (A) The region of administration was prepared by first shaving the animal's fur using hair clippers, applying hair removal cream for 5 minutes, and then thoroughly removing the cream from the animal's skin. The animal was under isofluorane anesthesia (administered via a nose cone) throughout this process. (B) Silk microneedle devices were then applied to the animal's back and were adhered using Tegaderm® film dressing. No patches were observed to have been removed by the mice after a 24-hour period of administration.

5.4.2 Dose response

The first phase of this *in vivo* vaccine delivery study was to examine the immune response of the BALB/c mice to varying doses of influenza vaccine. This would provide insight over the minimum delivery dose needed to elicit a robust immune response. For this aim, microneedle patches were prepared by coating 1 ug, 6 ug, and 12 ug of commercial influenza vaccine antigen formulated with 1% silk fibroin onto the surface of the silk microneedle patches. Two controls groups were also included in this experiment: a negative control microneedle patch coated with water only and a positive control subcutaneous injection of 12 ug of vaccine (no silk). The animals were immunized and then boosted at two-weeks, with blood samples collected prior to each immunization and at day 34 to characterize the response over time. These blood samples were processed to isolate serum (no cells or clotting proteins) which was then stored at -20ºC. Aliquots of serum from each animal of an experiment group were combined to form a pooled sample which was then assayed through indirect ELISA for anti-silk and anti-influenza immunoglobulins. The three blood collection time-points were examined for anti-influenza antibody titer, while only the terminal blood samples were used for anti-silk titer. Endpoint titers and the fold-change in absorbance (relative to negative control) indicate a strong total and IgG-specific immune response from microneedle patches coated with 6 and 12 ug of influenza vaccine, comparable to the injected positive control (Figure 31A-E). The anti-silk immune response was found to be mild in comparison to influenza, with detectable IgG-specific titers of 500 from only two microneedle patch conditions (Figure 32).

Figure 31A. Anti-influenza endpoint titer

		MN Patch, 0ug	MN Patch, 1ug	MN Patch, 6ug	MN Patch, 12ug	Injection (SQ), 12ug
Total Immune Response	Pre-Immunization (Day 0)	2500	2500	500	500	100
	Post-Immunization (Day 14)	500	500	2500	2500	62500
	Post-Boost (Day 34)	500	500	62500	62500	312500
IgG-Specific Immune Response	Pre-Immunization (Day 0)	100	100	500	100	500
	Post-Immunization (Day 14)	100	100	500	500	2500
	Post-Boost (Day 34)	500	500	12500	12500	312500

Figure 31B. Total immune response, 1:500 dilution

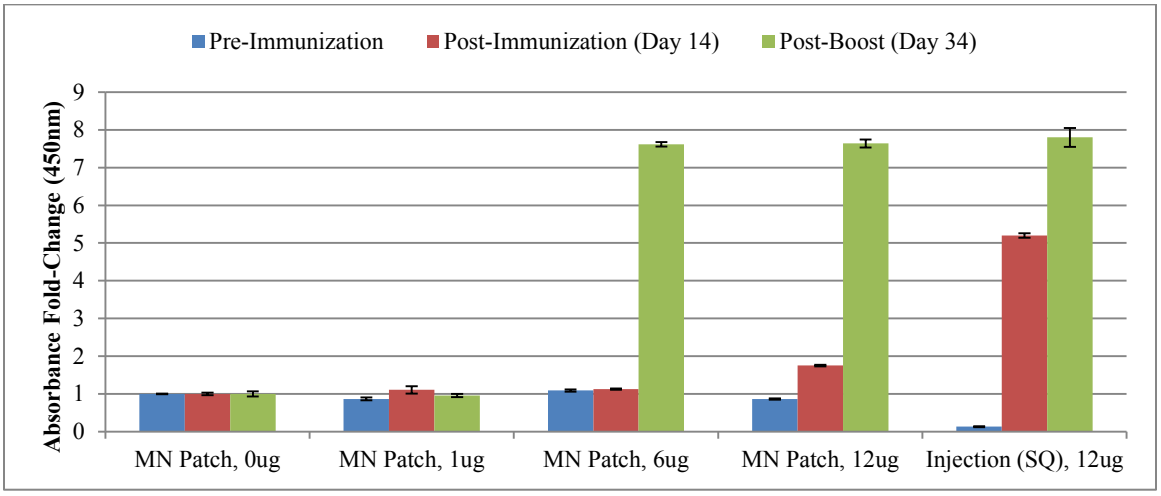

Figure 31C. Total immune response, 1:2500 dilution

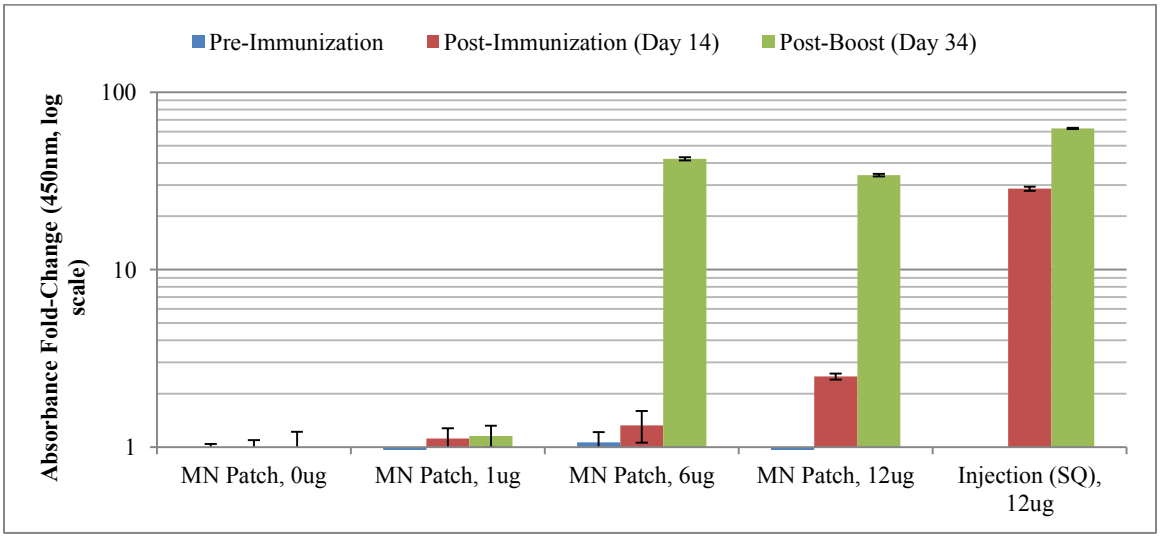

Figure 31D. IgG-specific immune response, 1:500 dilution

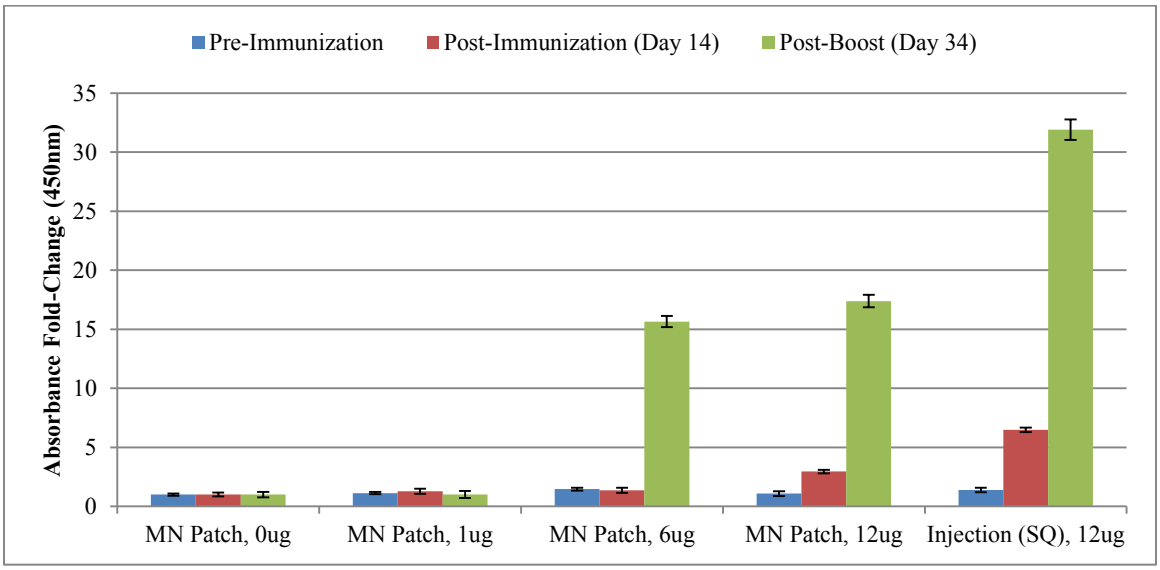

Figure 31E. IgG-specific immune response, 1:2500 dilution

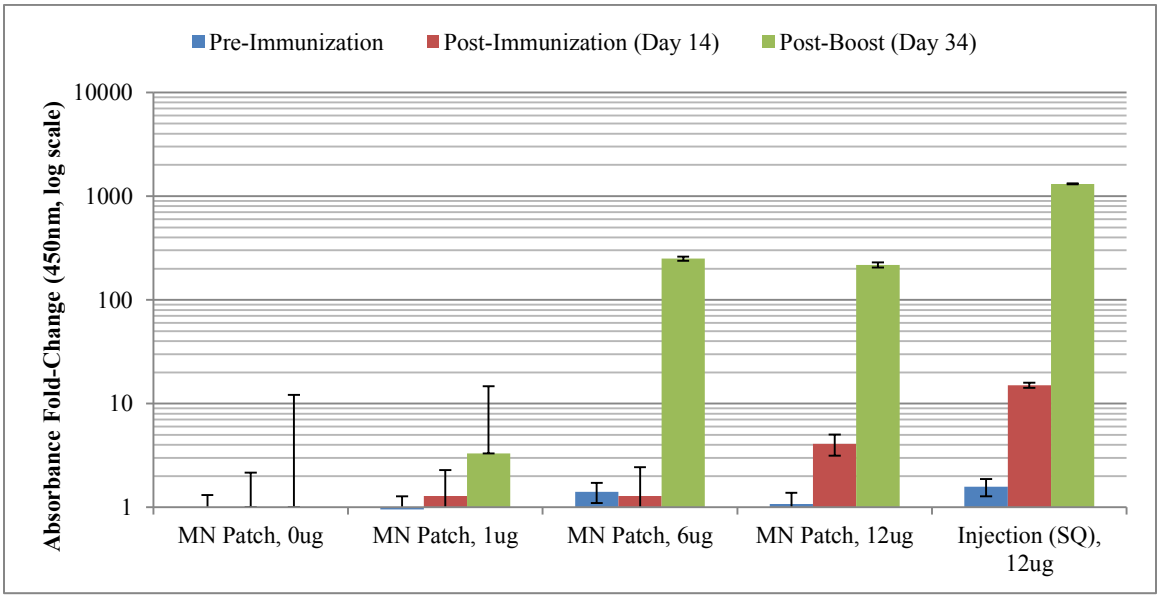

Figure 31. Anti-influenza dose response results. To examine the serological immune response of BALB/c mice to influenza vaccine doses through transdermal administration with microneedle patches, indirect ELISAs were performed. (A) Endpoint titers were calculated as the reciprocal of the highest dilution at which an absorbance signal greater than twice the background signal (no serum). (B, C) The total anti-influenza immune response at two dilutions, calculated as the fold-change in absorbance relative to the negative control after subtracting background signal. (D, E) The IgG-specific immune response to influenza vaccine calculated as fold-change in absorbance relative to the negative control (MN patch, 0ug). Comparable total and specific immune responses are observed after booster, with a reduced primary response. A diminished response is observed from the 1ug dose condition.

(A) Total anti-silk immune response

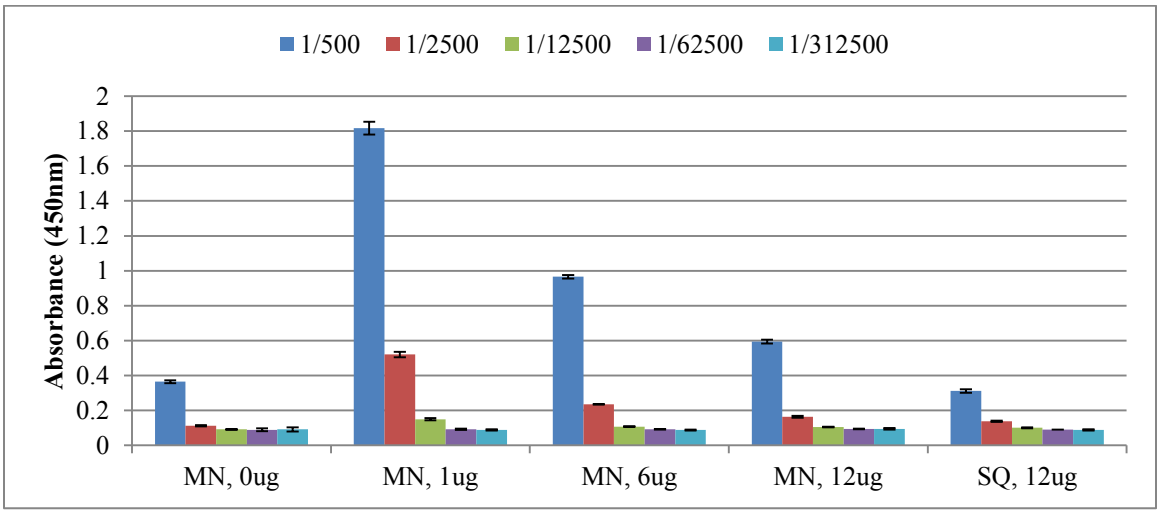

(B) IgG-specific immune response

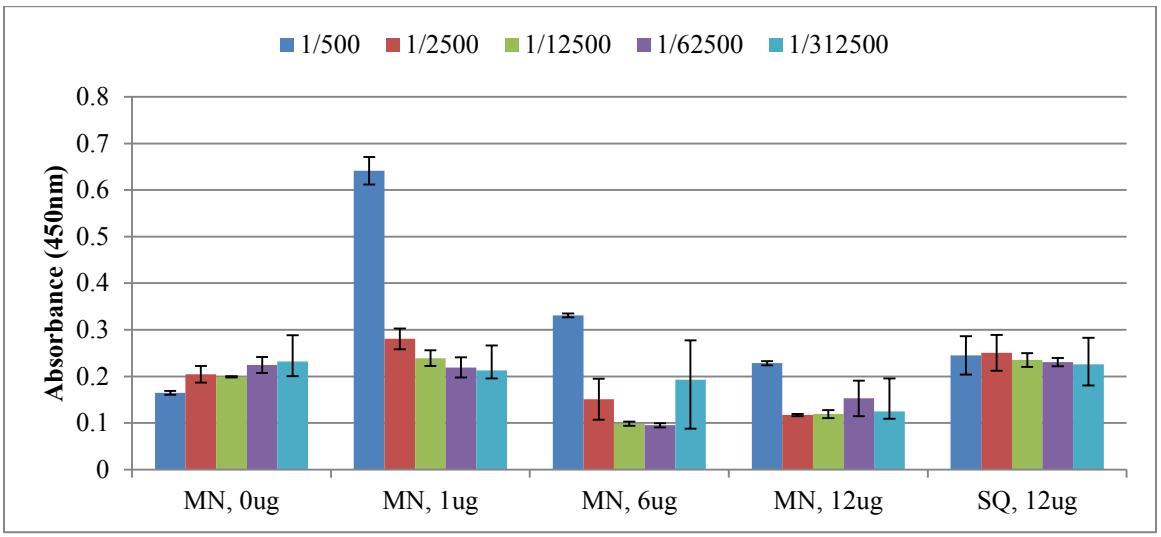

Figure 32. Anti-silk dose response results. Terminal blood samples (day 34) were assayed for anti-silk antibody levels following two exposure events. (A) The total immune response to silk shows elevated signal from the 1/500 dilution series for the vaccine-coated microneedle groups. There is also elevated signal from the silk-absent injected control group. (B) IgG-specific response of BALB/c mice against silk is significantly lower (1/500 dilution) than the response to influenza, suggesting silk biocompatibility as vaccine excipient and delivery vehicle.

5.4.3 Thermal stability

The second major aspect of this *in vivo* study was to examine the temperature stabilization properties of silk fibroin protein on influenza vaccine. Previous studies have demonstrated the ability of silk fibroin to preserve the activity of enzymes, antibiotics, and vaccines at elevated storage temperatures [8, 168]. We aimed to translate these findings to the solid microneedle format and validate the stability findings with a commercial influenza vaccine. Microneedle patches were prepared and coated with a 12 microgram dose of influenza vaccine formulated with 1% (w/v) final concentration of silk protein. After drying, these patches were stored at elevated temperatures (25ºC, 37ºC, and 60ºC) for two weeks before immunization. Liquid vaccine vials were left unaltered and were stored under the same conditions as matched controls. The immunization and blood collection schedules were identical to the dose response study to permit comparison to the negative and positive controls from that experiment. Indirect ELISAs against influenza and silk were performed to determine the endpoint antibody titers and fold-change in detected signal between groups. After boosting, comparable total and IgG-specific immune responses are observed from patches and paired injection controls (Figure 33A-E). Despite a decreased primary immune response from the microneedle patches, a robust secondary immune response is still generated. Again, anti-silk immune responses are generated but are mild in comparison to the anti-influenza immune response with much lower IgG titers (Figure 34).

Figure 33A. Anti-influenza endpoint titer

		MN Patch, 25ºC	MN Patch, 37ºC	MN Patch, 60°C	Injection (SQ), 25°C	Injection (SQ), 37°C	Injection (SQ), 60°C
Total Immune Response	Pre-Immunization (Day 0)	500	500	500	2500	500	500
	Post-Immunization (Day 14)	2500	2500	2500	12500	12500	12500
	Post-Boost (Day 34)	312500	62500	12500	312500	312500	62500
IgG-Specific Immune Response	Pre-Immunization (Day 0)	100	100	100	100	100	100
	Post-Immunization (Day 14)	500	500	500	500	2500	2500
	Post-Boost (Day 34)	62500	62500	12500	62500	62500	62500

Figure 33B. Total immune response, 1:500 dilution

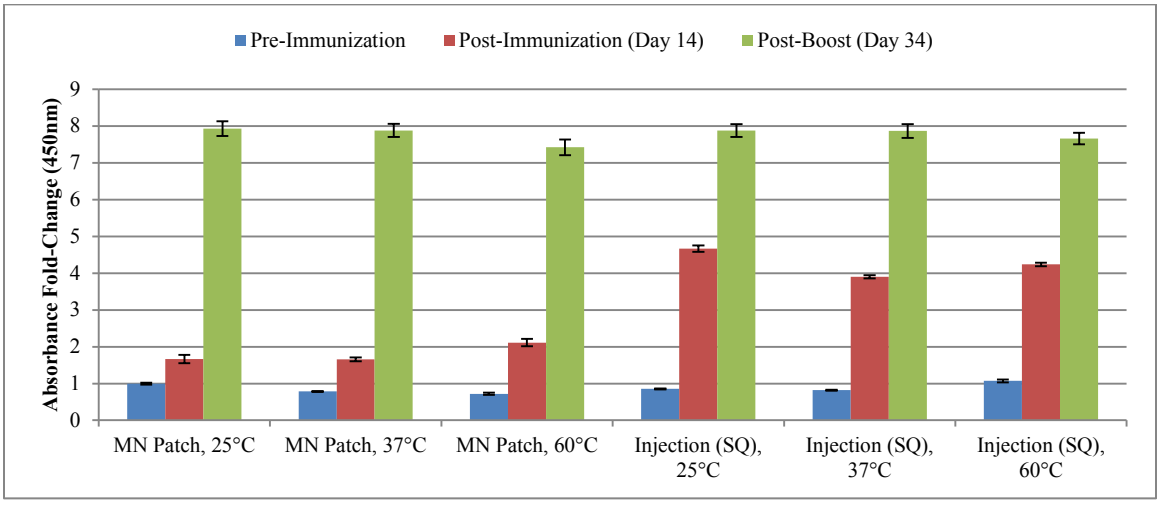

Figure 33C. Total immune response, 1:2500 dilution

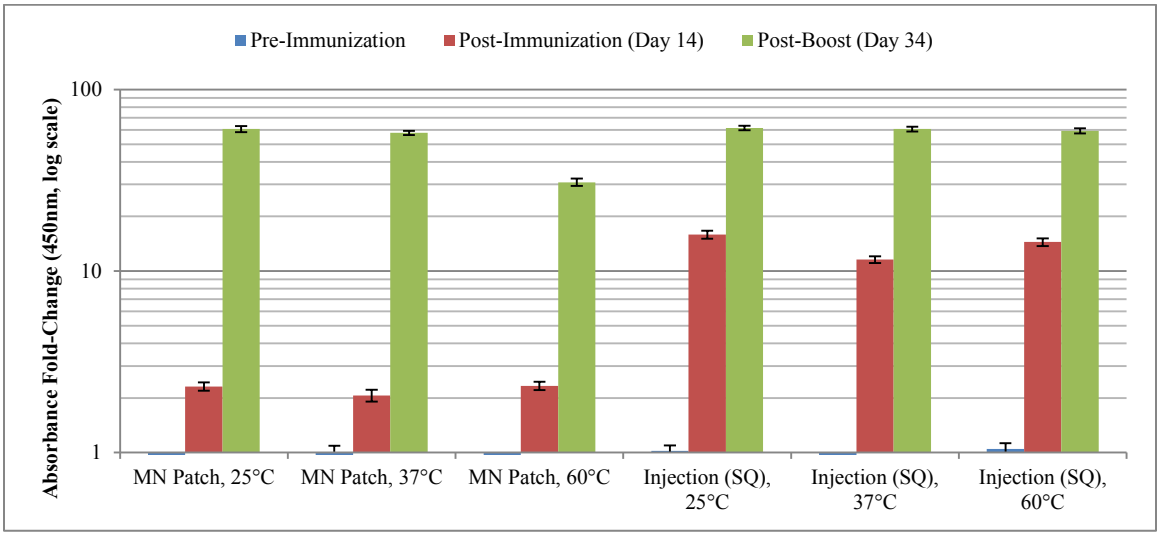

Figure 33D. IgG-specific immune response, 1:500 dilution

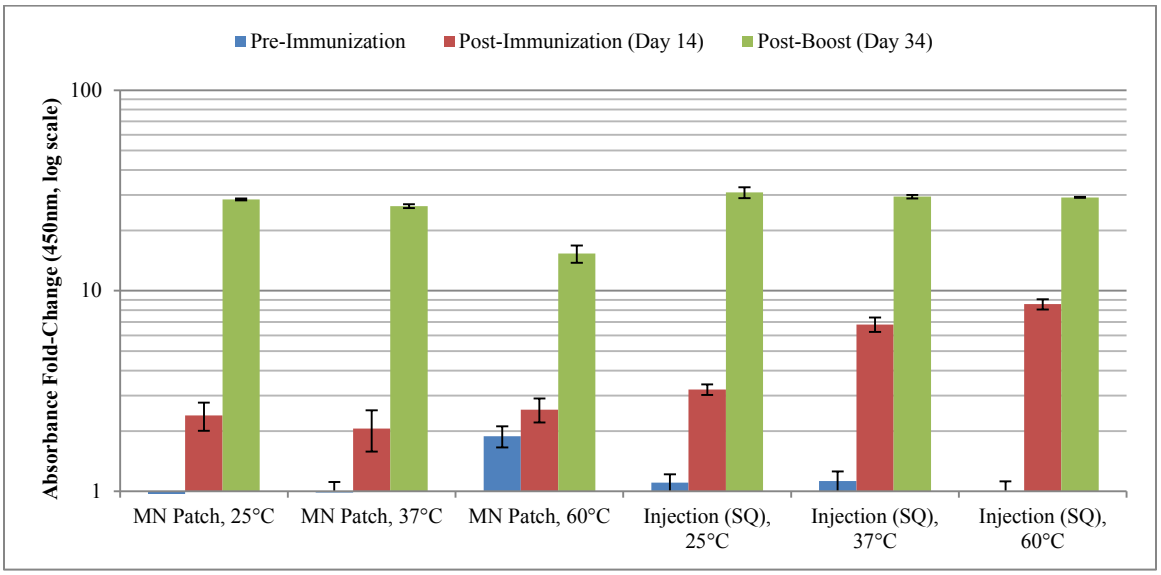

Figure 33E. IgG-specific immune response, 1:2500 dilution

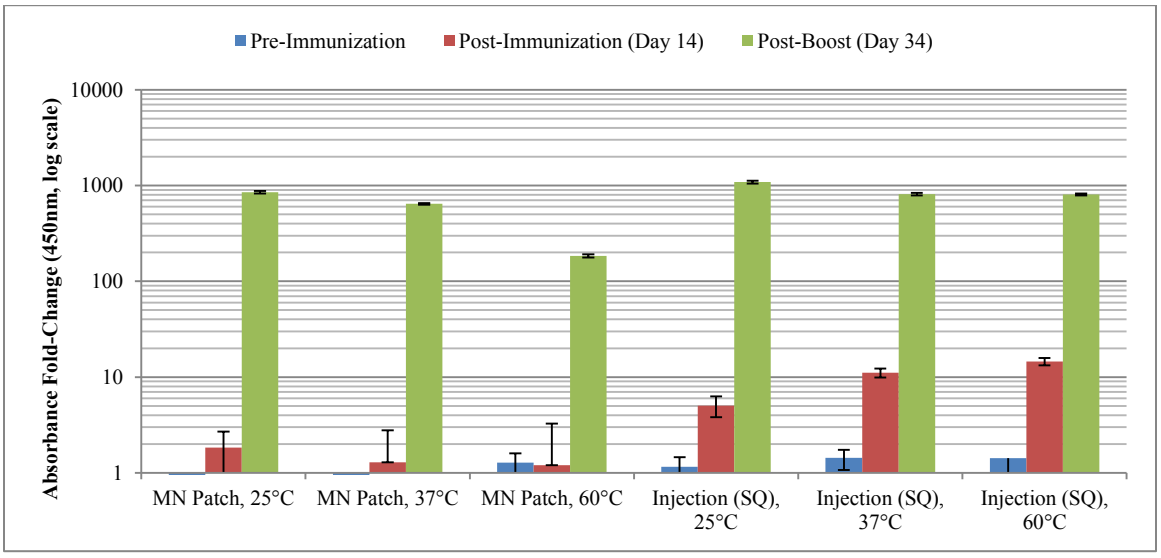

Figure 33. Anti-influenza temperature stability results. Indirect ELISAs were performed to assess the seroconversion of animals immunized with vaccine stored at different temperatures for 2-week periods. (A) Endpoint titers indicate a diminished total immune response with microneedle patches stored at elevated temperatures without any sacrifice in IgG-specific response relative to paired liquid controls. (B, C) Total immune response was determined using a biotinylated secondary antibody against heavy and light chain regions of the primary mouse antibodies. Similar immune responses are observed after boosting for patches compared to injections, with a lower primary immune response. (D, E) For IgG-specific responses, a decrease in fold-change is observed for the microneedle patches stored at 60°C.

(A) Total anti-silk immune response

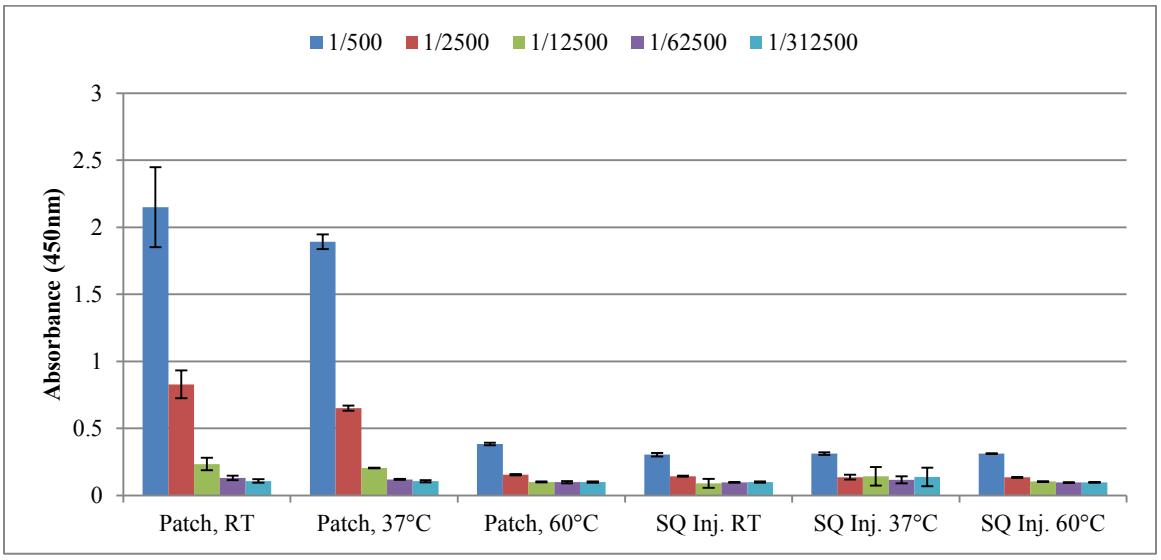

(B) IgG-specific immune response

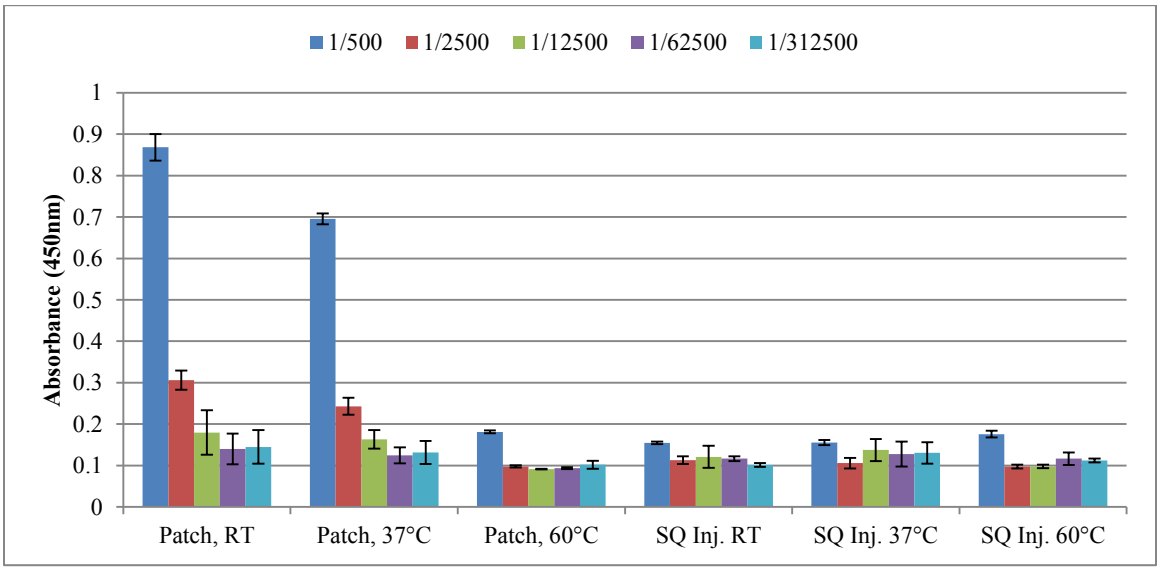

Figure 34. Anti-silk temperature stability results. We performed anti-silk indirect ELISAs using the final time-point blood samples to determine the immunogenicity of the silk fibroin formulated into the vaccine coating. The patches stored at 60°C display no significant increase in total or IgG-specific anti-silk response as compared to the injected controls. A mild response is generated from the room temperature and 37°C stored microneedle patches, but is significantly smaller in magnitude than the anti-influenza responses of the animals.

5.5 Rapid and Scalable Microneedle Fabrication

5.5.1 Drop-cast microneedle patches

We revisited the drop-casting fabrication technique after briefly investigating it in the context of creating flexible multi-material microneedle patch devices. The technique offers the advantage of more rapid drying, freeing up molds to allow faster throughput and a more efficient process. Standard microneedle molds were prepared for this process by removing the vertical edges that normally compose the trench to be filled with 3-4 mL of silk solution. With these molds, we optimized the initial casting process by investigating the first volume addition, step to force silk solution into the needle wells, bubble removal, and final silk volume. We found 500 uL of drop-cast volume to be sufficient to allow solution to fully cover the surface area of the mold while providing enough depth to allow bubbles to be removed. Both mechanical disruption of the needle wells and vacuum pulling were attempted as methods to remove air from the needle wells. Cycling the vacuum on and off five times over a twenty minute period was the more effective and reproducible method to remove air from the microneedle mold. The remaining bubbles were carefully removed and an additional 500 uL of silk solution was added to reach a final volume of just under 1 mL. The maximum drop-cast volume is about 1.2 mL; beyond this volume there is risk that the solution droplet will spill over the edges of the mold.

The first comparison between the drop-cast and spin-cast microneedle patches that was performed examined the difference in material waste. With the spin-cast microneedles, a significant portion of the dried silk is found in the vertical edges of the device, which must be trimmed off before drug coating and administration. Four devices

were created by filling PDMS molds with 800 uL of silk solution, centrifuging, and then filling up the molds with varying volumes of silk solution to create a range of masses. The devices were weighed after drying and again after being water-vapor annealed and trimmed. Percent loss was calculated as the change in mass divided by the initial mass value and was found to be an average of 71.63% (Table 5). The mass change of the silk material before and after water-vapor annealing and drying was assumed to be negligible.

Table 5. Material loss calculation for spin-cast microneedles. Masses of spin-cast patches were obtained before annealing, drying, and trimming and after this process. Material loss percentages were calculated to be the material loss in the silk edges divided by the initial mass of the device. Mass change of the silk protein before and after the annealing process was assumed to be negligible. With drop-cast needles there is no trimming step performed after annealing and drying since the material is limited to the surface area of the needle backing.

Sample	Initial Mass (g)	Final Mass (g)	Mass Loss (g)	Material Lost (%)
1	0.18478	0.05375	0.13103	70.91
2	0.24541	0.05967	0.18574	75.69
3	0.19854	0.05889	0.13965	70.34
4	0.24723	0.07515	0.17208	69.60
			AVERAGE	71.63

We then compared patches prepared through the two fabrication techniques to examine if there were any differences at the macroscopic and microscopic levels. Specifically, we looked at the flexibility of the patches through three point bend testing to compare with the results from section 5.2.1 and performed ATR-FTIR to examine differences in the secondary structure content of the microneedle devices. For mechanical testing, drop-cast patches were prepared with four weight ratios of glycerol—0%, 5%, 10%, and 20%. The patches were flexed in the 3-point bend test apparatus shown in

Figure 10 to examine their compressive extension with applied load. The results were processed in the same manner as described for the flexible patch investigation (Figure 35).

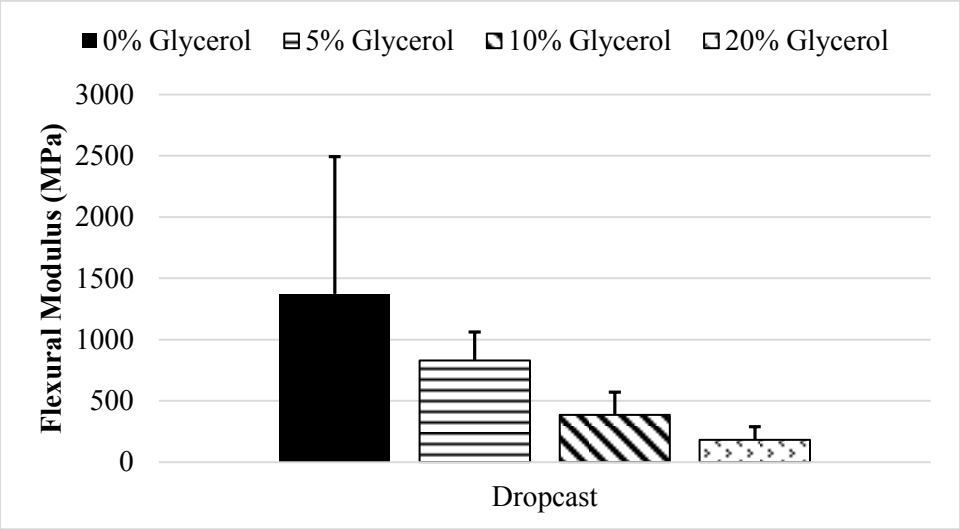

Figure 35. Flexural bend test results for drop-cast microneedle patches. Without examining the masses for each tested patch, the flexural modulus results appear on the same order of magnitude as the spun-cast microneedle patches. The flexural modulus values appear to mimic those of the 'HI' mass condition of 0.2g of dried silk (0.06g after trimming). These devices were produced with 1mL of 6.1% silk solution (0.061g), thus corroborating the original results.

The final comparison was to use ATR-FTIR to determine the relative secondary structure content of the devices produced through both fabrication techniques. Spin-cast patches were prepared with 5.4% silk fibroin solution (30 MB) and were annealed, trimmed, and dried. In parallel, 8.3% drop-cast microneedle patches were created with a volume (739 uL) designed to produce devices with the same mass as the spin-cast needles, assuming a 71.63% mass loss. The smooth film backing of the microneedle devices was placed in contact with the instrument crystal to ensure accurate measurement. The absorbance spectra were collected and used to calculate the relative changes in content (β-sheet and random coil) at known wavenumbers from the literature (Figure 36).

(A)

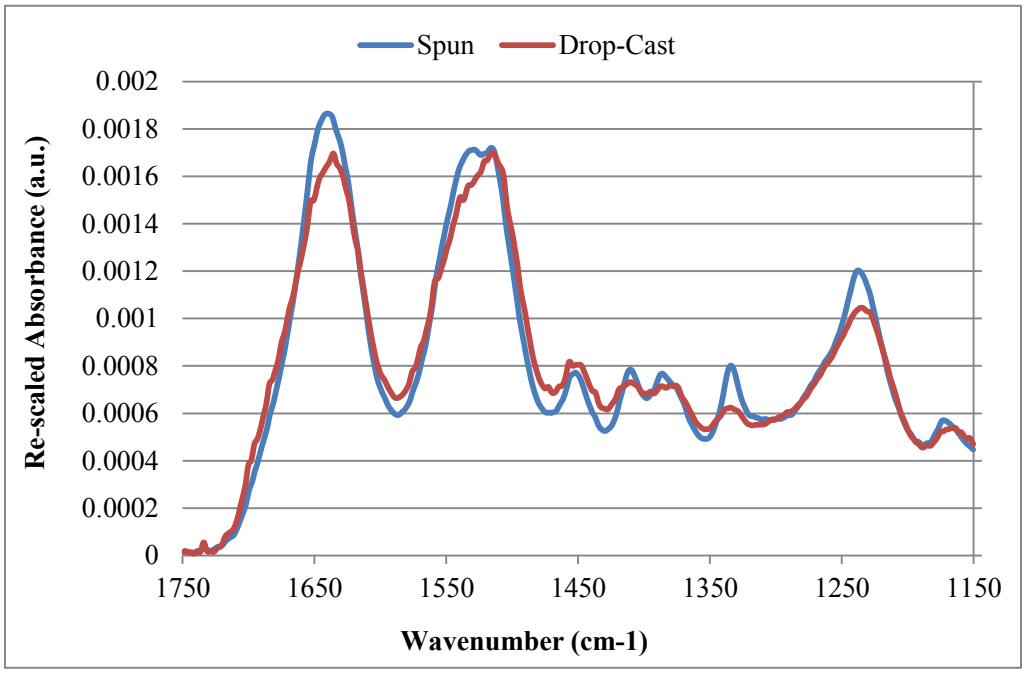

(B)

Structure (Wavenumber)	Spin-Cast (a.u.)	Drop-Cast (a.u.)	Change (%)
β-turns (1695)	0.000356451	0.000476649	+33.72%
β-turns (1680)	0.000678843	0.000780653	+14.99%
β-sheets (1667)	0.00104224	0.001074865	-25.10%
α-helices (1656)	0.00149794	0.001366313	-8.79%
Random coil (1644)	0.001844365	0.001611922	-12.60%
β-sheets (1630)	0.001736519	0.001626384	-6.34%
Random coil (1540)	0.001638016	0.001507696	-7.96%
β-sheets (1520)	0.001696802	0.001667174	-1.75%
β-sheets (1270)	0.000749201	0.000733381	-2.05%
Random coil (1225)	0.001018804	0.000976159	-4.19%

Figure 36. ATR-FTIR spectra comparison for spun and drop-cast microneedles. ATR-FTIR spectra were recorded for three microneedle patches in each condition and the spectra were averaged. (A) The curves for each condition were preprocessed by truncating to the 1150-1750 cm^{-1} region of interest, rescaling e
ach to a range of 0 to 1, and then standardizing the total area under the curve. (B) Changes in the absorbance of the drop-cast patches relative to the spun patches at wavenumbers corresponding to different silk secondary structures were compiled and converted to percentages [170, 189].

5.5.2 Dissolving silk microneedles

The drop-cast method allows silk microneedle devices to dry much more quickly, theoretically allowing them to dry to a more amorphous crystalline state and preserving their solubility. We investigated this hypothesis by producing multi-component (needles and backing) microneedles, as well as soluble full patches with the standard drop-cast molds. Three-needle devices were the first dissolving microneedles studied as the needle structures were slightly larger and allowed easier visual inspection of dissolution. As the process was developed, the appearance of the devices improved and the lamination between the two layers became more uniform (Figure 37). Since the needle structures in this mold were larger, the silk film formed a divot inside the needle well. As demonstration that this could be filled with a separate material to create a three-component device, blue food coloring was added to silk solution and incorporated into this middle phase.

Figure 37. Progression of three needle devices with process development. Initial devices displayed poor lamination between layers (left). As the lamination process was improved, the appearance of the devices did as well (middle) and it was even demonstrated that a third component could be included between the needles and backing in the needle divot that formed during drying of these larger structures. This could allow further development into a device with multiple programmable release kinetics.

To examine how the three-needle devices degraded we performed a series of dissolution experiments to evaluate the effects of different material and process variables. The devices were fabricated with and without a 40% (w/w) glycerol silk blend to laminate the two components together, two different silk boil times in the needle component layer (30 minute boil and 60 minute boil), and three different concentrations of silk with the same drop-cast volume (Figure 38). These devices were dissolved for either one minute or 15 minutes in deionized water, and weighed after drying. Percent mass loss was calculated and we observed a significant increase in dissolution when glycerol was added to the lamination layer (t-test, $n = 3$, $p < 0.05$) and when the devices were allowed to dissolve for 15 minutes instead of one minute (t –test, $n = 3$, $p < 0.05$).

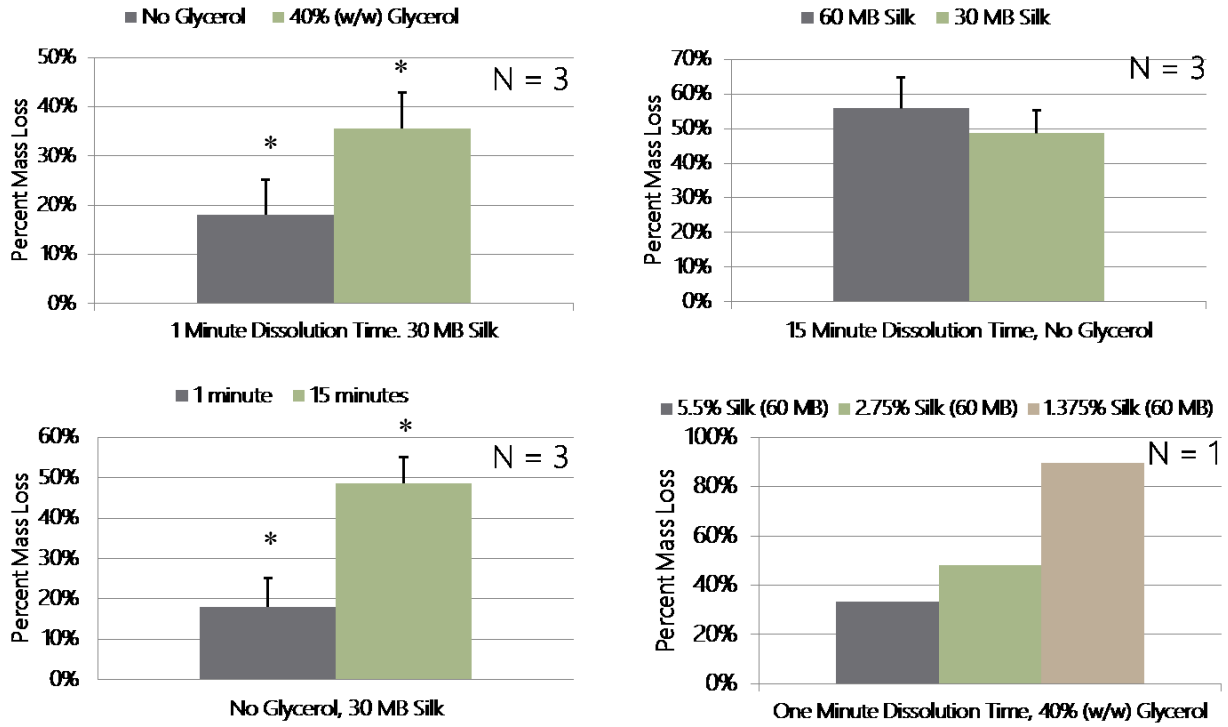

Figure 38. Dissolution comparison of two-component devices with different processing variables. A significant increase was observed when glycerol was added to the solution used to laminate the needle and backing layer together (top left, $n = 3$, $p < 0.05$). With longer dissolution time, more degradation was also observed (bottom left, $n = 3$, $p < 0.05$). There was no significant difference in the two boil time silk solutions.

We also loaded the three-needle devices with HRP to visualize the spatial release of enzyme into a model gel loaded with the colorimetric substrate TMB. The two-component devices were fabricated with HRP loaded in the microneedle solution (0.5 mg/mL). The gelatin gels were also prepared and contained 5% (v/v) TMB substrate to allow visualization of the HRP release. The three-needle devices were applied directly to the substrate-laden gel and allowed to release their HRP payload for 5 minutes. The gel was then developed in 2 M sulfuric acid and was sandwiched between two glass slides for imaging (Figure 39). This same process was later repeated with whole dissolving microneedle devices to confirm their ability to penetrate a stratum corneum model and release bulk-loaded HRP.

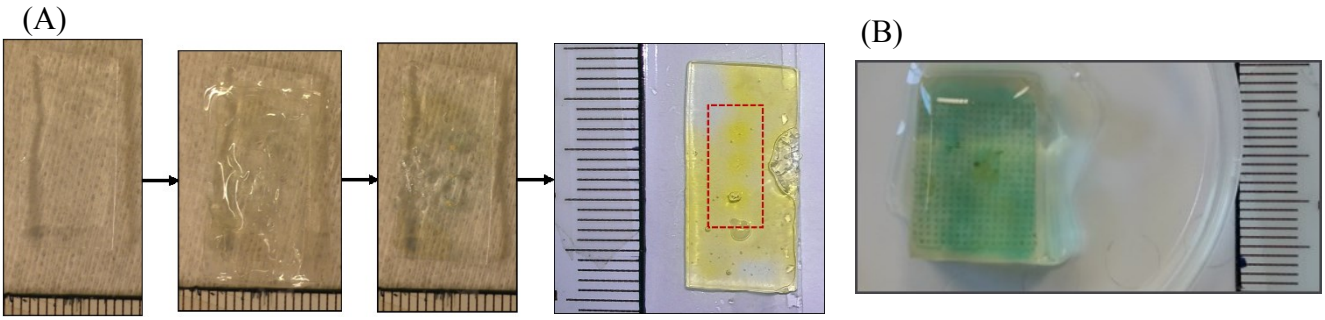

Figure 39. Spatial release pattern of dissolving microneedle devices. (A) Gelatin gels are prepared with incorporated TMB substrate before a three-needle device is applied for five minutes before being removed. The gel is then placed in sulfuric acid to develop the colored TMB product into yellow. A region around the three needle structures (red dotted line) has been highlighted. The area of release outside this space is due to release from the HRP-loaded needle film that is laminated to the backing; the HRP is not localized to the needles themselves. (B) This approach was repeated using full microneedle patches into a gel covered with Parafilm to demonstrate the ability of the device to maintain strength to cross the skin barrier and release a bulk-loaded payload.

The dissolution of full 20 x 20 arrays of silk microneedles was next addressed. Because the rate at which the silk microneedle dry determines their solubility, we investigated variables that we believed may impact the drying rate of these devices: silk concentration and device mass (drop-cast volume). Full microneedle patches were produced with two different silk concentrations (5.5% and 8.3%) at a range of masses by varying the final drop-cast volume. The patches were weighed before and after being dissolved in water for three minutes and subsequently dried. We found well-correlated negative linear relationships between the initial device mass and the overall mass lost during the dissolution step (Figure 40).

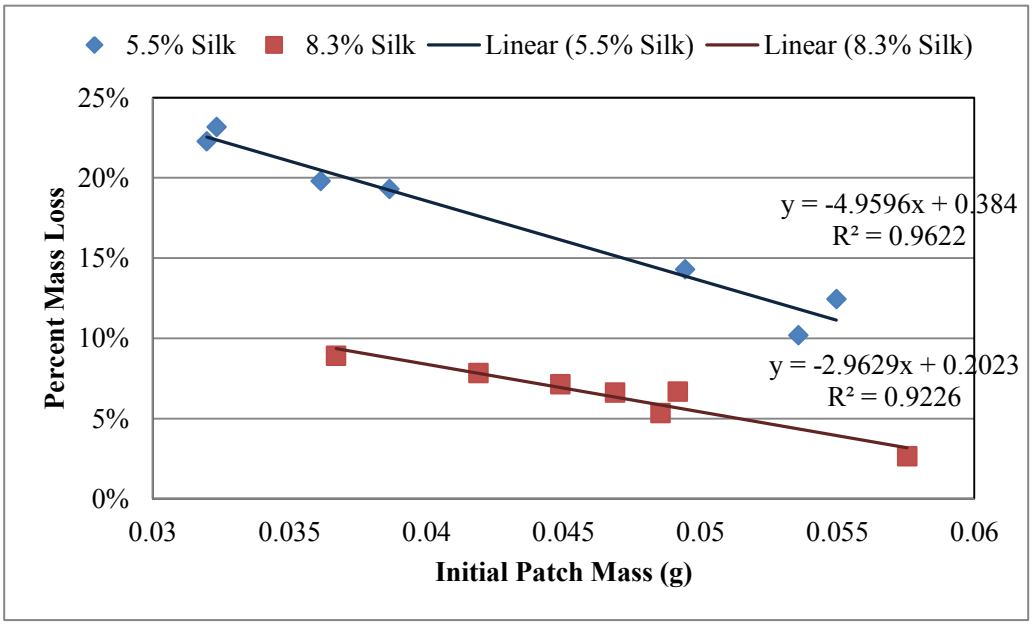

Figure 40. The relationship between initial device mass and percent mass lost for full silk microneedle patches. The devices were produced from two different concentrations of silk with different dropcast volumes to create series of patches with different total weights. These microneedle devices were weighed before and after three minutes of dissolution in water (needles down). Strong linear correlations are observed for both silk concentrations, with greater slope from the lower silk concentration.

In addition to the visual release study with the standard array microneedle design as described in Figure 39, HRP-loaded microneedles were used in two more release studies. The first experiment was designed to evaluate the use of an applicator device to standardize the administration process of the needles to the skin. This experiment would also validate that the drop-cast devices maintain their ability to penetrate the skin, even without water-vapor annealing, allowing rapid dissolution *in situ* and therapeutic release. We prepared silk microneedles with bulk-loaded HRP and used our 3D-printed applicator to administer them to Parafilm-covered gelatin gels. This layer of Parafilm is designed to mimic the stratum corneum barrier of the human epidermis. The needles were left on the gels for three durations: 60 seconds, 30 seconds, and 0 seconds (immediately removed). While no clear release kinetics were observed, it was demonstrated that the devices can deliver roughly 30-50% of their bulk HRP payload after penetrating the Parafilm barrier (Figure 41).

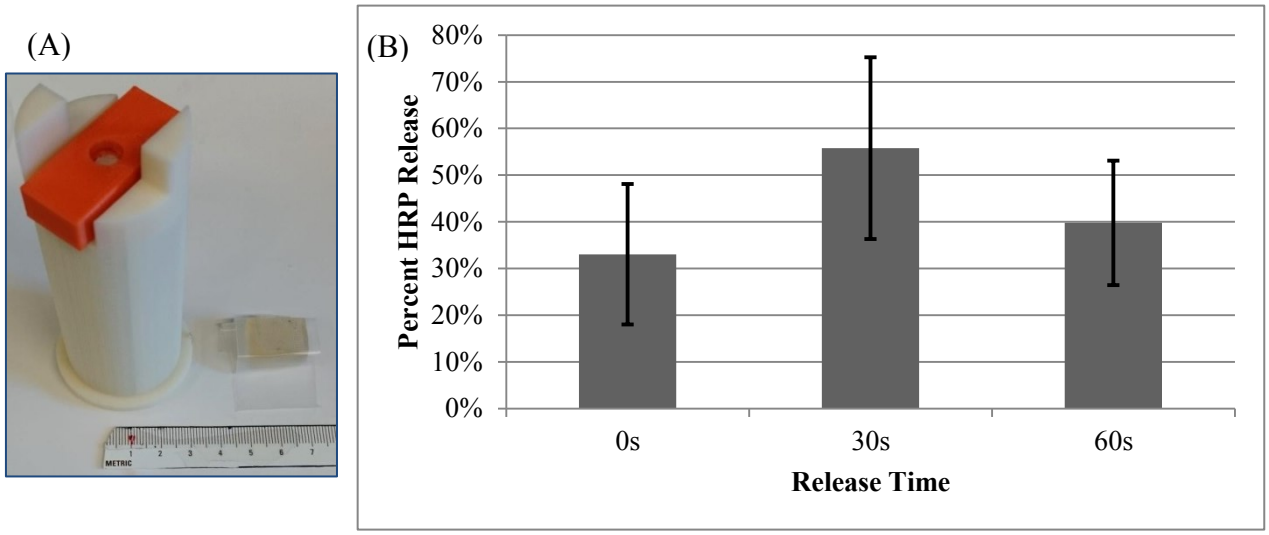

Figure 41. HRP-loaded silk microneedle release into *in vitro* skin model using a 3D-printed applicator. (A) A spring-loaded device was prototyped using a 3D-printer to standardize the administration of silk microneedles to a Parafilm-covered gel as a skin model. (B) Although inconsistent release results were observed over three quick time-points, approximately 30-50% of the bulk-loaded HRP cargo was released.

The second release study with whole microneedle arrays was to determine whether the release kinetics could be controlled by changing the degree of insolubility of the devices using a glycerol blend. While glycerol was demonstrated to have a non-significant effect on the flexibility of the microneedle patches (Figure 25), it could have the benefit of changing the release kinetics of the devices. Therefore, we created HRP-doped microneedle devices from 10, 20, and 30% weight ratio blends of glycerol to silk. These devices were applied directly to gelatin gels without a Parafilm barrier and were allowed to release their payload for 15 minutes. We saw more release from the 10% (w/w) glycerol devices than from the 20 and 30% devices (Figure 42). Unfortunately, no pure silk microneedle devices were run as 0% glycerol control samples in this experiment.

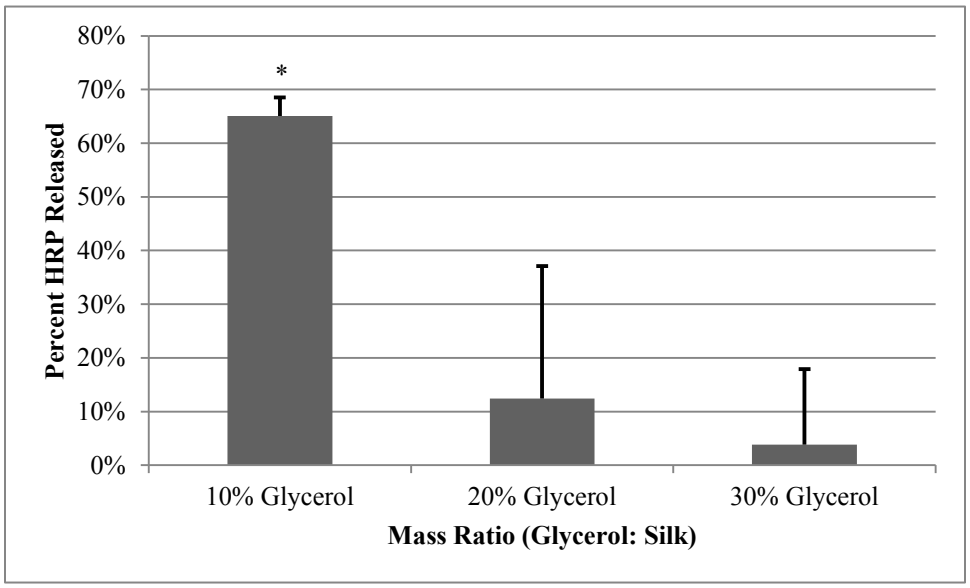

Figure 42. Relationship between HRP release and mass ratio of glycerol used in the device material. As the mass ratio of glycerol increased, the extent of HRP release decreased. The 10% glycerol condition was determined to have significantly higher release than each of the other two conditions (t-tests, n = 3, p = 0.0327 [10% vs 20%], p = 0.0158 [10% vs 30%]).

5.5.3 Alternative microneedle device formats

With other microneedle materials and fabrication processes, the final devices are generally limited to either in-plane or out-of-plane structures—there is no method to combine the two types of needles or change from one design to the other. Silk fibroin offers an excellent balance of material strength and flexibility, especially in film form, and we attempted to exploit this property to develop novel microneedle devices. First, we patterned a thick silk film with in-plane needle structures. These raised features were designed to be manually cut out from the film, and were successfully bent out-of-plane in an initial prototyping effort (Figure 43A). A more complex version of this device was engineered, allowing a user to manually press down on the needle to selectively break the joints along the edge of the needle profile, and then bent the shape out-of-plane by bending the film backing (Figure 43B). These two devices demonstrate that with a single process, silk fibroin can be used to generate both in-plane and out-of-plane needle geometries.

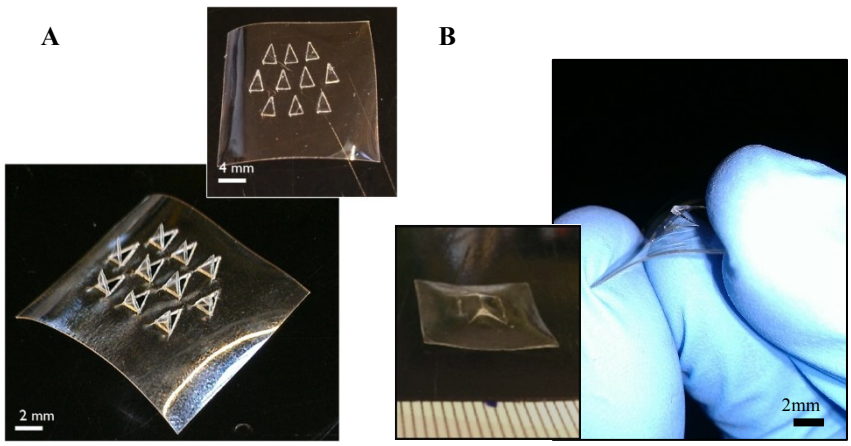

Figure 43. Examples of out-of-plane microneedle structures converted from in-plane features on a silk substrate. (A) Triangular needle profiles are patterned on a PDMS mold and transferred to a silk film through a casting step. After cutting the edges of the needles out, the features can be manually bent out-of-plane. (B) A more advanced design has a raised structure with weak joints that are designed to break and allow the device to be converted out-of-plane without any additional tools.

Finally, we sought to leverage the flexibility of the silk film backing to enable the generation of non-flat microneedle patch structures. We developed two processes to create ring-shaped silk devices, with both axial and radial microneedles. The radial microneedle devices were produced via the fabrication of a new master mold with angled needles to allow twisting of the device to insert the structures (Figure 44A-C). As demonstration of these devices for drug delivery, a silk ring was loaded with HRP and applied to a circular gel with TMB substrate. In a similar manner to previous spatial release studies, the regions where the needles penetrated the gel and released HRP can be clearly observed (Figure 44E). Axial microneedles were also successfully produced from a sawtooth-shaped mold and have been placed inside another plastic ring demonstrating the potential of these devices to provide biosensing readout to a separate ring device (Figure 44D).

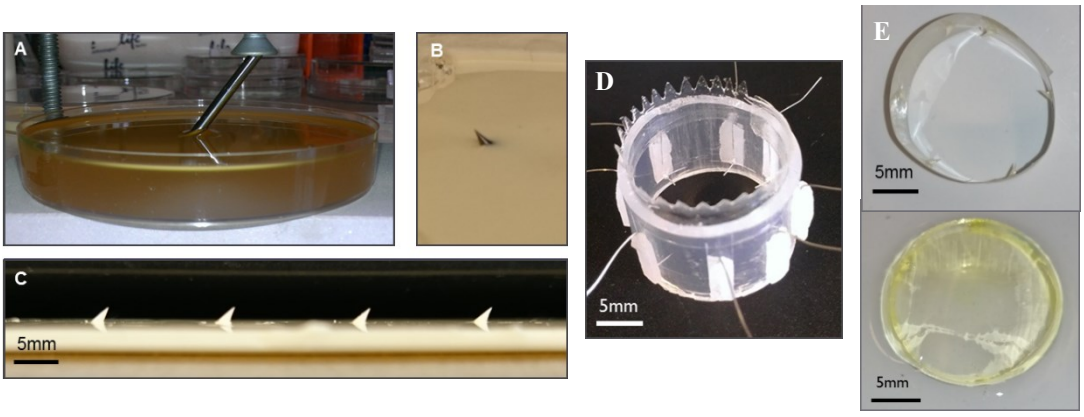

Figure 44. Silk fibroin ring-shaped microneedle devices. (A, B) A mold was created for radial microneedles by casting plastic around a drill bit at 45 degrees. (C) After a series of molding steps to transfer the structure between PDMS and plastic, the number of needles could be increased until a linearly-arranged set was produced. (D) Axial needles were produced from a sawtooth mold and could be interfaced with a plastic ring to help with insertion and potentially biosensing readout. (E) The radial silk microneedle rings were demonstrated to release an HRP payload after twist insertion to a gel model.

5.6 Adapting Silk Microneedles for Additional Research Uses

5.6.1 Hollow silk microneedles

To generate hollow silk fibroin microneedles, we began by trying to adapt existing solid microneedle fabrication techniques using a laser cutter (Figure 45A). While this approach was successful in boring a central lumen through the solid needle structure, issues were encountered with the reproducibility of this technique. The alignment of the laser with the single silk microneedle was performed manually for each device, resulting in location variation of the needle bore. Unfortunately, slight differences in radial needle bore location also produce variation along the height of the needle. While this height variation is not necessarily critical to the delivery of liquid drugs or vaccines, it will affect the ability of the device to extract fluid. The laser cutter also does not produce a clean cut through the material—there are burned areas surrounding the bore of the needle. Laboratory tape was used to remove some of the burned silk material, but this process was not 100 percent effective. Residual burned material may elicit a different inflammatory response upon administration to the skin for delivery of drugs or vaccines.

An initial penetration study using the device on rat skin *in vivo* demonstrated the ability of the devices to penetrate the skin (Figure 45B). However, many of the prepared devices were not robust enough to remain intact during the needle administration process. The single needles would shear off from the backing if the device was not applied completely normal to the skin surface. For the devices that did work, we attempted to administer a small volume of sterile PBS saline into the skin. A significant volume was lost onto the surface of the skin, demonstrating the poor seal of the skin around the needle bore due to variation in the bore location.

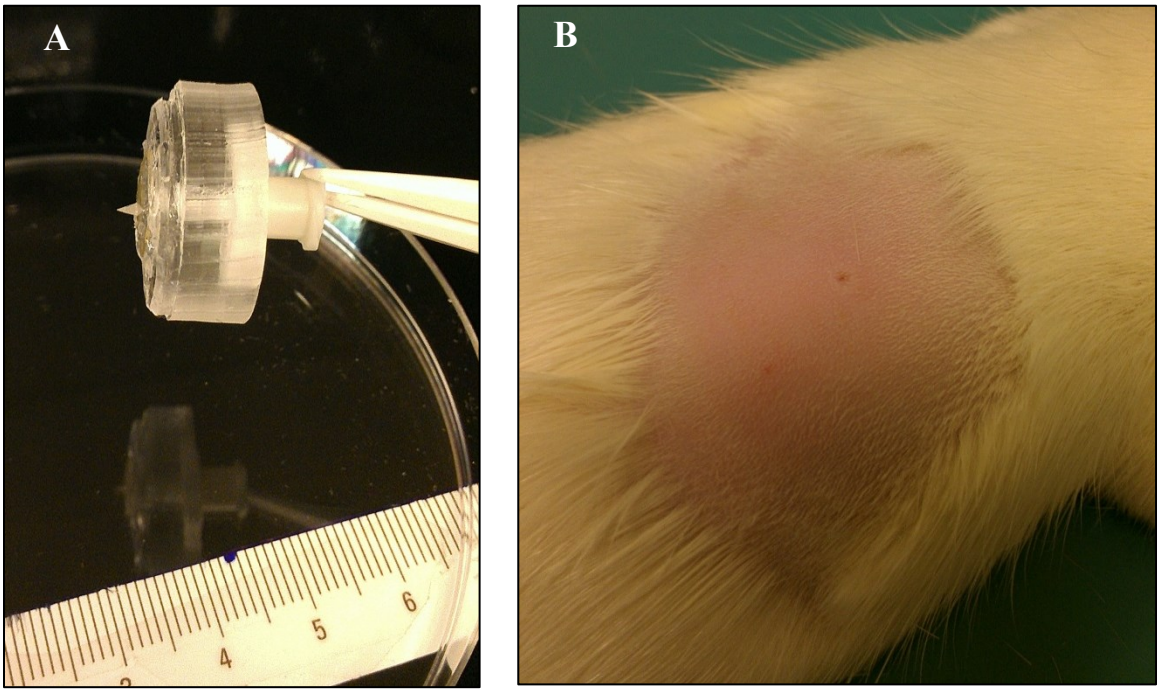

Figure 45. Hollow silk microneedle device produced from a solid microneedle through laser ablation. (A) The microneedle bore is created through laser ablation and then is combined with a PDMS backing and Luer fitting to enable connection between this device and a standard syringe. (B) The microneedle is able to penetrate the skin of a rat, but faces issues with needle placement variation, mechanical failure of the needle, and leakage of the administered solution onto the surface of the skin.

The second fabrication approach to create hollow silk microneedles was to use a separate mold component to form the needle bore. Teflon-coated wires and stainless-steel acupuncture needles were used as these needle bore mold materials as they featured sub-200 um diameter widths. Initially, we sought to insert these devices into the center of a microneedle well to cast silk and form a hollow needle structure as outlined in Figure 18. However, it was quickly observed that the structures were not forming as desired in the

PDMS feature depressions. Instead, the silk was forming a cone shape along the vertical axis of the acupuncture needles as it dried. This finding was investigated further and was found to be able to produce arrays of hollow structures over 1 mm in height, with some features as long of 3-4 mm (Figure 46). Poor outcomes were encountered when sharpening the tips of this structures was attempted—the features are very small and manual sharpening was not consistent. The next efforts were made to improve the sharpness of the silk structures during the casting step and combine the devices with microfluidics to create a more useful device.

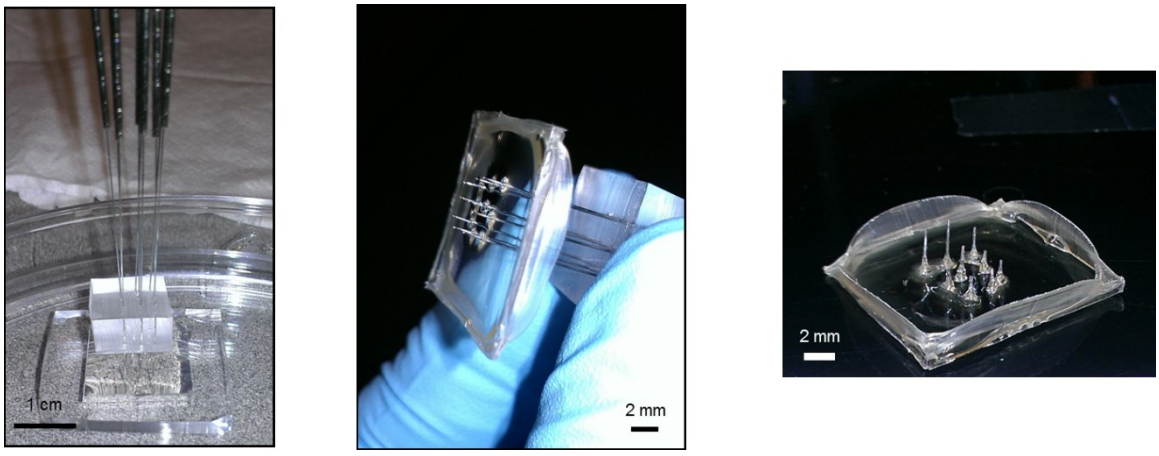

Figure 46. Hollow microneedle arrays were produced in silk through out-of-plane fabrication via capillary action up the channel bore substrate and subsequent drying. The technique reproducibly created millimeter-length hollow devices, with some needles ranging up to 3-4 mm in height. The sharpening of the needle tips using the rotary device was challenging due to the size of the features.

To improve the hollow silk microneedle devices produced through drop-casting, we examined the device outcomes using a needle-shaped profile in the bore-molding material. Specifically, a positive PDMS mold was produced and silk was cast onto the surface to determine if the feature would replicate as was observed with the acupuncture needles (Figure 47A). Good feature transfer was observed, and the devices were integrated with a separate silk film patterned with a microfluidic channel to test the principle of this fabrication technique for fluid delivery or extraction (Figure 47B). Colored solution was flowed through the device using a 33-gauge needle with little leakage between the layers or at the inlet port (Figure 47C). While successful, the device-to-device variation was quite high in terms of flatness and general appearance. The other investigated method to produce all-silk hollow microneedles containing microfluidic channels used an acupuncture needle-based molding technique and produced devices with much more uniform appearance (Figure 47D, E). After combining the devices with PDMS blocks to seal the hollow microneedle, colored solution was flowed through the channels to the hollow needles to examine leaking. Minimal leaking was observed at the inlet of the device and good flow was achieved through the channel and out the silk microneedle. To examine the ability of these hollow microneedle devices to be combined with electrode materials for biosensing applications, gold was deposited onto acupuncture needles before channel casting. After the silk fibroin material dried, the acupuncture needles were removed with complete transfer of the gold material to silk observed (Figure 47F, G).

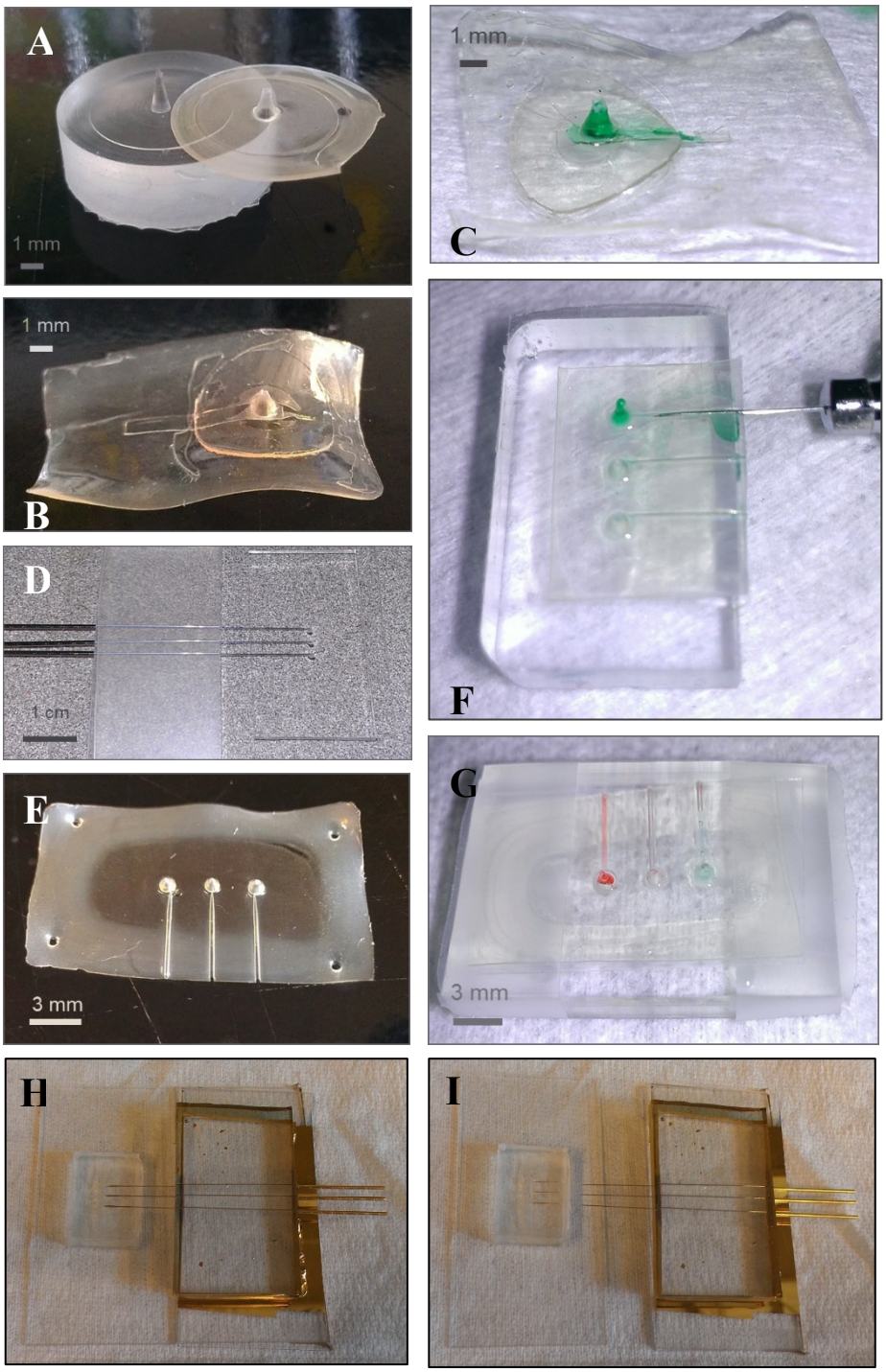

Figure 47. Examples of more advanced hollow silk microneedle devices. (A) Using a positive PDMS mold, silk films can be patterned to contain a hollow needle structure. (B) This hollow needle can be combined with a silk microfluidic channel for fluid delivery or recovery with good demonstrated success (C). (D) A separate approach was to use acupuncture needles as channel guides for a single-step cast-fabrication process. (E) Output devices had better physical appearance and uniformity and were capable of microfluidic flow with little leakage (F, G). (H) A gold layer was sputter-deposited onto the acupuncture needles and was successfully transferred to the silk material after drying (I), demonstrating the potential to adapt these devices for biosensing applications.

5.6.2 Silk Microneedle electrodes

Building upon the previous work performed at Tufts on silk fibroin microneedle electrodes, we aimed to create more reproducible electrode devices with signal detection localized to the tip of the needle to minimize collected background noise. To this end, we developed fabrication techniques compatible with the standard silk microneedle production process, drop-cast process for hollow silk microneedles, and folding microneedle fabrication method. We began by creating a new master mold with a less dense array (4 by 4) to simplify the sputter deposition process. After machining the structure out of wax, both PDMS and plastic were cast in the negative mold to produce positive molds. To generate standard solid silk microneedles, the plastic positive mold was re-cast in PDMS to form negative molds similar to those with the 20x20 microneedle arrays. Silk solution was cast in these molds, centrifuged, dried, annealed, and trimmed as described for the baseline microneedle patches. After processing, the devices were functionalized with gold conductive pathways through a tape-based deposition mask (Figure 48A). The electrical conductivity of the device was confirmed with a non-zero resistance reading for each row of microneedle electrodes on the multimeter.

The hollow silk microneedles were produced by drop-casting silk solution onto the positive PDMS mold. Before casting, the PDMS mold was patterned with gold electrodes for transfer liftoff to the silk material (Figure 48B). Laboratory tape was used to create a deposition mask before a 300 nm layer of gold was deposited onto the PDMS surface. Silk solution was cast after the mask had been removed. Once the device had dried it was lifted off the PDMS with excellent gold liftoff results (Figure 48C). The hollow silk microneedle devices were water annealed with no issues in delamination of

the gold from the silk material. We also found these devices to have non-zero resistance values demonstrating their potential to be used as biosensing devices.

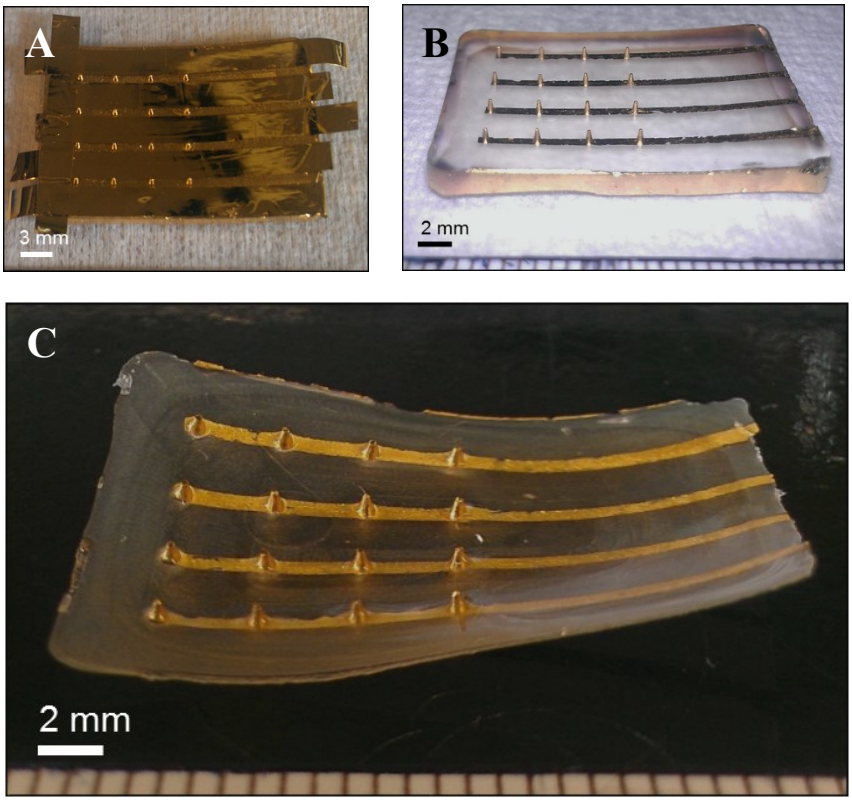

Figure 48. Out-of-plane microneedle fabrication with gold-electrode functionalization. (A) Solid silk microneedles can be formed in this 4 by 4 array and then sputtered with gold. (B) A positive PDMS mold can be deposited with gold that will then transfer to cast silk fibroin with good efficacy (C).

The folding microneedles were briefly investigated to demonstrate the ability to rapidly prototype devices on the benchtop and functionalize them through sputter deposition. Three-needle devices were produced by casting over a patterned PDMS mold and then create deposition masks to control the area of the needle functionalized with conductive gold. As a demonstration of this planar fabrication approach, different needle electrode geometries were produced with some connection pad variations as well (Figure 49). This work was all done manually and could be improved through a hard, re-useable mask with better resolution.

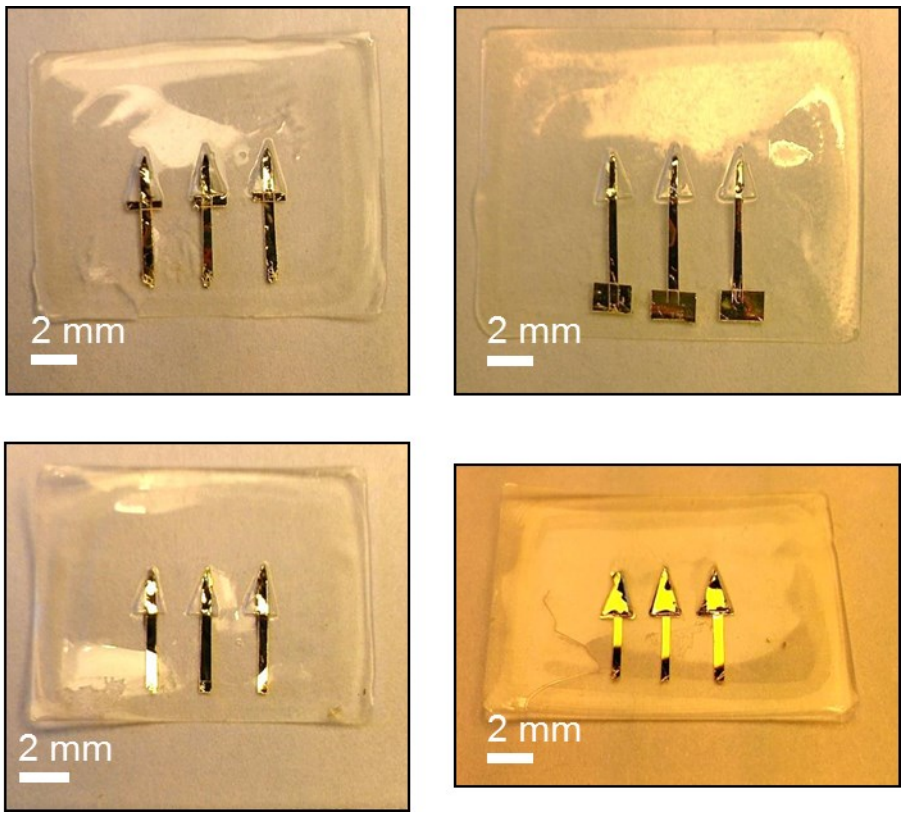

Figure 49. Planar fabrication can create silk microneedles with electrode functionality. In-plane sputter deposition of more complex electrical conduits is significantly easier than out-of-plane deposition. As demonstration of the ability to manually create various geometries, we prototyped devices with large contact points and different electrode coverage on the silk microneedles.

5.6.3 Silk microneedles for tissue engineering

Microneedles are traditionally thought of as drug delivery devices, but we recognized the resemblance of these structures with microvilli encountered in human small intestine tissue. With ongoing work at Tufts in creating novel silk-based scaffolds for small intestine tissue engineering, we aimed to develop a process to generate microvilli topology on the inside surface of the scaffold. This approach centered on the use of gelatin, or denatured collagen, as a sacrificial molding material to transfer the physical features to silk before being degraded in a later process step. We began by testing this fabrication principle in a flat scaffold using existing microneedle positive molds before advancing to a three-dimensional molding process. We found gelatin could be easily demolded from the epoxy positive masters and visually retained the microneedle depressions (Figure 50A). Silk solution was cast in these gelatin molds, was frozen down, and lyophilized to create the silk scaffold with no process issues (Figure 50B). After an autoclave cycle, the gelatin did not fully dissolve (Figure 50C) so the devices had to be placed in water at 60°C overnight. The final silk scaffolds maintained the microneedle structures, demonstrating the utility of the gelatin-molding fabrication process (Figure 50D, E, F, G, H).

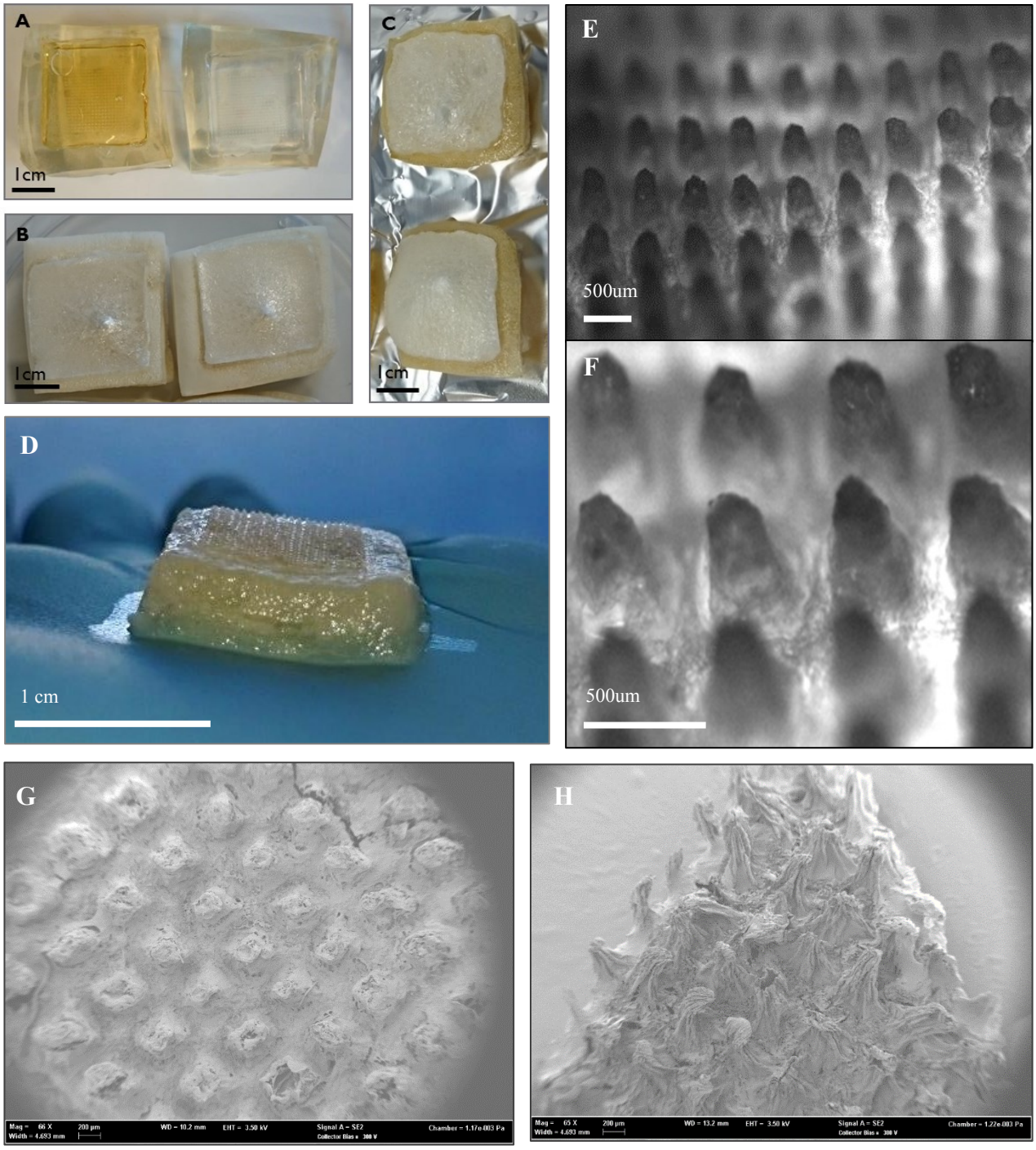

Figure 50. Fabrication outcome of flat microvilli-patterned silk scaffolds using gelatin as a sacrificial substrate. (A) The gelatin successfully preserved microneedle well features after casting around the positive epoxy mold. (B) No process issues were encountered after casting silk, freezing, and lyophilizing. (C) Gelatin remained partially intact after autoclaving, demanding the need for an additional dissolution step to create the final scaffold (D). Macroscope images showed the excellent preservation of microvilli features with some loss of sharpness at the needle tip (E, F). SEM images also demonstrated the pattern and feature transfer to the silk scaffold, but with some loss of geometry due to the dehydration step necessary for the imaging process (G, H).

We advanced the fabrication technique using gelatin into 3-D to create a central patterned rod to replace the Teflon-coated wire in the existing fabrication process for intestinal silk scaffolds. Plastic was cast inside a 2-mm internal diameter tube and was manually machined using a handheld rotary tool and 30° half-round milling bit (Bits & Bits, Silverton, OR; Figure 51A, B). The master plastic mold was then cast in PDMS and diced in half, with the needle features being successfully preserved (Figure 51C). Gelatin solution was prepared (0.5 g/mL) and cast inside the press-fit PDMS mold, with the negative features preserved after demolding (Figure 51D). When inserting the gelatin rod into the PDMS chamber, we found it easier to modify the chamber pores to be a larger diameter to allow easier insertion of the rod into the device. The ends are then capped with additional molten gelatin to provide a strong seal with the chamber (Figure 51E). The output silk scaffolds appear to contain a hollow channel (Figure 51F). Subsequent dicing of the scaffold and imaging under the macroscope shows the successful fabrication of villi features inside the channel of the scaffold, albeit with feature variability (Figure 51G, H, I).

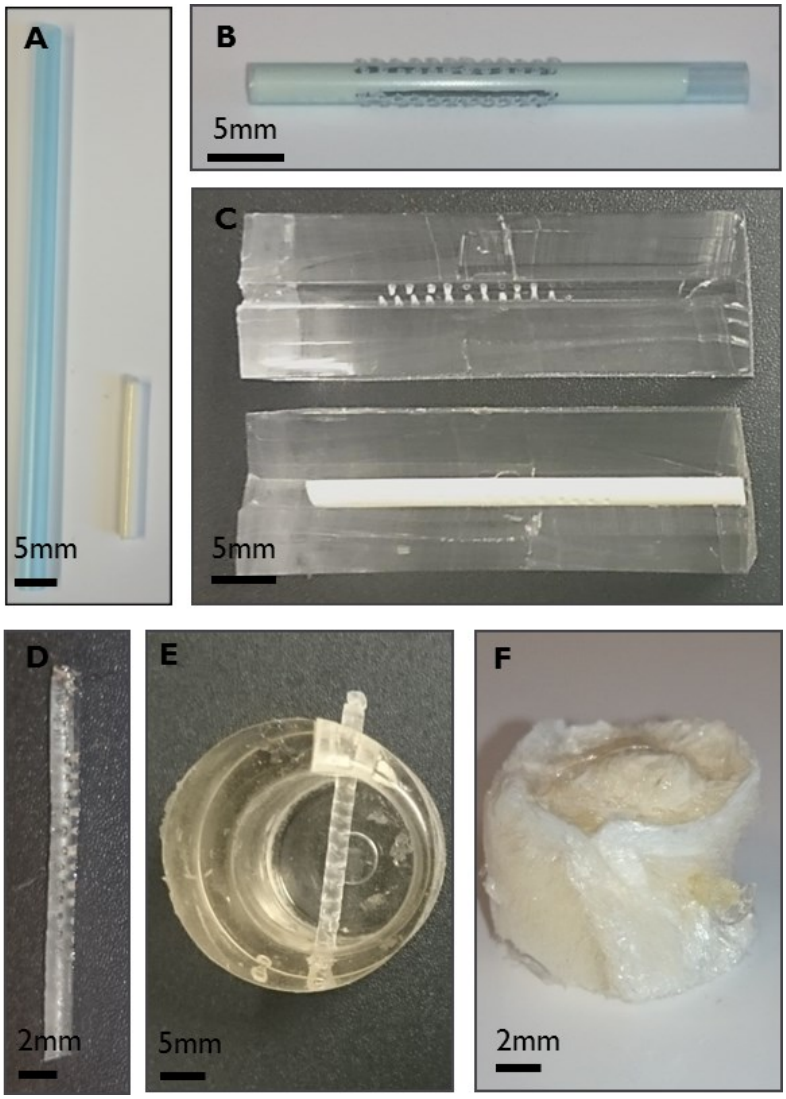

Figure 51. The fabrication process outcomes using gelatin as a patterned luminal mold in the creation of small intestine silk scaffolds. (A) Urethane plastic was cast in a separate tube to form the substrate for master mold creation. (B) Manual micromachining was used to create the villi structures in the plastic material. (C) The urethane master mold was removed and cast in PDMS, which was then diced in half after curing. The needle features successfully transferred to the PMS mold. (D) The two PDMS halves are press-fit together and gelatin is cast inside the mold, allowed to cure, and is then demolded. (E) The gelatin rod appears to contain the microvilli structures when inserted to the PDMS chamber. (F) The output silk scaffold does not have the best morphology but appears to maintain a hollow channel through the process. (G, H, I) The scaffold was diced and imaged under the macroscope, displaying microvilli features inside the lumen, demonstrating the success of this fabrication process.

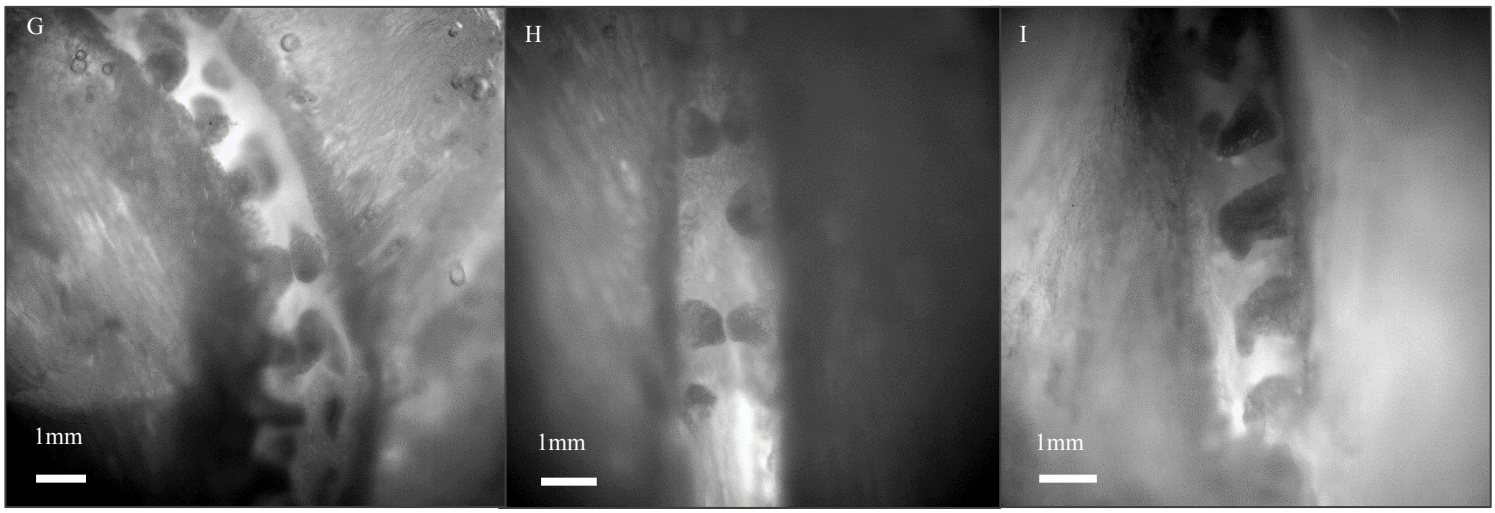

6. Discussion

6.1 Improving Flexibility of Silk Microneedle Patches

6.1.1 Fabrication

We approached the design challenge of creating flexible silk microneedle patches from a materials standpoint. Based on previous research reported in the literature, we chose to incorporate glycerol, a common plasticizer, into the silk microneedles as silk-glycerol blends had been studied in thin-films and had been shown to improve their flexibility [170]. We believed that these results could be translated into the microneedle devices, increasing their conformance to curved skin surfaces. The initial strategy was to create microneedle devices out of two materials—a pure silk fibroin solution for the needles themselves, and a blend silk-glycerol solution to form the film backing in the patch. We hypothesized that this approach would improve the flexibility of the devices without any loss of needle mechanical strength or overall performance. To accommodate this approach, we had to adapt the standard fabrication techniques and investigate different methods of device production.

After significant troubleshooting and attempts at process optimization, we were unsuccessful in reproducibly creating quality multi-material microneedle devices. The process consisted of first generating a baseline silk microneedle device with a very thin backing and then adding the silk-glycerol blend. This blend material would provide mechanical integrity to the device while imparting more flexibility than a pure silk backing. During the water-vapor annealing process, the thin silk backing would delaminate from the PDMS mold. When we added the blend material, it would often flow

underneath the silk needles and create a second layer of needles (Figure 23). To improve this interface, we tried creating silk-glycerol films and inserting them into the devices as they were drying. This improved the interface between the layers, but the fabricated devices were ultimately too brittle. We found drop-casting to be the most promising alternative production method for multi-material devices, as it would permit layer-by-layer fabrication. This process was not optimized though during this phase of research, as investigation into whole-patch blends had already begun. The drop-casting technique offers the benefit of reduced material waste as well, and was investigated as a later direction for this research.

We were much more successful in producing microneedle devices from whole-patch blends of silk and glycerol. Relative to the multi-material patches, the processing was simpler as we were able to use the standard silk microneedle fabrication methods. Based on observations of the output devices, we viewed this fabrication method as a viable approach to create flexible microneedles. The patches appeared more flexible and bent easily under manual force as we changed the composition of the material used to create the devices (Figure 24). This led us to refine our hypothesis; we believed that the mechanical properties of the microneedle patches could be controlled through the composition of the material used to fabricate the patches. In particular, the initial study of the blend devices led us to think that the mass of silk protein in the patches and the weight ratio of glycerol to silk would have the most significant impact on mechanical properties.

Overall, we examined a variety of fabrication methods to produce flexible microneedle patches, and had different levels of success with each. However, all of these

methods maintain the advantages of silk and its benign processing conditions relative to the methods used to create microneedle devices out of other materials such as metal, silicon, and non-degradable polymers. We do not have to use high temperature, ultraviolet light, or harsh chemicals to produce the microneedles and are thus able to formulate therapeutic drugs and proteins directly into our devices. Glycerol is also a safe material and should have no adverse effects on the skin or in the body if it is released from the blend microneedle patches.

6.1.2 Mechanical Outcomes

Two of the engineering design criteria for this research objective were related to the mechanical properties of the devices: (1) improving the flexibility of the devices and (2) preserving the ability of the microneedles to penetrate the skin. We evaluated the flexibility of the devices through three-point bend testing and the needle strength was examined through axial compression tests. We tested a range of whole-patch blend microneedle devices, with sixteen total material composition conditions spread across four levels of silk mass and four levels of glycerol weight ratio.

We found that the glycerol weight ratio had a statistically significant effect on the flexural moduli of the microneedle patches, making them more flexible as the amount of glycerol increased (one-way ANOVA, $p < 0.01$ for all silk masses, Figure 25). At lower glycerol concentrations, increasing the silk mass also significantly decreased flexibility. This result is consistent with what would be expected as the amount of material in the device changes. Glycerol does not dry and will thus maintain the same volume in the device. As the backing thickness increases with increases in silk and glycerol, the

glycerol helps plasticize the material and render it more flexible. At lower concentrations of glycerol, this effect is less significant and the overall thickness of silk matters more. From the literature, it is understood that increasing the thickness of silk films also increases their bending stiffness [186]. From these results, we can decrease the amount of silk fibroin protein in the microneedle patches or increase the amount of glycerol to increase their flexibility and thus improve their conformance to the skin surface.

We now know that the total mass lost when trimming the edges off the patches accounts for a significant portion of mass lost. We designed the devices for the total silk included in the devices, and not the final mass of the device. In the future, this final mass should be recorded as well as the thickness of the backing to provide a more accurate means of calculating the conversion factor to translate compressive-extension slopes to flexural modulus values. When including more silk in the molds for the 'XHI' condition, the higher concentration may have preferentially dried into the edges of the device that are trimmed off. Thus, the tested devices may have been thinner than the 'HI' condition, resulting in the more flexible modulus values observed in Figure 25.

This testing method was also sensitive to the geometry of the microneedle patches and while we took great care to produce devices as flat as possible, there were some devices with surface irregularities. These irregularities likely account for the large standard deviations observed in the flexural moduli (Figure 25) and may have contributed to the non-significance of the glycerol weight ratio in influencing the device mechanical properties. Near the end of the semester, we began to experiment with using double-sided tape to keep the patches flat after water-vapor annealing and observed much flatter patches than were produced by pinning them to PDMS. In the future, we would suggest

using the tape method to generate very flat microneedle patches, which would improve the reliability of the three-point flexural testing results.

We examined the strength of single needles made from the highest three silk masses at all four glycerol weight ratios (the 'LO' condition single needles could not be fabricated due to issues with the backing thickness). We found that there were no significant relationships between needle fracture force and the glycerol weight ratio of the silk mass used in the needles, and that the majority of the tested needle conditions were above the skin penetration of 100 mN as reported in the literature [62] (Figure 26). However, a very small sample size was tested (n = 2 for three conditions, n = 3 for all others), so we would suggest performing additional needle testing to better define the properties of the needles. The strengths of the needles we did test were consistent with previous silk microneedles, with a range of 100–700 mN/needle and an average of ~400 mN/needle [98]. We are optimistic that further testing will prove that the incorporation of glycerol has no negative effect on the strength of individual microneedles, and will not compromise the ability of the devices to penetrate the skin.

6.1.3 Release Performance

The final objective of this research was to demonstrate that the flexible microneedle patches maintained the drug release performance characteristic to baseline patches. In the most ideal case, the conformance of the patch to curved skin surfaces would improve the amount of drug that could be released and increase the reliability of the devices for transdermal drug delivery. We examined the drug release kinetics from baseline microneedle patches ('XHI', 0% glycerol w/w) as well as a more flexible patch

condition ('HI', 20% glycerol w/w) which was chosen based on the tested mechanical properties. These patches were also subjected to skin penetration and release testing on a curved porcine skin substrate to demonstrate their ability to conform to non-flat surfaces.

We found that after the microneedle patches had been applied to the collagen gel models there was no significant difference between the baseline and flexible patches as they had released their full drug payload (Figure 27). The baseline patches released 100 percent of their HRP coating after one hour, while the flexible patches released just more than 40 percent after the same amount of time. The flexible patches have a large standard deviation at that time point, and both conditions have large standard deviations at the 10 minute time point. It is difficult to conclude that the flexible patches have slightly slower, or more controlled, release than the baseline patches due to these large error bars. The sources of error may stem from how tightly the plastic wrap was stretched over the collagen gels. If the wrap was loose, some of the needles would be unable to penetrate and would require more time to allow the full drug coating to diffuse across the barrier through the needle areas that did breach the plastic wrap.

While the incorporation of glycerol into the microneedle patches has an unclear effect on the release kinetics due to the large reported errors, it does affect the coating of drug solutions onto the surface of the patches. When coating the microneedle patches we pre-wet the surface by pipetting droplets of DI water on and off the patches. This pre-wetting step helps improve the evenness of the final drug coating and increases the overall area of the patch that can be coated. In the flexible patches, we did not observe the formation of water droplets on the needles, which occurs with the baseline patches.

This suggests that glycerol changes the hydrophobicity of the material in the microneedles. The better spreading of water during the pre-wetting of the flexible patches produced better coverage over the surface area of the microneedle patches (Figure 28). The glycerol molecule has three hydroxyl groups, which allow it to participate in hydrogen bonding with water and other materials. In blended starch films, the weight ratio of glycerol was shown to change the hygroscopic properties of the films depending on ambient humidity of the environment [190]. Based on this observation, I believe it would be interesting to examine whether changing the hygroscopic nature of the microneedle patches has any effect on the release kinetics of drug coatings formulated with silk.

Finally, we examined the ability of the flexible and baseline microneedle patches to penetrate a curved skin surface and release a model protein, ovalbumin. The images demonstrate that the flat, baseline patches are unable to conform to the surface of the skin and are only able to penetrate the area of the patch (center) that is in contact with the skin surface (Figure 29). The flat, flexible patches penetrate the skin across the entire area of the patch, demonstrating their ability to effectively conform to the curved substrate (Figure 29). The two pre-formed patch conditions are also able to conform to the curvature of the skin, although the baseline microneedle condition displayed areas of irregular penetration (Figure 29). Unfortunately, cryosectioning and histology was not performed with these skin samples. These processes would allow us to verify that the microneedles had penetrated the skin and the extent to which drug was released. It is recommended that this be done in the future to confirm that the flexible patches provide a performance benefit over baseline patches for transdermal drug delivery.

6.2 Silk Microneedle Vaccine Delivery

6.2.1 Dose response

Previous work at Tufts had demonstrated the ability of silk fibroin microneedles to deliver the model drug ovalbumin both in an *in vitro* model and *in vivo*. While ovalbumin is known to elicit an immune response from host organisms, it is not necessarily relevant from a commercial standpoint as it is not a real vaccine. For this reason, we sought to examine the performance of silk fibroin microneedles in delivering commercially-available influenza vaccine (Fluzone Quadrivalent inactivated influenza vaccine, Sanofi-Pasteur, Swiftwater, PA). Three doses (1ug, 6ug, and 12ug) of influenza antigen were selected based on published literature suggesting 6-9ug of vaccine could elicit a strong immune response in a mouse model [61, 182]. The influenza vaccine was formulated with 1% (w/v) final concentration of silk fibroin to coat onto the surface of the silk microneedles, providing some measure of controlled release and temperature stability. A negative control was included in this experiment against which the transdermal immune response could be measured; silk microneedle patches were coated with water in this condition (no silk). Similarly, a positive control was included to serve as a standard for vaccination; 12 ug of vaccine was administered subcutaneously through an injection after being stored at 4°C as recommended by the manufacturer. Animals were immunized twice—an initial administration followed by a booster at two weeks. Blood samples were collected immediately before these administration events and at a final timepoint of 34 days. The serum from the animals in each experimental group was isolated and pooled for serological analysis via indirect ELISA.

We aimed to determine the minimum dosage of influenza vaccine necessary to elicit a robust immune response through microneedle administration. We measured the total immune response against influenza at each time point to determine the success of vaccine delivery and immunogenicity of each coated dose. Additionally, we examined the IgG-specific response to determine the extent of immunological memory formed against the influenza antigens. We found that the 6ug and 12ug doses coated on microneedle patches generated a strong total immune titer after the two administration events, with a reduced anti-influenza IgG titer compared to the positive control (Figure 31A). In comparing the fold-change of signal generated through the assay, we observed comparable total immune responses from these same two conditions compared to the positive control, indicating a robust immune response to the microneedle-delivered vaccine (Figure 31B, C). No significant total immune response was observed from the 1ug dose condition relative to the negative control. However, a mild IgG response is observed from the 1ug dose condition following a booster with comparable responses from the 6ug and 12ug conditions relative to the positive control (Figure 31D, E). There does not appear to be a significant difference in total and IgG-specific responses between the 6ug and 12ug dose conditions.

Overall, these results demonstrate the successful delivery of commercial influenza vaccine using silk microneedle patches. While there was only a mild IgG-specific response from the 1ug dose, the 6ug and 12ug dose conditions elicited robust immune responses comparable in magnitude to the 12ug positive control. This suggests the devices could be used in a solid coated format for transdermal vaccination. There are limitations with this approach however. The lack of difference in total and IgG-specific

titers between the 6ug and 12ug doses suggests that a near-equal dose was actually delivered across the skin. This is reasonable as only the vaccine localized to the silk microneedles themselves would be introduced to the skin—any vaccine coating on the flat film backing would not be delivered into the skin. Although a higher concentration of vaccine was used in the 12ug coating experimental group, most of the vaccine may have localized to the backing itself. Thus, the exposure of vaccine antigen between the 6ug and 12ug groups would have been similar and elicited the same immune response.

While this lack of delivery control is sub-optimal, it does suggest the principle of dose-sparing using silk microneedle devices. Although we did not quantify the residual vaccine remaining on the microneedle patches, it is expected that the delivered dose is far less than the total antigen dose coated onto the devices (1, 6, 12ug). The comparable total and IgG-specific immune response generated through transdermal administration compared with subcutaneous injection is quite exciting as it suggests a reduced dose could be used for vaccination of the subject. Moving forward, it will be important to quantify the amount of vaccine remaining on the patch so the immune responses can be better correlated with the actual dose delivered. Additionally, this finding suggests the benefit of a bulk-loaded microneedle designed for biodegradation in the skin. Localizing the drug or vaccine to the needles themselves will provide better control over the total dose released, minimizing variability in therapeutic/immune response and validating the dose sparing principle through this administration route.

6.2.2 Thermal stability

Silk fibroin protein has been demonstrated to temperature stabilize a variety of therapeutics, including enzymes, antibiotics, and vaccines [8, 168]. We sought to validate this finding in the microneedle device format as it would allow a fully-stable, self-administrable vaccination device to be produced. For this aim, we examined the immunogenicity of influenza vaccine after storage in the solid phase on silk microneedles (formulated with 1% w/v silk in the coating) and in the liquid phase (unaltered commercial vaccine) to compare stability head-to-head. The same immunization schedule (primary and 2-week boost) was used for this study as for the dose response study, with the same bleed timepoints (day 0, 14, 34). Indirect ELISAs to measure the total and IgG-specific immune responses were also performed as the analysis for this experiment. All animals received a 12ug dose of liquid vaccine, or a patch coated with 12ug of antigens.

Microneedle patches stored at room temperature and 37°C displayed strong total and IgG-specific immune titers that were comparable to the subcutaneous injection controls (Figure 33A). The microneedle patches stored at 60°C produced a reduced total immune response and IgG-specific immune response at both tested dilutions (Figure 33B-E). Interestingly, after the primary immunization the total and IgG-specific responses of the microneedle patches is much lower than those of the injected controls. However, this does not appear to affect the final immune responses of the animals. These results suggest that the microneedle patches can stabilize the influenza vaccine up to 37°C with some potential activity lost at 60°C. The injected controls appear to be relatively stable at all tested temperatures.

As mentioned for the dose response study, these results are exciting as they suggest a reduced transdermal dose can elicit the same final immune response post-boost as a subcutaneous injection. Additionally, it may not be the most relevant comparison to examine transdermal delivery side-by-side with subcutaneous injection. The injected material may be more readily taken into the lymphatic system where it generates a more humoral response to the antigen through B-cells. This could result in the faster production of IgG antibodies against the material following the first administration event. However, the influenza antigen delivered transdermally would be processed through a more cell-mediated response (T-cells) which may be slower but results in just as strong of an immune response following the second exposure event. If the processes by which the antigen generates an immune response are different, it is challenging to compare the stability of the vaccine through an immune response metric. Thus, a more relevant stability study would be to coat microneedle patches with vaccine without any silk to standardize the immune response process and compare the stability imparted by silk protein.

The reduced immune response from the microneedle patches stored at 60°C may be due to a loss in stability or it may be due to another factor. As will be discussed in the following section through analysis of the anti-silk immune response, it is likely that the elevated storage temperature resulted in a degree of crystallization of the silk fibroin coating containing the vaccine. This crystallization would reduce the solubility of the vaccine coating a prevent release into the skin. Thus, the reduced immune response may be due to slower release kinetics than the loss of stability at elevated temperatures. Again, to confirm this finding a non-silk coating should be used as a paired control to evaluate

the stability effects of the silk protein. Additionally, an inactived vaccine may not provide the best target for stability as the antigens remain intact after heat-inactivation of the virus. Instead, a live attenuated vaccine may provide a more challenging target to temperature stabilize and could provide more insight to the stabilization properties of silk fibroin. Such live attenuated vaccine targets would include oral polio virus, measles, rotavirus, and yellow fever.

6.2.3 Silk immunogenicity

We desired to confirm that silk is non-immunogenic and biocompatible in a microneedle format as has been reported in the literature for a variety of other silk formats. Especially since the vaccine coating on the microneedle devices is formulated with 1% silk in a soluble format to release into the skin, we wanted to measure the formation of antibodies against silk fibroin protein. In a similar manner to the anti-influenza evaluation, we developed and performed indirect ELISAs against silk fibroin protein to determine the total and IgG-specific immune response. As this evaluation was to determine the immunogenicity and not the temporal response, we examined only the blood samples from the final collection time point. Overall, we observed a mild total immune response to the silk material from the microneedle patches coated with silk (Figure 32A, 34A). The total response is inconsistent—for microneedle patches coated with less vaccine (1ug vs. 6ug, 12ug) the total anti-silk response is stronger; similarly, patches stored at lower temperatures (25, 37°C) have a stronger response than higher temperatures (60°C). Similar results are observed for the IgG-specific responses, although these responses are much milder than the responses to influenza antigen (Figure

32B, 34B). This result suggests that the silk material is largely biocompatible and safe for use in the solid coated microneedle format.

The increased immune response to silk protein at lower vaccine doses and lower temperatures is unexpected. These results may suggest that the availability of the protein was not consistent between the experimental groups. For the microneedle patches stored at 60°C, the reduced immune response may be due to poor dissolution of the silk coating—indicating that some degree of crystallization of the protein may have occurred. Although the patches were stored with desiccant to prevent inadvertent water-annealing, the desiccant may have become saturated over the two week period. This would allow the silk coating to form β-sheet structures at this temperature, making it largely insoluble. In this state the silk coating would inhibit release of influenza vaccine which may account for the diminished total and IgG-specific immune responses of the animals to the patches stored at 60°C. In the future, more control over humidity should be provided to prevent variability in the solubility of silk coatings.

For the results observed for the different doses, the same explanation can be used to rationalize the finding of increased immune response from lower vaccine doses. The soluble silk material available on the needle structures introduced into the skin will increase with decreasing vaccine concentration. Thus the total immune response against silk is dose-dependent. However, the IgG antibodies generated against silk protein are largely observed at a 1/500 dilution, which is much lower in magnitude than the anti-influenza titers generated with the same microneedle patches. These results suggest that silk fibroin protein is generally biocompatible and safe for use in the microneedle devices for transdermal vaccination.

6.3 Rapid and Scalable Microneedle Fabrication

6.3.1 Replication of spin-cast devices

Microneedle devices offer many advantages over other parenteral administration forms that make them very attractive for drug and vaccine delivery. To date however, commercial products and microneedle patches reported in the literature fall short in either device design or functional aspects due to the materials available to fabricate these devices through common techniques. Silk fibroin is an attractive material candidate for these devices because it offers the complete package of biocompatibility, tunable mechanics, tunable degradation and/or release kinetics, temperature stability, and all-aqueous processing. Silk protein is able to bridge the material-property gaps that have been encountered with other popular microneedle substrates such as silicon, SU-8 photoresist, PLGA, nickel metal, and sugars such as maltose and galactose. While silk microneedles have been produced and studied previously at Tufts, the processing methods used to create the devices lead to the loss of some of the functional advantages silk has over other materials. In this research aim, we desired to develop a fabrication process that would output the same silk microneedles while also permitting rapid drug release and other needle formats. Achieving this objective would provide strong evidence that silk fibroin protein is a leading candidate material for a microneedle platform that could be optimally programmed for the delivery of specific drugs or vaccines.

To this end, we aimed to study the drop-cast fabrication technique first described in the context of the fabrication of multi-material flexible microneedle patches. The process was noted to produce silk microneedles in far less time, with drying occurring in less than 24 hours compared to the standard 2-3 days required for spin-cast microneedle

devices. Reducing the total processing time and material waste are important objectives for any engineered process as they lead to decrease costs and increased throughput and efficiency. Once we had optimized the drop-casting process, using an on-off vacuum cycle to improve microneedle mold filling, we compared the material lost in the drop-cast and spin-cast fabrication techniques. With the drop-cast needles, silk fibroin is confined to the square area above the needles, with little to no requirement to trim the millimeter border. With the spin-cast microneedles, silk solution dries along the vertical walls of the PDMS chamber to create a film edge that must be trimmed off after the water-vapor annealing process. In a brief study with four spin-cast devices, we found the silk waste to be an average of 71.63 percent (Table 5). From a manufacturing standpoint, this amount of waste is unacceptable. By eliminating all silk fibroin waste with drop-casting, more than three devices could be produced with the same amount of material as is used in spin-casting. This provides a cost-savings that could be transferred to the final user and allow these devices to be distributed to low-resource settings.

For this process to be adopted, we had to first confirm that the output silk microneedle devices could be produced with near-identical characteristics. We characterized the devices through ATR-FTIR and mechanical bend testing to compare their properties. Infrared spectroscopy provides insight to the secondary structure composition of the silk protein after processing into the dry state. We compared an insoluble spin-cast microneedle device (water-annealed) to an insoluble drop-cast microneedle device (high silk concentration used, no post-processing). The absorbance spectra were collected from triplicate samples and were preprocessed by averaging to a single curve, rescaling to a 0 to 1 range, truncating to the 1150-1750 range, and

standardizing area under the curve to 1 (Figure 36). The absorbance values at peak wavelengths associated with different secondary structure components were then compared to determine the relative changes due to processing conditions. We observed increases in the β-turn content and decreases in β-sheet and random coil structures in the drop-cast fabrication method. This is consistent with our expectation that water-vapor annealing will direct the silk towards a more ordered silk II conformation marked by high β-sheet content. With the drop-cast method, we observe self-assembly of the protein into an insoluble silk I state with high β-turn content, consistent with the literature [170, 184]. We expect that through water-vapor annealing of the drop-cast patches, the observed differences between output patches will be reduced to similar levels. This analysis was performed quickly, and it is recommended that pre-annealed spin-cast and post-annealed drop-cast patches be examined to validate the secondary structure consistency of patches produced with both methods. A peak-fitting analysis using deconvolution is also suggested to improve the accuracy of the quantitative results.

We characterized the flexural moduli of drop-cast silk microneedles to compare with the previous results obtained with a range of spin-cast microneedle masses and glycerol weight ratios. We drop-cast a 1 mL volume of 6.1% silk (30 minute boil) at 20%, 10%, 5%, and 0% weight ratios of glycerol. The patches were three-point bend tested on the Instron apparatus (Figure 10) and the force-extension curves were processed into flexural modulus values by extracting and converting the slope of the linear deformation region (Figure 35). We observed flexural moduli values that ranged from ~1400 MPa to ~250 MPa for the 0% glycerol and 20% glycerol conditions respectively, with the 5% and 10% conditions following a decreasing trend in between these limits.

The calculated flexural moduli values were on the same order as those of the 'MID' and 'HI' conditions from the spin-cast mechanical testing, suggesting uniformity of patch mechanics with the two fabrication techniques. The 'HI' condition microneedles were designed for a total mass of 0.200 grams before annealing and trimming. Assuming the 71.63% material loss observed during the trimming process, the final mass of these spin-cast microneedles is approximately 0.05674 grams. The devices produced through drop-casting were similar in mass (0.06 grams, approximately), validating the finding that the 'HI' spin-cast devices have similar mechanics as the drop-cast ones. This result suggests that the drop-cast fabrication technique is able to produce microneedle devices with the same mechanics as those made through the centrifugation-based process and could be adopted as the new primary method for creating these silk devices.

6.3.2 Dissolving microneedle devices and other formats

The drop-cast fabrication technique offers the ability to more produce silk microneedle devices and has the potential to be scaled-up. This production process could provide additional advantages the current spin-casting technique. With the spin-casting process, silk microneedles take 2-3 days to fully dry. Although water-vapor annealing of these devices is performed to increase their β-sheet content, they are often already insoluble. It has been previously demonstrated that the slow drying process allows the silk to self-assemble into an insoluble silk I conformation. While this is an excellent outcome for extended release formulations or coated microneedle devices, it prevents rapidly-degrading and/or bulk-loaded microneedles from being produced. We believed that the drop-casting process would preserve the solubility of the final silk product by

increasing drying speed. In this aim, we sought to demonstrate this principle and show that effective bulk-loading of the silk microneedles could be achieved.

We began this research phase by investigating the ability to produce two-component microneedles consisting of a soluble needle layer and an insoluble microneedle backing layer. If successful, these devices would provide an excellent means to localize drug or vaccine to the needles themselves, reducing any waste observed by loading into the bulk material in the backing [164]. We created a three-needle mold with larger features to allow easier prototyping to occur as well as easier visualization of successful microneedle dissolution. The fabrication process was investigated and it was found that the inclusion of glycerol at a weight ratio of 40% had a significant effect in maintaining the solubility of the needle layer during the component lamination process (Figure 38). Glycerol is known to participate in electrostatic interaction with hydrophobic regions of proteins, providing an amphiphilic interface between the protein and water [191]. This property may provide a "shielding" effect between the soluble silk needle layer and the liquid phase used to bind the needle and backing layers together. This finding should be investigated further, as it could provide a good method to create elaborate layered microneedle devices for multi-stage release.

As demonstration of the potential for these devices to be bulk-loaded, we created three-needle devices and whole microneedle patches loaded with HRP enzyme. This enzyme is an excellent model for drug release as it can be used in a straightforward colorimetric assay to quantify release from microneedles. We tested release into TMB-loaded gelatin gels to visually validate the penetration of microneedles into the gel model and subsequent drug release (Figure 39). In both cases, a blue intermediate product was

observed before development in acid to turn the product yellow. Thus, this assay provided quick confirmation that these devices could be used for delivery into mucosal tissues in the oral cavity (Figure 39A) or into the skin (Figure 39B).

More quantitative evaluation was performed with the full-patch microneedle devices to test their functional ability to penetrate a stratum corneum model (Parafilm over gel) and release a model therapeutic payload. First, a spring-loaded applicator device was prototyped to standardize the administration process of silk microneedles (Figure 41A). Gelatin gels were covered with Parafilm in an *in vitro* model of the skin as previously described [6]. The HRP-loaded microneedles were applied for three different durations (0, 30, 60 seconds) with the applicator (Figure 41B) and were quantified for percent release based on the initial loading mass. There was no clear increase with HRP release over this investigated short release time (less than a minute), but the important finding is that the devices released at least 30% of their payload after penetrating the skin. This result confirms that silk fibroin could be used in a bulk-loaded microneedle format for more rapid drug release.

Taking this finding one step further, we wanted to evaluate whether the drop-cast silk microneedles could be programmed for specific release profiles based on material parameters. Specifically, we examined the dissolution rates of microneedles produced with different silk concentrations and total silk masses to characterize the relationship between these material properties and the total degradation in a three minute period. A follow-up study using different mass ratios of glycerol to control the degree of silk I content and degradation was also performed. The dissolution results showed strong negative linear correlation between the mass of the silk device prior to degradation and

the extent of this degradation (Figure 40). With a larger drop-cast volume used to create devices of a higher mass, the drying time would increase and could result in more self-assembly into an insoluble silk I form. The decreased release from the higher investigated silk concentration can also be explained through assembly of the protein into more stable secondary structures. With decreased water-protein interactions/increased protein-protein interactions, the higher concentration silk is more likely to assemble into an insoluble form even though a smaller total volume was used to create these devices. This result provides strong evidence that great control over total degradation could be achieved simply through the concentration and volume of silk used to fabricate the microneedle devices. Similar control could be provided by doping the silk solution with glycerol, as decreased release was achieved by increasing the weight ratio of silk protein. Again, glycerol can have the effect of minimizing protein-water interactions, allowing the silk protein to assemble into thermodynamically-stable conformations.

This research concerning the drop-casting fabrication technique has demonstrated the ability of silk fibroin to be used to create insoluble solid microneedles for coated formulations, as well as bulk-loaded devices with tunable degradation. The ability of a single material to be easily processed into either device format based simply on the material parameters is a property not achievable through other fabrication methods or with other biomaterials. We have also examined the ability of the silk protein to be used to create alternative formats of microneedle devices with folding needles (Figure 43), a circular ring design for application through twisting (Figure 44), and three-stage microneedles (Figure 37). These results demonstrate the flexibility of our silk microneedles to be adapted or programmed for the delivery of specific therapeutics.

6.4 Expanding Silk Microneedle Applications

The flexibility of silk fibroin material platform extends beyond the delivery of different drug and vaccine products. The properties of the material can be leveraged to create new microneedle devices for the delivery of drug products in the liquid phase, biosensing applications including electrical signal recording and analyte detection, or recapitulating *in vivo* structures in engineered tissues. We briefly prototyped devices for each of these three applications to demonstrate the adaptability of the silk protein platform for traditional and non-traditional microneedle applications.

Hollow microneedle devices are appealing as they can have two distinct uses—delivery of liquid formulations of drug or vaccine and extraction of interstitial fluid or capillary blood for biosensing or bioanalysis. We desired to demonstrate that these devices could be produced from silk fibroin material in a non-cleanroom fabrication process for easier prototyping and access than traditional microfabrication approaches. Hollow microneedles were first produced from solid silk microneedles through laser ablation (Figure 45). While these devices were able to penetrate rat skin they had poor reproducibility of the needle bore location because the ablation process was manually-aligned. To standardize the location of the needle bores, a drop-casting technique was developed using a positive feature-patterned PDMS substrate and microfluidic channel molds (Figure 46, 47). While these devices were not extensively characterized, the microfluidic principle was demonstrated by flowing colored solution through the channels and out the hollow needle tip. Electrodes could even be included on the inside of the microfluidic channels to permit a silk device with lab-on-a-chip capabilities. The mechanics of these hollow microneedles were not investigated, but these devices attest to

how silk fibroin provides a simple and straightforward conduit to prototype devices for new applications and uses.

Similarly, microneedle electrode devices with silk fibroin were prototyped in both a solid and hollow format. Microelectrode arrays for biosignal sensing and recording are another logical use for microneedle devices. We created silk microneedles with electrode functionalization by sputter-depositing gold metal through laboratory tape masks as a straightforward exercise in prototyping. The gold electrodes and electronic pathways were found to be conductive with no delamination issues in the devices (Figure 48). Electrode-functionalized microneedles were also produced on folding silk devices as described previously. These folding devices are a novel microneedle format and another example of the advantages silk protein provides over alternative biomaterials for microneedle fabrication. The planar fabrication approach allowed different electrode geometries to be easily created with a low-resolution, tape-based deposition mask. We expect that this planar approach would allow the creation of more detailed microneedle electrode devices to be produced. This work is in progress and is being pursued by two undergraduate students at Tufts.

Finally, silk fibroin has proven to be an excellent material for tissue engineering applications [152, 153, 154, 160]. However, most of the silk scaffolds used for these 3-D engineered tissues have had very basic geometries. On-going work at Tufts has resulted in the development of a novel 3D scaffold with a hollow lumen to mimic the human small intestine. While basic surface topology has been achieved in this model by patterning the lumen with the threads from a screw, it falls short of an accurate representation of *in vivo* tissue architecture. Microvilli are small projections from the

surface of the small intestine that increase surface area and play a significant role in nutrient absorption. We saw resemblance between the geometry of these structures and the silk microneedles and aimed to recapitulate these features in the silk scaffold to generate the most physiologically-relevant small intestine model to date.

We designed a fabrication method to create microvilli-like surface topology in the lumen of 3D silk scaffolds with minimal disruption to the existing fabrication technique. Using a similar soft-lithography molding approach as is employed to create solid silk microneedle devices, we created microneedle molds out of a material to be sacrificed later in the fabrication process. Gelatin was chosen as this sacrificial molding material as it has been used previously for micromolding applications with good results while also being low-cost and biocompatible [188]. We first tested the ability of gelatin to transfer microneedle structures to a flat silk scaffold (Figure 50). After brief optimization, we observed very consistent microneedle structures with a rounded tip due to the swelling of the gelatin substrate. This loss of aspect ratio is quite beneficial as the *in vivo* structures do not terminate in a sharp tip. We moved into our proposed fabrication process to create patterned gelatin lumen molds. The process successfully transferred the microvilli structures to the lumen of the silk scaffold, demonstrating the potential for this fabrication technique. While the consistency of these features was not very good, the process can be improved through the creation of a better master mold. The master mold used in these designs was produced manually—leading to a high degree of feature variability.

Overall, we demonstrate that the silk microneedle platform is not constrained to delivery of solid-phase drugs or vaccines. While not extensively studied or characterized, hollow silk microneedles and silk microelectrode arrays were prototyped using simple

benchtop processes. With more time and resources, we are confident that these devices could be developed to exploit further advantages of the silk material. For example, silk microneedle electrodes could be designed to partially dissolve and adhere to the tissue of interest, as has been done with silk films previously [186]. Silk microneedles have broad application for these traditional uses, but also in the non-traditional application of tissue engineering. The formation of microvilli-like microneedles in a silk scaffold is exciting due to the better anatomical and physiological parity that could be observed in the *in vitro* tissue model. These devices could provide better models of drug absorption or toxicity, leading to better outcomes from pre-clinical research studies. All of these devices show how the silk microneedle platform can be extended to a broad variety of applications that could not all be achieved with other biomaterials.

7. Conclusions

The current parenteral drug delivery paradigm is imperfect. While intramuscular and subcutaneous injections result in the successful delivery of therapeutics in the liquid phase, a significant portion of the population suffers from needle-phobia and there are logistical access and waste-handling issues associated with this route of administration [5, 19]. Recently, transdermal delivery of drugs and vaccines has gained significant research momentum as it offers minimally- or non-invasive delivery of these same therapeutics with similar efficacy [17]. While transdermal patches have been developed, the types of therapeutics amenable to this delivery format are limited by molecular size and charge. For this reason, microneedle devices have been developed to offer a straightforward method to deliver a broad range of drug products across the skin. The simplicity of these devices is a major advantage that could allow self-administration, which is particularly appealing for vaccination [17].

Microneedle devices have been created from a variety of materials through both cleanroom and non-cleanroom based fabrication techniques. These devices range in their properties and functionality, including: biocompatibility, excellent mechanics to penetrate the skin, tunable release kinetics, processing under benign conditions, thermal stability of the therapeutic, and most importantly, the ability to be self-administered. However, no material to date has been used to create a microneedle platform with the full set of these properties and functionality. The closest material that meets all of these criteria is silk fibroin protein from the silkworm *Bombyx mori*. The material has excellent properties and has been previously used in a microneedle format. Although these silk microneedle

devices successfully delivered model drugs both *in vitro* and *in vivo*, certain advantages over other materials were sacrificed through the fabrication process limiting the overall scope of this material platform.

In this body of work, we have reported on a number of research efforts to recapture these lost material advantages and demonstrate the broad utility of silk microneedle devices. Conformable microneedle patches have been produced through blending the silk material with the plasticizer glycerol, enabling application to curved skin surfaces—something that cannot be easily achieved with stiff substrates such as metal or silicon. We have investigated *in vivo* influenza vaccination with these devices to demonstrate their continued performance relative to other microneedle systems. The material is found to be non-immunogenic while eliciting a robust immune response. The existing fabrication process has been further developed and optimized to solve challenges encountered with the previous methods and to allow more efficient device production. This new fabrication method also has the potential to be scaled-up for the mass-manufacturing of silk microneedles. Unlike other materials in microneedle systems, silk can be processed into a variety of formats. This property was exploited in this research to create novel folding microneedles, ring devices, and to enable the non-traditional use of microneedles for tissue engineering. Silk fibroin provides an all-in-one material for a microneedle platform that can be quickly adapted and optimized for the delivery of a range of therapeutics. With a number of tunable properties described in this research, the silk material can be engineered for a number of broad applications. A self-administrable microneedle device is the ultimate goal for transdermal delivery research and we strongly believe that silk fibroin is the best candidate material for this device platform.

8. Future Directions

Much of this work has provided evidence for the broad utility of the silk microneedle platform. While we made improvements to the devices made through the existing spin-casting technique as well as through the drop-cast method, these devices were not characterized in great depth for performance. The *in vitro* delivery of both flexible and dissolving patches should be characterized in a porcine skin model to confirm (a) insertion of needles into the skin and (b) release of a labeled therapeutic into the skin. This would help validate that the flexible silk microneedle devices retain performance in a more accurate representation of their use. Similarly, it would confirm that the drop-cast needles designed for rapid therapeutic release could be used *in vivo* with no post-processing step to increase their strength. These studies represent important steps closer to a silk microneedle platform that could be advanced to a clinical stage.

For dissolving microneedle patches in particular, further characterization is needed to validate that upstream material parameters can be used to dictate the downstream release kinetics. The ability to control the release of therapeutics through changing the silk concentration and device mass alone would offer huge processing time advantages by obviating the post-processing treatment step. Silk boil time could also be investigated as an additional material parameter for these devices as longer boil times help reduce the average molecular weight of the silk solution. Obviously, validation of the performance of these devices *in vivo* would be needed after these characterization studies. We also believe that these dissolving devices could offer significant potential as vaccination devices for the mucosal surfaces of the body, particularly in the mouth. It has

been shown that these vaccination at these tissues may induce more robust immune response both locally and systemically [192, 193]. Previous microneedle devices used for mucosal vaccination have been in the solid coated format. A dissolving microneedle device could offer the benefit of being swallowed after administration, completely removing all biohazardous sharps waste that may still exist with solid microneedle devices.

We briefly investigated the areas of hollow microneedle development, microneedles for biosensing, and microvilli intestinal scaffolds. There is significant work remaining for each of these three research areas as prototyping was the extent of research efforts in these silk microneedle platform areas. The mechanics of hollow microneedles should be investigated to confirm that they could still penetrate the skin. If not, they may be suitable for blood collection from capillaries in the mouth, which would have a lower mechanical requirement for access and sampling. Similarly, microneedle electrodes could be developed for sensing in the skin or another tissue such as the heart or brain. There is a lot of potential for the folding microneedle devices, as they could be deployed into these tissues without any concern about damaging the tips of the microneedles which can be a concern for standard microneedle devices. Finally, we made significant progress with the microvilli-patterned silk scaffolds for small intestine tissue modeling. However, the master molds should be improved through more controlled micromachining (at the Tufts machine shop) to ensure the consistency of the microneedle features. The size of these scaffolds could also be increased to allow a higher density of needles to be produced inside the lumen of these scaffolds.

For vaccination, we mentioned a few improvements that could be made to better validate the silk microneedle system. First, the amount of residual vaccine should be measured to calculate the actual dose delivered and better correlate the immune response with delivered dose. Additionally, dissolving microneedles should be compared as they can localize the vaccine to the needle tips providing more consistent administration of dose which should be corroborated by more consistent immune response results. For stability, non-silk formulated vaccine coatings should be included as more relevant paired controls. The immune response mediated by the humoral/cellular components of the immune system through the two routes of administration may vary in magnitude; thus it would be more accurate to use the same route of administration to provide insight to the temperature stabilization properties of silk. A more difficult vaccine target to stabilize could also be used, such as a live attenuated vaccine like rotavirus, measles, or yellow fever. These studies would help characterize the performance of the silk microneedle system, as well as the overall stability performance that is necessary in producing a temperature-stable and self-administrable microneedle device.

In less than two years, we have demonstrated a number of methods to improve the existing silk microneedle devices and adapt them for a number of broader applications. No device design or fabrication process is perfect, and there is still room for development and innovation in this space. The microneedle designs were kept constant for this study, but could be made to mimic some of the arrowhead designs seen in literature or a more bio-inspired features such as a mosquito proboscis. The delivery of multiple therapeutics from a single patch could be investigated. All that remains is detailed investigation of these individual applications to confirm the advantages of silk fibroin over other existing

microneedle materials. We are confident that silk fibroin protein is the best available material for a microneedle platform with broad utility and represents the best opportunity for the creation of a commercially successful self-administrable vaccination device.

List of References

1. Smith, J, Lipsitch, M, & Almond, JW. Vaccine production, distribution, access, and uptake. The Lancet, 378:, 428–438 (2011).

2. Chen, X, Fernando, GJ, Crichton, ML, Flaim, C, Yukiko, SR, Fairmaid, EJ, Corbett, HJ, Primiero, CA, Ansaldo, AB, Frazer, IH, Brown, LE, & Kendall, MA. Improving the reach of vaccines to low-resource regions, with a needle-free vaccine delivery device and long-term thermostabilization. J. Control. Release, 152: 349–355 (2011).

3. Guy, B, & Nicolas, J-F. Intradermal, epidermal, and transcutaneous vaccination: from immunology to clinical practice. Expert Rev. of Vaccines, 7: 1201–1214 (2008).

4. Zaric, M, Lyubomska, O, Touzelet, O. Poux, C, Al-Zahrani, S, Fay, F, Wallace, L, Terhorst, D, Malissen, B, Henri, S, Power, UF, Scott, CJ, Donnelly, RF, & Kissenpfennig, A. Skin dendritic cell targeting via microneedle arrays laden with antigen-encapsulated poly-D,l-lactide-co-glycolide nanoparticles induces efficient antitumor and antiviral immune responses. ACS Nano, 7: 2042–2055 (2013).

5. Hamilton, JG. Needle phobia: a neglected diagnosis. J. Fam. Prac., 41(2): 169-175 (1995).

6. Raja, WK, Maccorkle, S, Diwan, IM, Abdurrob, A, Lu, J, Omenetto, FG, & Kaplan, DL. Transdermal delivery devices: Fabrication, mechanics and drug release from silk. Small, 9(21): 3704-3713 (2013).

7. Tsioris, K, Raja, WK, Pritchard, EM, Panilaitis, B, Kaplan, DL, & Omenetto, FG. Fabrication of silk microneedles for controlled-release drug delivery. Adv. Func. Mater., 22(2): 330-335 (2012).

8. Zhang, J, Pritchard, E, Hu, X, Valentin, T, Panilaitis, B, Omenetto, FG, & Kaplan, DL. Stabilization of vaccines and antibiotics in silk and eliminating the cold chain. PNAS, 109(30): 11981-11986 (2012).

9. Scheuplein, RJ. Mechanism of percutaneous adsorption I: Routes of penetration and the influence of solubility. J. Invest. Dermatol., 45: 334–345 (1965).

10. Scheuplein, RJ & Blank, IH. Permeability of the skin. Physiol. Rev., 51: 702–747 (1975).

11. Michaels, AS, Chandrasekaran, SK, & Shaw, JE. Drug permeation through human skin: theory and in vitro experimental measurement. AIChE J., 21: 985–996 (1975).

12. Swarbrick, J, Lee, G, & Brom, J. Drug permeation through human skin: I. Effect of storage conditions of skin. J. Invest. Dermatol., 78: 63–66 (1982).

13. Gemmell, D. & Morrison, J. The release of medicinal substances from topical applications and their passage through the skin. J. Pharm. Pharmacol., 9: 641–656 (1957).

14. Prausnitz, MR, Mitragotri, S, & Langer, R. Current status and future potential of transdermal drug delivery. Nat. Rev. Drug Disc., 3: 115–124 (2004).

15. Pastore, MN, Kalia, YN, Horstmann, M, & Roberts, MS. Transdermal patches: history, development and pharmacology. Brit. J. Pharm., 172(9): 2179–2209 (2015).

16. Center for Drug Evaluation and Research, Food and Drug Administration. Orange Book: Approved Drug Products with Therapeutic Equivalence Evaluations. US Department of Health and Human Services. March 2015. Accessed April 2015, http://www.accessdata.fda.gov/scripts/cder/ob/docs/queryai.cfm.

17. Prausnitz, MR & Langer, R. Transdermal drug delivery. Nat. Biotech., 26: 1261–1268 (2008).

18. Nasrollahi, SA, Taghibiglou, C, Azizi, E, & Farboud, ES. Cell-penetrating peptides as a novel transdermal drug delivery system. Chem. Biol. & Drug Design, 80, 639–646 (2012).

19. Miller, M.A. & Pisani, E. The cost of unsafe injections. Bull. World Health Organ., 77, 808–811 (1999).

20. Romanovsky, AA. Skin temperature: its role in thermoregulation. Acta Physio., 210(3): 498–507 (2014).

21. Rawlings, AV & Harding, CR. Moisturization and skin barrier function. Dermat. Ther., 17(S1): 43–48 (2004).

22. Lips, P. Vitamin D physiology. Prog. Biophys. Mol. Bio., 92(1): 4–8 (2006).

23. Menon, GK. New insights into skin structure: scratching the surface. Adv. Drug Del. Rev., 54(S1): 3–17 (2002).

24. Sengel, P. Pattern formation in skin development. Int. J. Dev. Bio., 34(1): 33–50 (1990).

25. Kanitakis, J. Anatomy, histology, and immunohistochemistry of normal human skin. Eur. J. Dermatol., 12(4): 390–401 (2002).

26. Palmer, CN, Irvine, AD, Terron-Kwiatkowski, A, Zhao, Y, Liao, H, Lee, SP, Goudie, DR, Sandilands, A, Campbell, LE, Smith, FJ, O'Regan, GM, Watson, RM, Cecil, JE, Bale, SJ, Compton, JG, DiGiovanna, JJ, Fleckman, P, Lewis-Jones, S, Arseculeratne, G, Sergeant, A, Munro, CS, El Houate, B, McElreavey, K, Halkjaer, LB, Bisgaard, H, Mukhopadhyay, S, & McLean, WH. Common loss-of-function variants of the epidermal barrier protein filaggrin are a major predisposing factor for atopic determinants. Nat. Genet., 38(4): 441–446 (2006).

27. Proksch, E, Brandner, JM, & Jensen, J-M. The skin: an indispensable barrier. Exper. Derm., 17(12): 1063–1072 (2008).

28. Baranoski, GVG & Krishnaswamy, A. Chapter 4—Bio-optical properties of human skin. In Light and Skin Interactions, M. Kaufmann ed., Boston, 61–79 (2010).

29. Nemes, Z & Steinert, PM. Bricks and mortar of the epidermal barrier. Exp. Mol. Med., 31(1): 5–19 (1999).

30. Barry, BW & Williams, AC. Permeation enhancement through skin. In: Encyclopedia of Pharmaceutical Technology. 11, 449–493 (1995).

31. Narvaez, D, Kanitakis, J, & Claudy, A. Dendritic cells of human dermis. Eur. J. Dermatol., 5: 69–76 (1995).

32. Foldvari, M., Babiuk, S. & Badea, I. DNA delivery for vaccination and therapeutics through the skin. Curr. Drug Deliv., 3, 17–28 (2006).

33. Karande, P., Jain, A., Ergun, K., Kispersky, V. & Mitragotri, S. Design principles of chemical penetration enhancers for transdermal drug delivery. Proc. Natl. Acad. Sci. USA, 102, 4688–4693 (2005).

34. Touitou, E & Godin, B. Vesicular carriers for enhanced delivery through the skin. In Enhancement in Drug Delivery (eds. Touitou, E & Barry, B). 255–278 (2007).

35. Naik, A, Kalia, YN & Guy, RH. Transdermal drug delivery: overcoming the skin's barrier function. PSTT, 3, 318–326 (2000).

36. Prausnitz, MR, Bose, VG, Langer, R & Weaver JC. Electroporation of mammalian skin: a mechanism to enhance transdermal drug delivery. PNAS USA, 90, 10504–10508 (1993).

37. Mitragotri, S & Kost, J. Low frequency sonophoresis: a noninvasive method of drug delivery and diagnostics. Biotech. Prog., 16, 488–492 (2000).

38. Paliwal, S, Menon, GK, & Mitragotri, S. Low-frequency sonophoresis: ultrastructural basis for stratum corneum permeability assessed using quantum dots. J. Invest. Dermatol., 126(5): 1095–1101 (2006).

39. Park, JH, Lee, JW, Kim, YC, & Prausnitz, MR. The effect of heat on skin permeability. Int. J. Pharm., 359: 94–103 (2008).

40. Langer, R. Drug delivery and targeting. Nature, 392: 5-10 (1998).

41. Torchilin, VP. Recent advances with liposomes as pharmaceutical carriers. Nat. Rev. Drug Disc., 4(2): 145-160 (2005).

42. Langer, R. New methods of drug delivery. Science, 249(4976): 1527-1533 (1990).

43. Henry, S, McAllister, DV, Allen, MG, & Prausnitz, MR. Microfabricated microneedles: A novel approach to transdermal drug delivery. J. Pharm. Sci., 87(8): 922-925 (1998).

44. Amsden, BG & Goosen, MFA. Transdermal delivery of peptide and protein drugs: An overview. AIChE, 41(8): 1972-1997 (1995).

45. Mahato, RI, Narang, AS, Thoma, L, & Miller, DD. Emerging trends in oral delivery of peptide and protein drugs. Crit. Rev. Thera. Drug Carrier Sys., 20(2-3): 153-214 (2003).

46. McAllister, DV, Wang, PM, Davis, SP, Park, J-H, Canatella, PJ, Allen, MG, & Prausnitz, MR. Microfabricated needles for transdermal delivery of macromolecules and nanoparticles: Fabrication methods and transport studies. PNAS, 100(24): 13755-13760 (2003).

47. Prausnitz, MR. Microneedles for transdermal drug delivery. Adv. Drug Deliv. Rev., 56: 581-587 (2004).

48. Indermun, S, Luttge, R, Choonara, YE, Kumar, P, du Toit, LC, Modi, G, & Pillay, V. Current advances in the fabrication of microneedles for transdermal delivery. J. Control. Rel., 185: 130-138 (2014).

49. Birchall, JC. Microneedle array technology: the time is right but is the science ready? Exp. Rev. Med. Dev., 3(1): 1-4 (2006).

50. Gill, HS & Prausnitz, MR. Coated microneedles for transdermal delivery. J. Control. Release, 117(2): 227-237 (2007).

51. Davidson, A, Al-Qallaf, B, & Das, DB. Transdermal drug delivery by coated microneedles: Geometry effects on effective skin thickness and drug permeability. Chem. Eng. Res. Des., 86: 1196-1206 (2008).

52. Arora, A, Prausnitz, MR, & Mitragotri, S. Micro-scale devices for transdermal drug delivery. Int. J. Pharmaceutics, 364(2): 227-236 (2008).

53. McAllister, DV, Allen, MG, & Prausnitz, MR. Microfabricated microneedles for gene and drug delivery. Annu. Rev. Biomed. Eng., 2: 289-313 (2000).

54. Kim, Y-C, Park, J-H, & Prausnitz, MR. Microneedles for drug and vaccine delivery. Adv. Drug Del. Rev., 64: 1547–1568 (2012).

55. McAllister, DV, Wang, PM, Davis, SP, Park, J-H, Canatella, PJ, Allen, MJ, & Prausnitz, MR. Microfabricated needles for transdermal delivery of macromolecules and nanoparticles: Fabrication methods and transport studies. PNAS, 100(24): 13755-13760 (2003).

56. Mikszta, JA, Alarcon, JB, Brittingham, JM, Sutter, DE, Pettis, RJ, & Harvey, NG. Improved genetic immunization via micromechanical disruption of skin-barrier function and targeted epidermal delivery. Nat. Med., 8: 415-419 (2002)

57. Cormier, M, Johnson, B, Ameri, M, Nyam, K, Libiran, L, Zhang, DD, & Daddona, P. Transdermal delivery of desmopressin using a coated microneedle array patch system. J. Control. Release, 97(3): 503-511 (2004).

58. Choi, H-J, Bondy, BJ, Yoo, D-G, Compans, RW, Kang, S-M, & Prausnitz, MR. Stability of whole inactivated influenza virus vaccine during coating onto metal microneedles. J. Control. Release, 166(2): 159-171 (2013).

59. Kommareddy, S, Baudner, BC, Bonificio, A, Gallorini, S, Palladino, G, Determan, AS, Dohmeier, DM, Kroells, KD, Sternjohn JR, Singh, M, Dormitzer, PR, Hansen, KJ, & O'Hagan, DT. Influenza subunit vaccine coated microneedle patches elicit comparable immune responses to intramuscular injection in guinea pigs. Vaccine, 31(34): 3435-3441 (2013).

60. Park, J-H, Allen, MG, & Prausnitz, MR. Polymer microneedles for controlled-release drug delivery. Pharm. Res., 23(5): 1008-1019 (2006).

61. Sullivan, SP, Koutsonanos, DG, del Pilar Martin, M, Lee, JW, Zarnitsyn, V, Choi, S-O, Murthy, N, Compans, RW, Skountzou, I, & Prausnitz, MR. Dissolving polymer microneedle patches for influenza vaccination. Nature Med., 16(8): 915-920 (2010).

62. Park, J-H, Allen, MG, & Prausnitz, MR. Biodegradable polymer microneedles: Fabrication, mechanics, and transdermal drug delivery. J. Control. Release, 104(1): 51-66 (2005).

63. Ambrose, CG & Clanto, TO. Bioabsorbable implants: review of clinical experience in orthopedic surgery. Ann. Biomed. Eng., 32(1): 171-177 (2004).

64. Chu, LY & Prausnitz, MR. Separable arrowhead microneedles. J. Control. Release, 149: 242–249 (2011).

65. Li, CG, Lee, CY, Lee, K, & Jung, H. An optimized hollow microneedle for minimally invasive blood extraction. Biomed. Microdev., 15(1): 17-25 (2013).

66. Sullivan, SP, Murthy, N, & Prausnitz, MR. Minimally invasive protein delivery with rapidly dissolving microneedles. Adv. Mater., 20: 933-938 (2008).

67. Mansoor, I, Liu, Y, Haefeli, UO, & Stoeber, B. Arrays of hollow out-of-plane microneedles made by metal electrodeposition onto solvent cast conductive polymer structures. J. Micromech. Microeng., 23 (2013).

68. Van Der Maaden, K, Jiskoot, W, & Bouwstra, J. Microneedle technologies for (trans)dermal drug and vaccine delivery. J. Control. Rel., 161: 645-655 (2012).

69. Hilt, JZ & Peppas, NA. Microfabricated drug delivery devices. Int. J. Pharmaceu., 306(1-2): 15-23 (2005).

70. Gardeniers, HJGE, Luttge, R, Berenchot, EJW, Boer, MJD, Yeshurun, SY, Hefetz, M, Oever, RVT, Berg, AVD. Silicon micromachined hollow microneedles for transdermal liquid transport. J. Microelectromech. Syst., 12(3): 855-862 (2003).

71. Smart, WH & Subramanian, K. The use of silicon microfabrication technology in painless blood glucose monitoring. Diabetes Technol. Ther., 2(4): 549-559 (2000).

72. Paik, S-J, Byun, S, Lim, J-M, Park, Y, Lee, A, Chung, S, Chang, J, Chun, K, & Cho, D. In-plane single-crystal-silicon microneedles for minimally invasive microfluidic systems. Sens. Actu. A, 114(2-3): 276-284 (2004).

73. Mukerjee, EV, Collins, SD, Isseroff, RR, & Smith, RL. Microneedle array for transdermal biological fluid extraction and in situ analysis. Sens. Actu. A, 114(2-3): 267-275 (2004).

74. Edell, DJ, Toi, VV, McNeil, VM, & Clark, LD. Factors influencing the biocompatibility of insertable silicon microshafts in cerebral cortex. IEEE Trans. Biomed. Eng., 39(6): 635-643 (1992).

75. Baron, N, Guicheret-Retel, V, Coudevylle, J-R, Cabodevila, G, & Lexcellent, C. Microfabricated silicon array of microneedles: prediction of its behavior during insertion through the skin.

76. Ami, Y, Tachikawa, H, Takano, N, & Miki, N. Formation of polymer microneedle arrays using soft lithography. J. Micro/Nanolith. MEMS MOEMS, 10(1): 1-6 (2011).

77. Park, J-H, Yoon, Y-K, Choi, S-O, Prausnitz, MR, & Allen, MG. Tapered conical polymer microneedles fabricated using an integrated lens technique for transdermal drug delivery. IEEE Trans. BME, 54(5): 903-913 (2007).

78. Moon, SJ & Lee, SS. A novel fabrication method of a microneedle array using inclined deep x-ray exposure. J. Micromech. Microeng., 15: 903-911 (2005).

79. Xia, Y & Whitesides, GM. Soft lithography. Ann. Rev. Mat. Sci., 28: 153-184 (1998).

80. Matteucci, M, Fanetti, M, Casella, M, Gramatica, F, Gavioli, L, Tormen, M, Grenci, G, De Angelis, F, & Di Fabrizio, E. Poly vinyl alcohol re-usable masters for microneedle replication. Microelec. Eng., 86: 752-756 (2009).

81. Lee, JW, Han, M-R, & Park, J-H. Polymer microneedles for transdermal drug delivery. J. Drug Target., 21(3): 211-223 (2013).

82. Kim, MY, Jung, B, & Park, J-H. Hydrogel swelling as a trigger to release biodegradable polymer microneedles in skin. Biomater., 33(2): 668-678 (2012).

83. DeMuth, PC, Garcia-Beltran, WF, Ai-Ling, ML, Hammond, PT, & Irvine, DJ. Composite dissolving microneedles for coordinated control of antigen and adjuvant delivery kinetics in transcutaneous vaccination. Adv. Func. Mater., 23(2): 161-172 (2013).

84. Aoyagi, S, Izumi, H, Isono, Y, Fukuda, M, & Ogawa, H. Laser fabrication of high aspect ratio thin holes on biodegradable polymer and its application to a microneedle. Sens. Actua. A Phys., 139: 293-302 (2007).

85. Jin, CY, Han, MH, Lee, SS, & Choi, YH. Mass producible and biocompatible microneedle patch and functional verification of its usefulness for transdermal drug delivery. Biomed. Microdev., 11(6): 1195-1203 (2009).

86. Han, M, Hyun, D-H, Park, H-H, Lee, SS, Kim, C-H, & Kim, C. A novel fabrication process for out-of-plane microneedle sheets of biocompatible polymer. J. Microelec. Microeng., 17(6): 1184-1191 (2007).

87. You, SK, Noh, YW, Park, HH, Han, M, Lee, SS, Shin, SC, & Cho, CW. Effect of applying modes of the polymer microneedle-roller on the permeation of L-ascorbic acid in rats. J. Drug Target., 18(1): 15-20 (2010).

88. Moon, SJ, Lee, SS, Lee, HS, & Kwon, TH. Fabrication of microneedle array using LIGA and hot embossing processes. Microsys. Tech., 11: 311-318 (2005).

89. Perennes, F, Marmiroli, B, Matteucci, M, Tormen, M, Vaccari, L, & Di Fabrizio, E. Sharp beveled tip hollow microneedle arrays fabricated by LIGA and 3D soft lithography with polyvinyl alcohol. J. Micromech. Microeng., 16(3): 473-479 (2006).

90. Donnelly, RF, Majithiya, R, Singh, TRR, Morrow, DIJ, Garland, MJ, Demir, YK, Migalska, K, Ryan, E, Gillen, D, Scott, CJ, & Woolfson, AD. Design, optimization, and characterization of polymeric microneedle arrays prepared by a novel laser-based micromoulding technique. Pharmaceu. Res., 28: 41-57 (2011).

91. Chu, LY, Choi, S-O, & Prausnitz, MR. Fabrication of dissolving polymer microneedles for controlled drug encapsulation and delivery: bubble and pedestal microneedle designs. J. Pharm. Sci., 99(10): 4228-4238 (2010).

92. Yung, KL, Xu, Y, Kang, C, Liu, H, Tam, KF, Ko, SM, Kwan, FY, & Lee, TMH. Sharp tipped plastic hollow microneedle array by microinjection molding. J. Micromech. Microeng., 22: 015016 (2012).

93. Lee, JW, Park, J-H, & Prausnitz, MR. Dissolving microneedles for transdermal drug delivery. Biomater., 29(13): 2113-2124 (2008).

94. Yan, L, Raphael, AP, Zhu, X, Wang, B, Chen, W, Tang, T, Deng, Y, Sant, HJ, Zhu, G, Choy, KW, Gale, BK, Prow, TW, & Chen, X. Nanocomposite-strengthened dissolving microneedles for improved transdermal delivery into human skin. Adv. Healthc. Mater., 3(4): 555-564 (2014).

95. Ito, Y, Yoshimitsu, J-I, Shiroyama, K, Sugioka, N, & Takada, K. Self-dissolving microneedles for the percutaneous absorption of EPO in mice. J. Drug Target., 14(5): 255-261 (2006).

96. Ito, Y, Murano, H, Hamasaki, N, Fukushima, K, & Takada, K. Incidence of low bioavailability of leuprolide acetate after percutaneous administration to rats by dissolving microneedles. Int. J. Pharmaceu., 407(1-2):126-131 (2011).

97. Chen, M-C, Ling, M-H, Lai, K-Y, & Pramudityo, E. Chitosan microneedle patches for sustained transdermal delivery of macromolecules. Biomacromol., 13(12): 4022-4031 (2012).

98. Chen, M-C, Huang, S-F, Lai, K-Y, & Ling, M-H. Fully embeddable chitosan microneedles as a sustained release depot for intradermal vaccination. Biomater., 34(12): 3077-3086 (2013).

99. Liu, S, Jin, M-N, Quan, Y-S, Kamiyama, F, Kusamori, K, Katsumi, H, Sakane, T, & Yamamoto, A. Transdermal delivery of relatively high molecular weight drugs using novel self-dissolving microneedle arrays fabricated from hyaluronic acid and their characteristics and safety after application to the skin. Eur. J. Pharmaceu. Biopharmaceu., 86(2): 267-276 (2014).

100. Donnelly, RF, Morrow, DIJ, Singh, TRR, Migalska, K, McCarron, PA, O'Mahony, C, & Woolfson, AD. Processing difficulties and instability of carbohydrate microneedle arrays. Drug Devel. Indust. Pharm., 35(10): 1242-1254 (2009).

101. Li, G, Badkar, A, Nema, S, Kolli, CS, & Banga, AK. In vitro transdermal delivery of therapeutic antibodies using maltose microneedles. Int. J. Pharmaceu., 368: 109-115 (2009).

102. Miyano, T, Tobinaga, Y, Kanno, T, Matsuzaki, Y, Takeda, H, Wakui, M, & Hanada, K. Sugar micro needles as transdermic drug delivery system. Biomed. Microdev., 7(3): 185-188 (2005).

103. Parker, ER, Rao, MP, Turner, KL, Meinhart, CD, & MacDonald, NC. Bulk micromachined titanium microneedles. J. MEMS, 16(2): 289-295 (2007).

104. Chandrasekaran, S, Brazzle, JD, & Frazier, AB. Surface micromachined metallic microneedles. J MEMS, 12(3): 281-288 (2003).

105. Omatsu, T, Chujo, K, Miyamoto, K, Okida, M, Nakamura, K, Aoki, N, & Morita, R. Metal microneedle fabrication using twisted light with spin. Optics Exp., 18(17): 17967-17973 (2010).

106. Ovsianikov, A, Chichkov, B, Mente, P, Monteiro-Riviere, NA, Doraiswamy, A, & Narayan, RJ. Two photon polymerization of polymer-ceramic hybrid materials for transdermal drug delivery. Int. J. Appl. Ceram. Tech., 4(1): 22-29 (2007).

107. Wang, PM, Cornwell, M, Hill, J, & Prausnitz, MR. Precise microinjection into skin using hollow microneedles. J. Invest. Dermat., 126: 1080–1087 (2006).

108. Ito, Y, Hagiwara, E, Saeki, A, Sugioka, N, & Takada, K. Feasibility of microneedles for percutaneous absorption of insulin. Eur. J. Pharm. Sci., 29(1): 82-88 (2006).

109. Kolli, CS & Banga, AK. Characterization of solid maltose microneedles and their use for transdermal delivery. Pharm. Res., 25(1): 104-113 (2008).

110. Ito, Y, Kashiwara, S, Fukushima, K, & Takada, K. Two-layered dissolving micrneedles for percutaneous delivery of sumatriptan in rats. Drug Devel. Indust. Pharm., 37(12): 1387-1393 (2011).

111. Garland, MJ, Caffarel-Salvador, E, Migalska, K, Woolfson, AD, & Donnelly, RF. Dissolviing polymeric microneedle arrays for electrically assisted transdermal drug delivery. J. Control. Release, 159(1): 52-59 (2012).

112. Wermeling, DP, Banks, SL, Hudson, DA, Gill HS, Gupta, J, Prausnitz, MR, & Stinchcomb, AL. Microneedles permit transdermal delivery of a skin-impermeant medication to humans. PNAS, 105(6): 2058-2063 (2008).

113. Katsumi, H, Liu, S, Tanaka, Y, Hitomi, K, Hayashi, R, Hirai, Y, Kusamori, K, Quan, Y-S, Kamiyama, F, Sakane, T, & Yamamoto, A. Development of a novel self-dissolving microneedle array of alendronate, a nitrogen-containing bisphosphonate: Evaluation of transdermal absorption, safety, and pharmacological effects after application in rats. J. Pharm. Sci., 101(9): 3230-3238 (2012).

114. Jiang, J, Gill, HS, Ghate, D, McCarey, BE, Patel, SR, Edelhauser, HF, & Prausnitz, MR. Coated microneedles for drug delivery to the eye. Investigative Ophth. Vis. Sci., 48(9): 4038-4043 (2007).

115. Martanto, W, Davis, SP, Holiday, NR, Wang, J, Gill, HS, & Prausnitz, MR. Transdermal delivery of insulin using microneedles. Pharm. Res., 21(6): 947-952 (2004).

116. Gupta, J, Felner, EI, & Prausnitz, MR. Minimally invasive insulin delivery in subjects with type 1 diabetes using hollow microneedles. Diabetes Tech. Therapeu., 11(6): 329-337 (2009).

117. Lanke, SSS, Kolli, CS, Strom, JG, & Banga, AK. Enhanced transdermal delivery of low molecular weight heparin by barrier perturbation. Int. J. Pharmaceu., 365: 26-33 (2009).

118. Ito, Y, Murakami, A, Maeda, T, Sugioka, N, & Takada, K. Evaluation of self-dissolving needles containing low molecular weight heparin (LMWH) in rats. Int. J. Pharmaceu., 349: 124-129 (2008).

119. Fukushima, K, Ise, A, Morita, H, Hasegawa, R, Ito, Y, Sugioka, N, & Takada, K. Two-layered dissolving microneedles for percutaneous delivery of peptide/protein drugs in rats. Pharma. Res., 28(1): 7-23 (2011).

120. Lee, JW, Choi, S-O, Felner, EI, & Prausnitz, MR. Dissolving microneedle patch for transdermal delivery of human growth hormone. Small, 7(4): 531-539 (2011).

121. Daddona, PE, Matriano, JA, Mandema, J, & Maa, Y-F. Parathyroid-hormone (1,34)-coated microneedle patch system: Clinical pharmacokinetics and pharmacodynamics for treatment of osteoporosis. Pharma. Res., 28(1): 159-165 (2011).

122. Lara, MF, Gonzalez-Gonzalez, E, Speaker, TJ, Hickerson, RP, Leake, D, Milstone, LM, Contag, CH, & Kaspar, RL. Inhibition of CD44 gene expression in human skin models, using self-delivery short interfering RNA administered by dissolvable microneedle arrays. Human Gene Therapy, 23(8): 816-823 (2012).

123. Chong, RHE, Gonzalez-Gonzalez, E, Lara, MF, Speaker, TJ, Contag, CH, Kaspar, RL, Coulman, SA, Hargest, R, & Birchall JC. Gene silencing following siRNA delivery to skin via coated steel microneedles: in vitro and in vivo proof-of-concept. J. Control. Rel., 166(3): 211-219 (2013).

124. Yan, G, Arelly, N, Farham, N, Lobo, S, & Li, H. Enhancing DNA delivery into the skin with a motorized microneedle device. Euro. J. Pharm. Sci., 52(1): 215-222 (2014).

125. Pearton, M, Saller, V, Coulman, SA, Gateley, C, Anstey, AV, Zarnitsyn, V, & Birchall, JC. Microneedle delivery of plasmid DNA to living human skin: Formulation coating, skin insertion and gene expression. J. Control. Rel., 160(3): 561-569 (2012).

126. Matsuo, K, Hirobe, S, Yokota, Y, Ayabe, Y, Seto, M, Quan, Y-S, Kamiyama, F, Tougan, T, Horii, T, Mukai, Y, Okada, N, & Nakagawa, S. Transcutaneous immunization using a dissolving microneedle array protects against tetanus, diphtheria, malaria, and influenza. J. Control. Release, 160: 495-501 (2012).

127. Kim, YC, Quan, FS, Compans, RW, Kang, SM, & Prausnitz, MR. Formulation and coating of microneedles with inactivated influenza virus to improve vaccine stability and immunogenicity. J. Control. Release, 142: 187-195 (2010).

128. Raphael, AP, Prow, TW, Crichton, ML, Chen, X, Fernando, GJ, & Kendall, MA. Targeted, needle-free vaccinations in skin using multilayered, densely-packed dissolving microprojection arrays. Small, 6: 1785-1793 (2010).

129. Mikszta, JA, Dekker III, JP, Harvey, NG, Dean, CH, Brittingham, JM, Huang, J, Sullivan, VJ, Dyas, B, Roy, CJ, & Ulrich, RG. Microneedle-based intradermal delivery of the anthrax recombinant protective antigen vaccine. Infection and Immunity, 74(12): 686-6810 (2006).

130. Edens, C, Collins, ML, Goodson, JL, Rota, PA, & Prausnitz, MR. A microneedle patch containing measles vaccines is immunogenic in non-human primates. Vaccine, in press (DOI: 10.1016/j.vaccine.2015.02.074), 2015.

131. Edens, C, Collins, ML, Ayers, J, Rota, PA, & Prausnitz, MR. Measles vaccination using a microneedle patch. Vaccine, 31(24): 3403-3409 (2013).

132. Andrianov, AK, DeCollibus, DP, Gillis, HA, Kha, HH, Marin, A, Prausnitz, MR, Babiuk, LA, Townsend, H, & Mutwiri, G. Poly[di(carboxylatophenoxy)phosphazene] is a potent adjuvant for intradermal immunization. PNAS, 106(45): 18936-18941 (2009).

133. Corbett, HJ, Fernando, GJP, Chen, X, Frazer, IH, & Kendall, MAF. Skin vaccination against cervical cancer associated human papillomavirus with a novel micro-projection array in a mouse model. PLOS One, 5(10): e13460 (2010).

134. Prow, TW, Chen, X, Prow, NA, Fernando, GJP, Tan, CSE, Raphael, AP, Chang, D, Ruutu, MP, Jenkins, DWK, Pyke, A, Crichton, ML, Raphaelli, K, Goh, LYH, Frazer, IH, Roberts, MS, Gardner, J, Khromykh, AA, Suhrbier, A, Hall, RA, & Kendall, MAF. Nanopatch-targeted skin vaccination against West Nile virus and Chikungunya virus in mice. Small, 6(16): 1776-1784 (2010).

135. Hiraishi, Y, Nandakumar, S, Choi, S-O, Lee, J-W, Kim, Y-C, Posey, J-E, Sable, S-B, & Prausnitz, MR. Bacillus Calmette-Guerin vaccination using a microneedle patch. Vaccine, 29: 2626-2636 (2011).

136. Van der Maaden, K, Trietsch, SJ, Kraan, H, Varypataki, EM, Romeijn, S, Zwier, R, Van Der Linden, HJ, Kersten, G, Hankemeier, T, Jiskoot, W, & Bouwstra, J. Novel hollow microneedle technology for depth-controlled microinjection-mediated dermal vaccination:A study with poliio vaccine in rats. Pharm. Res., 31(7): 1846-1854 (2014).

137. Edens, C, Dybdahl-Sissoko, NC, Weldon, WC, Oberste, MS, & Prausnitz, MR. Inactivated polio vaccination using a microneedle patch is immunogenic in the rhesus macaque. Vaccine, in press (DOI: 10.1016/j.vaccine.2015.01.089), 2015.

138. Kaplan, DL, Mello, SM, Arcidiacono, S, Fossey, S, & Senecal, KWM. Protein based materials, KKD McGrath (Ed.). Birkhauer, Boston, 103-131 (1998).

139. Altman, GH, Diaz, F, Jakuba, C, Calabro, T, Horan, RL, Chen, J, Lu, H, Richmond, J, & Kaplan, DL. Silk-based biomaterials. Biomaterials, 24(3): 401-416 (2003).

140. Wong Po Foo, C & Kaplan, DL. Genetic engineering of fibrous proteins: spider dragline silk and collagen. Adv. Drug Deliv. Rev., 54(8): 1131-1143 (2002).

141. Zoaming, W, Codina, R, Fernandez-Caldas, E, & Lockey, RF. Partial characterization of the silk allergens in mulberry silk extract. J. Inv. Allergy Clin. Immunol., 6: 237-241 (1996).

142. Panilaitis, B, Altman, GH, Chen, J, Jin, H-J, Karageorgiou, V, & Kaplan DL. Macrophage responses to silk. Biomaterials, 24(18): 3079-3085 (2003).

143. Vepari, C & Kaplan, DL. Silk as a biomaterial. Prog. Polym. Sci., 32(8-9): 991-1007 (2007).

144. Zhou, C-Z, Confalonieri, F, Medina, N, Zivanovic, Y, Esnault, C, Yang, T, Jacquet, M, Janin, J, Duguet, M, Perasso, R, & Li, Z-G. Fine organization of Bombyx mori fibroin heavy chain gene. Nucl. Acids Res., 28(12): 2413-2419 (2000).

145.Tanaka, K, Inoue, S, & Mizuno, S. Hydrophobic interaction of P25, containing Asn-linked oligosaccharide chains, with the H-L complex of silk fibroin produced by B. mori. Insect Biochem. Mol. Biol., 29(3): 269-276 (1999).

146. Zhou, C-Z, Confalonieri, F, Jacquet, M, Perasso, R, Li, Z-G, & Janin, J. Silk fibroin: Structural implications of a remarkable amino acid sequence. Proteins, 44: 119-122 (2001).

147. Murphy, AR & Kaplan, DL. Biomedical applications of chemically-modified silk fibroin. J. Mater. Chem., 19: 6443-6450 (2009).

148. Rockwood, DN, Preda, RC, Yucel, T, Wang, X, Lovett, ML, & Kaplan, DL. Materials fabrication from Bombyx mori silk fibroin. Nature Protocols, 6: 1612-1631 (2011).

149. Marin, MA, Mallepally, RR, & McHugh, MA. Silk fibroin aerogels for drug delivery applications. J. Supercrit. Fluids, 91: 84-89 (2014).

150. Yoshimizu, H & Asakura, T. Preparation and characterization of silk fibroin powder and its application to enzyme immobilization. J. App. Polym. Sci., 40(1-2): 127-134 (1990).

151. Marelli, B, Alessandrino, A, Fare, S, Freddi, G, Mantovani, D, & Tanzi, MC. Compliant electrospun silk fibroin tubes for small vessel bypass grafting. Acta Biomaterialia, 6(10): 4019-4026 (2010).

152. Li, C, Vepari, C, Jin, H-J, Kim, H-J, & Kaplan, DL. Electrospun silk-BMP-2 scaffolds for bone tissue engineering. Biomaterials, 27(16): 3115-3124 (2006).

153. Wang, Y., Kim, U-J, Blasioli, DJ, Kim, H-J, & Kaplan, DL. In vitro cartilage tissue engineering with 3D porous aqueous-derived silk scaffolds and mesenchymal stem cells. Biomaterials, 26(34): 7082-7094 (2005).

154. Mauney, JR, Nguyen, T, Gillen, K, Kirker-Head, C, Gimble, JM, & Kaplan, DL. Engineering adipose-like tissue in vitro and in vivo utilizing human bone marrow and adipose-derived mesenchymal stem cells with silk fibroin 3D scaffolds. Biomaterials, 28(35): 5280-5290 (2007).

155. Chen, et al. Manuscript prepared and submitted. (2015)

156. Tang-Schomer, MD, White, JD, Tien, LW, Schmitt, LI, Valentin,TM, Graziano, DJ, Hopkins, AM, Omenetto, FG, Haydon, PG, & Kaplan, DL. Bioengineered functional brain-like cortical tissue. Proc. Natl. Acad. Sci. USA, 111(38): 13811-13816 (2014).

157. Wenk, E, Merkle, HP, & Meinel, L. Silk fibroin as a vehicle for drug delivery applications. J. Control. Rel., 150(2): 128-141 (2011).

158. Wray, LS, Hu, X, Gallego, J, Georgakoudi, I, Omenetto, FG, Schmidt, D, & Kaplan, DL. Effect of processing on silk-based biomaterials: reproducibility and biocompatibility. J. Biomed. Mater. Res. B Appl. Biomater., 99: 89-101 (2011).

159. Yucel, T, Lovett, ML, & Kaplan, DL. Silk-based biomaterials for sustained drug delivery. J. Control. Rel., 190: 381-397 (2014).

160. Horan, RL, Toponarski, I, Boepple, HE, Weitzel, PP, Richmond, JC, & Altman, GH. Design and characterization of a scaffold for anterior cruciate ligament engineering. J. Knee Surg., 22(1): 82-92 (2009)

161. Meinel, L, Hofmann, S, Karageorgiou, V, Kirker-Head, C, McCool, J, Gronowicz, G, Zichner, L, Langer, R, Vunjak-Novakovic, G, & Kaplan, DL. The inflammatory responses to silk films in vitro and in vivo. Biomater., 26: 147-155 (2005).

162. Numata, K, Cebe, P, & Kaplan, DL. Mechanism of enzymatic degradation of beta-sheet crystals. Biomater., 31: 2926-2933 (2010).

163. Cao, Y & Wang, B. Biodegradation of silk biomaterials. Int. J. Mol. Sci., 10(4): 1514-1524 (2009).

164. Demuth, PC, Min, Y, Irvine, DJ, Hammond, PT. Implantable silk composite microneedles for programmable vaccine release kinetics and enhanced immunogenicity in transcutaneous immunization. Adv. Healthcare Mater., 3(1): 47-58 (2014).

165. Lee, J, Park, SH, Seo, IH, Lee, KJ, & Ryu, W. Rapid and repeatable fabrication of high A/R silk fibroin microneedles using thermally-drawn micromolds. Eur. J. Pharmaceut. Biopharmaceu., 94: 11-19 (2015).

166. You, X, Chang, J-H, Ju, B-K, & Pak, JJ. Rapidly dissolving fibroin microneedles for transdermal drug delivery. Mat. Sci. Eng. C, 31(8): 1632-1636 (2011).

167. Diwan, IM. Benchtop fabrication of silk microneedles for transdermal drug delivery. Master's thesis, Tufts University, 2013. Accessed 7/2015, ProQuest (Ann Arbor, MI).

168. Lu, S, Wang, X, Lu, Q, Hu, X, Uppal, N, Omenetto, FG, & Kaplan, DL. Stabilization of enzymes in silk films. Biomacromol., 10(5): 1032-1042 (2009).

169. Jin, H-J, Park, J, Karageorgiou, V, Kim, U-J, Valluzzi, R, Cebe, P, & Kaplan, DL. Water-stable silk films with reduced β-sheet content. Advan. Func. Mater., 15: 1241–1247 (2005).

170. Lu, S, Wang, X, Lu, Q, Zhang, X, Kluge, JA, Uppal, N, Omenetto, FG, & Kaplan, DL. Insoluble and flexible silk films containing glycerol. Biomacromol., 11: 143–150 (2010).

171. Perry, H, Gopinath, A, Kaplan, DL, Dal Negro, L, & Omenetto, FG. Nano- and micropatterning of optically transparent, mechanically robust, biocompatible silk fibroin films. Adv. Mater., 20: 3070–3072 (2008).

172. Borba, M, de Araujo, MD, de Lima, E, Yoshimura, HN, Cesar, PF, Griggs, JA, & Della Bona, A. Flexural strength and failure modes of layered ceramic structures. Dental Materials, 27: 1259–1266 (2011).

173. Kanie, T, Kadokawa, A, Arikawa, H, Fujii, K, & Ban, S. Flexural properties of ethyl or methyl methacrylate-UDMA blend polymers. Dental Materials Journal, 29: 575–581 (2010).

174. Rodrigues Jr., SA, Zanchi, CH, de Carvalho, RV, & Demarco, FF. Flexural strength and modulus of elasticity of different types of resin-based composites. Braz. Oral Res., 21: 16–21 (2007).

175. Halim, AS, Khoo, TL, & Yussof, SJM. Biologic and synthetic skin substitutes: An overview. Indian J. Plast. Surg., 43: S23-S28 (2010).

176. Jacobi, U, Kaiser, M, Toll, R, Mangelsdorf, S, Audring, H, Otberg, N, Sterry, W, & Lademann, J. Porcine ear skin: An in vitro model for human skin. Skin Res. Tech., 13(1): 19-24 (2007).

177. Geeraedts, F, Bungener, L, Pool, J, ter Veer, W, Wilschut, J, & Huckriede, A. Whole inactivated virus influenze vaccine is superior to subunit vaccine in inducing immune responses and secretion of proinflammatory cytokines by DCs. Influenza Resp. Viruses, 2(2): 41-51 (2008).

178. Romagnani, S. T-cell subsets (Th1 versus Th2). Ann. Allergy Asthma Immunol., 85(1): 9-18 (2000).

179. Vinuesa, CG, Tangye, SG, Moser, B, & Mackay, CR. Follicular B helper T cells in antibody responses and autoimmunity. Nat. Rev. Immunol., 5: 853–865 (2005).

180. Siegrist, C-A. Vaccine Immunology. Plotkin, SA, Orenstein, W, & Offit, PA (Eds.), Vaccines (6th ed.), Elsevier, 14-32 (2013).

181. Hirobe, S, Azukizawa, H, Hanafusa, T, Matsuo, K, Quan, Y-S, Kamiyama, F, Katayama, I, Okada, N, & Nakagawa, S. Clinical study and stability assessment of a novel transcutaneous influenza vaccination using a dissolving microneedle patch. Biomaterials, 57: 50-58 (2015).

182. Van Damme, P, Oosterhuis-Kafeja, F, Van Der Wielen, M, Almagor, Y, Sharon, O, & Levin, Y. Safety and efficacy of a novel microneedle device for dose sparing intradermal influenza vaccination in healthy adults. Vaccine, 27(3): 454-459 (2009).

183. Hamkar, R, Jalilvand, S, Mokhtari-Azad, T, Jelyani, KN, Dahi-Far, H, Soleimanjahi, H, & Nategh, R. Assessment of IgM enzyme immunoassay and IgG avidity assay for distinguishing between primary and secondary immune response to rubella vaccine. J. Virological Meth., 130(1-2): 59-65 (2005).

184. Lu, Q, Hu, X, Wang, X, Kluge, JA, Lu, S, Cebe, P, Kaplan, DL. Water-insoluble silk films with silk I structure. Acta Biomater., 6(4): 1380-1387 (2010).

185. Spira, ME, & Hai, A. Multi-electrode array technologies for neuroscience and cardiology. Nature Nanotech., 8: 83-94 (2013).

186. Kim, D-H, Viventi, J, Amsden, JJ, Xiao, J, Vigeland, L, Kim, Y-S, Blanco, JA, Panilaitis, B, Frechette, ES, Contreras, D, Kaplan, DL, Omenetto, FG, Huang, Y, Hwang, K-C, Zakin, MR, Litt, B, & Rogers, JA. Dissolvable films of silk fibroin for ultrathin, conformal bio-integrated electronics. Nat. Mater., 9: 511–517 (2010).

187. Palmer, C. The design and assessment of adherent and conformable high density electrode arrays for in vivo tissue monitoring, Senior Capstone Project, Department of Biomedical Engineering. Tufts University, 2014.

188. Golden, AP, & Tien, J. Fabrication of microfluidic hydrogels using molded gelatin as a sacrificial element. Lab Chip, 7: 720-725 (2007).

189. Lefevre, T, Rousseau, M-E, & Pezolet, M. Protein secondary structure and orientation in silk as revealed by Raman spectromicroscopy. Biophys. J., 92(8): 2885-2895 (2007).

190. Godbillot, L, Dole, P, Joly, C, Roge, B, & Mathlouthi, M. Analysis of water binding in starch plasticized films. Food Chemistry, 96: 380–386 (2006).

191. Vagenende, V, Yap, MG, & Trout, BL. Mechanisms of protein stabilization and prevention of protein aggregation by glycerol. Biochemistry, 48(46): 11084-11096 (2009).

192. Ma, Y, Tao, W, Krebs, SJ, Sutton, WF, Haigwood, NL, & Gill, HS. Vaccine delivery to the oral cavity using coated microneedles induces systemic and mucosal immunity. Pharm. Res., 31: 2393-2403 (2014).

193. McNeilly, CL, Crichton, ML, Primiero, CA, Frazer, IH, Roberts, MS, & Kendall, MAF. Microprojection arrays to immunise at mucosal surfaces. J. Control. Rel., 196: 252-260 (2014).